KU LEUVEN

ARENBERG DOCTORAL SCHOOL

FACULTY OF SCIENCE

Study of organic probes and strategies for DNA fluorescent labelling:

From basic photochemistry to super-resolution optical microscopy

Milena Helmer Lauer

Supervisors:

Prof. Marcelo H. Gehlen

Prof. Johan Hofkens

Thesis presented in partial fulfilment of the requirements for the degree of PhD in Science

2016

Milena Helmer Lauer

Estudo de sondas orgânicas e estratégias de marcação fluorescente de DNA: da fotoquímica básica à microscopia óptica de super-resolução

Tese apresentada ao Instituto de Química de São Carlos da Universidade de São Paulo e à Faculdade de Ciências da Katholieke Universiteit Leuven como parte dos requisitos para a obtenção do título de doutor em ciências

Área de concentração: Físico-Química

Orientadores: Prof. Dr. Marcelo Henrique Gehlen e Prof. Dr. Johan Hofkens

São Carlos
2016

“We are hard pressed on every side, but not crushed; perplexed, but not in despair; persecuted, but not abandoned; struck down, but not destroyed.”

2 Co 4:8-9

PREFACE

The development of this thesis was initiated in March 2011 at the Institute of Chemistry of São Carlos, under the supervision of Prof. Marcelo H. Gehlen. The first chapter includes the main fundamental concepts of the research. The second chapter comprises the photophysical study of several bisarylated maleic anhydride and maleimide derivatives, synthesized by the Heck-Matsuda reaction. These compounds are inspired by the natural products polycitrin A and B, found in the marine ascidian *Polycitor* sp. Moreover, the confocal fluorescence microscopy study of a set of compounds designed with condensed aromatic rings, which has the potential of being used as fluorescent probes is presented. All the compounds were supplied by our collaborators from the group of Prof. Dr. Carlos Roque Duarte Correia – UNICAMP, Brazil, and synthesized by Dra. Roberta Lopes Drekener. The fluorescence spectroscopic and microscopic experiments were performed in the Molecular Fluorescence Group, at IQSC – USP, Brazil.

The third chapter comprises the research conducted over the course of thirteen months (July 2013 until July 2014) at the Fluorocode Group, Katholieke Universiteit Leuven, Belgium, supervised by Prof. Dr. Johan Hofkens. In this period, the research was conducted towards platform experiments concerning the investigation of methodologies of sequence-specific fluorescent DNA labelling using methyltransferase enzymes. The strategies of labelling were studied by super-resolution optical microscopy. With this technique, we developed a single-molecule assay for counting the number of fluorophores associated with individual plasmids. In this chapter, a detailed AFM study of the plasmids morphology after the fluorescent labelling reactions is shown. Furthermore, experiments of vector transfection and protein expression into mammalian cells were used to demonstrate that the labelling does not interfere with the transcription of DNA.

During this time abroad, it was proposed to obtain of a double doctoral degree by USP and KU Leuven. I had the opportunity to return to KU Leuven for a short stay of two months (September to November 2015), in which a strategy for fluorescent labelling of oligonucleotide probes for fluorescence *in situ* hybridization purposes, as well as the elaboration of a DNA hybridization protocol, were developed. The main results of this additional research period are presented as a section of Chapter 3.

ACKNOWLEDGEMENTS

I would like to use this space to express my sincere gratitude to some people who have contributed to accomplish this PhD.

Firstly, I would like to thank my promoters, Prof. Marcelo H. Gehlen and Prof. Johan Hofkens, for accepting and welcoming me into their groups. Thanks to them, I had the unique opportunity to realise a double doctorate between USP and KU Leuven.

I would like to thank Fundação de Amparo à Pesquisa do Estado de São Paulo, FAPESP, for the regular direct doctoral scholarship, grant 2011/08727-1, and for the scholarship allowing me to conduct research abroad, BEPE, grant 2013/09965-9.

I would like to thank my group colleagues from MFG, IQSC – USP, Tiago Andrade, Carolina Sabatini, Rafael Frederice, Aline Lino, and Anderson Arandas, for the positive learning environment. Special thanks to Carol for her support.

I am also grateful to my colleagues of the Fluorocode group – KU Leuven, with whom I have had the privilege to work with. I would like to thank them for sharing their knowledge with me. They are Charlotte Vranken, Jochem Deen, Kris Janssen, Volker Leen, Sven Van Snick, Jia Su, Su Wang, and Cristina Martín-Álvarez. Special thanks to my friend Sven for his willingness to help me with revising this text and providing me the Dutch abstract.

I would like to give my warmest gratitude to Tiago, for his precious and ongoing support since the first day of my doctorate.

I would like to thank Prof. Robert Neely for patiently mentoring and supervising me during my research stay in Belgium.

Many thanks to Diego Lencione for contributing with all support related to the optical instrumentation at IQSC – USP and for the rich discussions about optics.

Many thanks to the Centre for Instrumental Chemical Analysis, CAQI, from IQSC – USP.

I would like to thank the collaboration of Prof. Carlos Roque Duarte Correia and Roberta Lopes Drekener, from the Institute of Chemistry at UNICAMP, for kindly supplying the compounds investigated in Chapter 2 of this thesis.

I would also like to thank Prof. Albérico B. F. da Silva and Gláucio Nagurniak, from IQSC – USP, for the support with the theoretical calculations.

I would like to thank Willem Vanderlinden and Wout Frederickx, from KU Leuven, for introducing me to the AFM area and for all the support with the measurements.

I would like to thank Susana Rocha, from KU Leuven, for kindly helping me with the cell experiments.

I have a lot to thank to Ann Petré, Karolien Moens, and Carine Jackers for the valuable support in Belgium.

I would like to thank Katholieke Universiteit Leuven and University of São Paulo, represented by Leen Cuypers and Alexandre Mazzola, respectively, for all the efforts concerning the agreement of double doctorate between the involved universities.

I would like to thank Prof. Robert Neely and Prof. Jelle Hendrix for agreeing to act as my assessors at KU Leuven. Also many thanks to Prof. Andrei Leitão and Prof. Maurício Baptista for accepting jury service during my doctoral qualification exam at IQSC – USP.

I am very grateful to Prof. Geovane Lopes de Sena and Prof. Denise Rocco de Sena for having encouraged my scientific career since my Bachelor studies.

I would like to thank my friends Adriel Martins, André Fazolo, Guto Baio, Irlon Maciel, and Ronaldo Fernandes for the friendship over the doctorate years.

Special thanks to my friend-sister Patricia Corradini for the uplifting and pleasant friendship since the Bachelor.

I would also like to take this opportunity to express my greatest gratitude to my family. To my parents Deusa Helmer and Hélio Lauer for supporting me. I am eternally thankful to my grandparents (*in memorian*) Hulda Margarida Espíndula Helmer and Luiz Helmer, who was the great encourager of my education.

ABSTRACT

Fluorescence microscopy is one of the most powerful techniques currently available, since it provides the unique combination of a high sensitivity in detection, a high specificity, and a considerable non-invasiveness. Recent developments have allowed the detection at a sub-diffraction resolution, which elevates its potentiality to investigate several systems and hence to go further in science.

The study of new fluorescent probes is crucial for the application in advanced methods in optical microscopy. In the first extent of this research, Chapter 2, a photophysical study of maleic anhydride and maleimide derivatives, synthesized by the Heck-Matsuda reaction, was performed. Aiming at the improvement of the design of these molecules, a photochemical cyclization was carried out, resulting in molecules with condensed rings, termed as phenanthrene derivatives, which promoted more photochemical stability. The excited state dynamics rely on the push-pull effect, in which a notable, but not complete, charge shift takes place. For the compounds with a 4-hydroxyl substituent, a charge shift combined with an excited state solvent-assisted proton transfer was observed. Additionally, the confocal microscopy study of the phenanthrene derivatives showed that the local properties of the solvent modulate the fluorescence relaxation dynamics in condensed media and hence such dyes can be potential candidates for use in advanced fluorescence microscopy techniques.

The second extent of this thesis, Chapter 3, explores a biological system at the single-molecule level. Specifically, this chapter concerns to an investigation of an optimal sequence-specific DNA fluorescent labelling, using super-resolution fluorescence microscopy. The reactions were performed using a two-step methodology, according to the mTAG approach. In the first step, moieties containing a terminal alkyne, azide, or primary amine group are transferred from an S-adenosyl-L-methionine analogue cofactor to the DNA by a methyltransferase enzyme. Herein, the enzyme M.TaqI was used, which targets the 5’-TCGA -3’ sequence for modification. In the second step, a fluorophore is coupled to the functional sites of the plasmid (pUC19) using bio orthogonal reactions, such as the click reaction catalysed by copper (CuAAC), the copper-free click reaction (SPAAC), and the amino-to-NHS-ester coupling reaction. A direct one-step approach in which the fluorophore is directly transferred to the DNA from the analogue cofactor in a single reaction step, was also developed.

A single-molecule assay was developed for counting the number of fluorophores associated with the individual plasmids. The topology of the plasmids after labelling was also

investigated by high-resolution AFM imaging. Combining both analysis, the SPAAC as well as the direct one-step reactions were found to promote near-complete labelling and the AFM showed that the fluorophore coupling did not damage the structure of the plasmids and that their native, supercoiled, morphology was preserved. Moreover, labelled plasmids were successfully applied for transfection into mammalian cells, implying that the DNA retained its ability to encode genetic information, even while carrying bound fluorophores.

Keywords: maleic anhydride, push-pull, single-molecule microscopy, DNA, AFM.

RESUMO

A microscopia de fluorescência é uma das técnicas mais poderosas disponíveis atualmente, uma vez que proporciona uma combinação excepcional de alta sensibilidade na detecção, alta especificidade, além de ser consideravelmente não invasiva. Avanços recentes permitiram a detecção em resolução de subdifração, o que eleva sua potencialidade de investigação de um maior número de sistemas e, consequentemente, de avanço científico.

O estudo de novas sondas fluorescentes é de fundamental importância para a aplicação em métodos avançados de microscopia óptica. Na primeira vertente da pesquisa, Capítulo 2, foi realizado o estudo fotofísico de uma série de compostos bisarilados derivados do anidrido maleico e de maleimidas sintetizados pela reação de Heck-Matsuda. Visando o aprimoramento do design dessas moléculas, foi realizada a ciclização fotoquímica de tais compostos, resultando em moléculas com anéis condensados, nomeados como derivados de fenantreno, as quais proporcionaram maior estabilidade fotoquímica. A dinâmica do estado excitado remete ao efeito *push-pull*, em que há um deslocamento de carga notável, mas não completo. Para os compostos com a substituição 4-hidroxifenil foi observado um processo de deslocamento de carga combinado com uma transferência de próton no estado excitado assistida por solvente. Ademais, o estudo dos compostos derivados de fenantreno em microscopia confocal demonstrou que as propriedades locais do solvente afetam a dinâmica de relaxação de fluorescência em diferentes meios condensados e que os mesmos são passíveis de serem aplicados a técnicas avançadas de microscopia de fluorescência.

A segunda vertente desta tese, Capítulo 3, explora um sistema biológico em nível de uma única molécula. Especificamente, este capítulo concerne à investigação de uma metodologia ótima para a marcação fluorescente de DNA em sequência específica, através de microscopia de fluorescência com super-resolução. As reações foram conduzidas utilizando uma metodologia de marcação de duas etapas, de acordo com o princípio mTAG. Na primeira etapa, grupamentos contendo alquino terminal, azida ou amina primária são transferidos do cofator análogo ao S-adenosil-L-metionina para o DNA através de uma enzima metiltransferase. Foi utilizada a enzima M.TaqI, a qual tem como alvo a sequência 5’- TGCA -3’ para modificação. Na segunda etapa é realizado o acoplamento do fluoróforo aos sítios funcionais do plasmídeo (pUC19) através de reações químicas bioortogonais, tais como reação *click* catalisada por cobre (CuAAC), reação *click* na ausência de cobre (SPAAC) e acoplamento do grupo amina primária com NHS-éster. Também foi desenvolvida

uma metodologia direta de uma etapa, na qual o fluoróforo é diretamente transferido do cofator análogo para o DNA em uma única etapa reacional.

Para acompanhar o desempenho das reações foi desenvolvido um ensaio *single-molecule* para a contagem do número de moléculas de corante ligadas a plasmídeos individuais. A topologia dos plasmídeos após a marcação foi investigada por imagens de AFM em alta resolução. A combinação de ambas as análises demonstrou que a reação SPAAC assim como a reação direta de uma etapa promoveram uma marcação fluorescente quase completa e a técnica de AFM confirmou que o acoplamento de fluoróforos não induziu danos à estrutura dos plasmídeos, os quais preservaram sua morfologia nativa, superenrolada. Além disso, os plasmídeos marcados foram aplicados com sucesso a procedimentos de transfecção em células de mamíferos, indicando que o DNA reteve sua capacidade de codificar informação genética, mesmo na presença de fluoróforos ligados.

Palavras-chave: anidrido maleico, *push-pull*, microscopia *single-molecule*, DNA, AFM

SAMENVATTING

Fluorescentiemicroscopie is momenteel verruit de meest krachtige, niet-invasieve optische microscooptechniek beschikbaar, welke een hoge detectiegevoeligheid en hoge specificiteit combineert. Recente ontwikkelingen aangaande deze techniek maken het mogelijk om structuren kleiner dan de diffractielimiet met hoge resolutie te visualiseren. Deze zogenaamde hoge resolutie fluorescentiemicroscopie vormt aldus een belangrijke uitbreiding van het arsenaal aan methodes en technieken om kleine systemen te onderzoeken.

De studie van nieuwe fluorescente *probes* is cruciaal voor hun toepassing in geavanceerde methodes voor optische microscopie. Het eerste deel van dit onderzoeksproject wordt uiteengezet in hoofdstuk 2 en omvat de fotofysische studie van maleïnezuuranhydride en maleïmide derivaten, gesynthetiseerd via de Heck-Matsuda reactie. Teneinde de fotochemische stabiliteit van deze moleculen te verbeteren werd een fotochemische cyclisatie uitgevoerd, resulterend in systemen met gecondenseerde ringen (fenantreen derivaten). De moleculaire dynamica van de geëxciteerde toestanden wordt bepaald door het *push-pull*-effect, waarbij een aanzienlijke, maar geen volledige ladingsverschuiving plaatsvindt. Voor de verbindingen met een 4-hydroxyl substituent werd een ladingsverschuiving en een slovengeassisteerde proton transfer waargenomen. Daarenboven heeft de studie van fenantreen derivaten met behulp van confocale microscopie aangetoond dat solventeigenschappen de fluorescentie relaxatie dynamica van gecondenseerde media moduleert. Dergelijke kleurstoffen zijn bijgevolg potentiële kandidaten voor gebruik in geavanceerde fluorescentie microscopie.

Het tweede deel van dit onderzoeksproject wordt besproken in hoofdstuk 3 en behandelt de analyse van een biologisch systeem op *single-molecule* niveau. Meerbepaald wordt in dit hoofdstuk het onderzoek naar een optimale, sequentiespecifieke DNA fluorescente labeling, met behulp van hoge resolutie fluorescentiemicroscopie, uiteengezet. Om dit te bewerkstelligen worden reacties uitgevoerd gebruik makende van een twee-staps-methodologie volgens de mTAG-benadering. In de eerste stap worden met behulp van een methyltransferase enzym functionaliteiten waaronder alkynen, azides of primaire amines getransfereerd van een S-adenosyl-L-methionine analoog naar DNA. Het hiervoor aangewende enzym, M.TaqI, herkent de 5'-TCGA-3' sequentie voor modificatie. In de tweede stap wordt een fluorofoor gekoppeld aan de functionele sites van het plasmide (pUC19) via bio orthogonale reacties, waaronder de koper-gekatalyseerde click-reactie (CuAAC), de kopervrije click-reactie (SPAAC) en de amino-NHS-ester koppeling reactie. Een

rechtstreekse, één-stap-methode, waarbij het fluorofoor rechtstreeks getransfereerd wordt van het cofactor analoog naar het DNA, werd eveneens ontwikkeld.

Tot slot werd een *single-molecule* essay ontwikkeld welke toelaat het aantal fluoroforen geassocieerd met individuele plasmiden te tellen. De topologie van de plasmiden na labeling werd onderzocht met behulp van hoge resolutie AFM beeldvorming. Door combinatie van de analysegegevens verkregen via deze twee technieken werd een nagenoeg complete labeling vastgesteld voor zowel de SPAAC, als de rechtstreekse één-stap-methode, daarenboven toonde de AFM-studie aan dat de koppeling van de fluoroforen met de plasmiden de structuur van laatstgenoemden niet beschadigd. De gelabelde plasmiden werden gebruikt voor de transfectie naar cellen van zoogdieren, wat impliceert dat het DNA zijn coderende eigenschappen niet verliest, ook al bevat het fluoroforen.

Kernwoorden: maleïnezuuranhydride, *push-pull*, *single-molecule* microscopie, DNA, AFM.

LIST OF FIGURES

LIST OF TABLES

LIST OF ABBREVIATIONS

AdoHcy	S-adenosine-L-homocysteine
AdoMet	S-adenosyl-L-methionine
AFM	Atomic force microscopy
APD	Avalanche photodiode
AU	Arbitrary unit
BALM	Binding-activated localization microscopy
BARAC	Biarylazacyclooctynone
BODIPY	refers to a family of dyes based on 4,4-difluoro-4-bora-3a,4a-diaza-s-indacene
BS	Beam splitter
BSA	Bovine serum albumin
CCD	Charged coupled device
CU	Control unit
CuAAC	Copper-catalysed azide-alkyne cycloaddition
CW	Continuous wave
DAPI	4',6-diamidino-2-phenylindole
DF	Dichroic filter
DFT	Density functional theory
DIBO	Di-benzo-cyclooctyne
DIFO	Difluorinated cyclooctynes
DiI	1,1′-dioctadecyl-3,3,3′,3′-tetramethylindocarbocyanine perchlorate
DMANS	*p*-dimethylamino-4-nitro-stilbene
DMEM	Dulbecco's modified eagle's medium
DMF	Dimethylformamide
DMSO	Dimethylsulphoxide
DNA	Deoxyribonucleic acid
dsDNA	Double-stranded DNA
dSTORM	Direct stochastic optical reconstruction microscopy
EDTA	Ethylenediaminetetraacetic acid
EdU	5-ethynyl-2'-deoxyuridine
EM-CCD	Electron multiplying charge-coupled device
EXP	Beam expander
FBS	Fetal bovine serum
FCS	Fluorescence correlation spectroscopy

FISH	Fluorescence *in situ* hybridization
fPALM	Fluorescence photoactivation localization microscopy
GFP	Green fluorescent protein
HOMO	Highest occupied molecular orbital
HPLC	High-performance liquid chromatography
IC	Internal conversion
ICT	Intramolecular charge-transfer
IR	Iris
irf	Instrumental response function
ISC	Intersystem crossing
L	Lens
LPF	Low-pass filter
LUMO	Lowest unoccupied molecular orbital
M	Mirror
MEA	β-mercaptoethylamine
MM	Mobile mirror
mTAG	Methyltransferase-directed transfer of activated groups
MTase	Methyltransferase
MTC	Methyltransferase cofactor
NA	Numerical aperture
NF	Notch filter
NHS	N-hydroxysuccinimide
NLC	Non-linear crystal
OB	Objective
OF	Optical fibre
PA	Piezoelectric stage
PA-FP	Photoactivatable fluorescent proteins
PAINT	Point accumulation for imaging in nanoscale topography
PALM	Photoactivation localization microscopy
PALMIRA	Photoactivation localization microscopy with independently running acquisition
PBS	Phosphate buffered saline
Pbs	Prism beam splitter
PH	Pinhole
PLL	Poly-L-lysine
MCP-PMT	Microchannel plate photomultiplier tube
PP	Pulse picker

PSF	Point-spread function
PVP	Polyvinylpyrrolidone
RNA	Ribonucleic acid
ROS	Reactive oxygen species
S	Sample
SD	Silicon detector
SDS	Sodium dodecyl sulphate
SPAAC	Strain-promoted azide-alkyne cycloaddition
SSC	Saline-sodium citrate
STED	Stimulated-emission depletion
STORM	Stochastic optical reconstruction microscopy
TBTA	Tris(benzyltriazolylmethyl)-amine
TCSPC	Time-correlated single-photon counting
THF	Tetrahydrofuran
THPTA	Tris[(1-hydroxypropyl-1H-1,2,3-triazol-4-yl)methyl]amine
TIRF	Total internal reflection fluorescence
Tris	Tris(hydroxymethyl)aminomethane
TTL	Transistor-transistor logic
UV	Ultraviolet
WP	Wave plate
YFP	Yellow fluorescent protein

CONTENTS

CHAPTER 1

Fundamentals of the research

1 BASIC PRINCIPLES OF FLUORESCENCE

The central topic of this thesis is the study of the emission properties of fluorophores by fluorescence spectroscopy and imaging. When a fluorophore absorbs a photon of the appropriate wavelength, an electron is excited to a higher energy state and, subsequently, the molecule relaxes to the ground state, releasing energy as an emitted photon of a different wavelength.[1]

The absorption of light can be mathematically described by the Lambert-Beer Law. This law states that the amount of light absorbed is proportional the concentration of the absorbing molecules (c), the optical path length (ℓ), that is the distance the light travels through the sample, and the extinction coefficient of the substance (ε).[2; 3] The resulting absorption can thus be defined by the following equation, where A is the absorbance.

$$A = c\ell\varepsilon \tag{1}$$

The light absorption is a very fast transition which occurs in about 10^{-15} s and it is considered as an instantaneous process. This time is considered too short for any notable displacement of the nuclei, a finding which is called the Franck-Condon principle.[4]

Upon light absorption, several processes may take place. To follow the different relaxation processes, a scheme of the energy levels, Jablonski diagram, of a dye molecule is depicted in Figure 1. It is worth mentioning that the electronic states of dye molecules are usually classified in singlet (S) and triplet states (T), depending on the different spin states of the excited electron.[1] In the singlet state, the electron spins in the relevant molecular orbital are antiparallel, while in the triplet state the spins are parallel. In the following Jablonski diagram, the bold horizontal lines represent the electronic states and the thin horizontal lines the vibrational energy states.

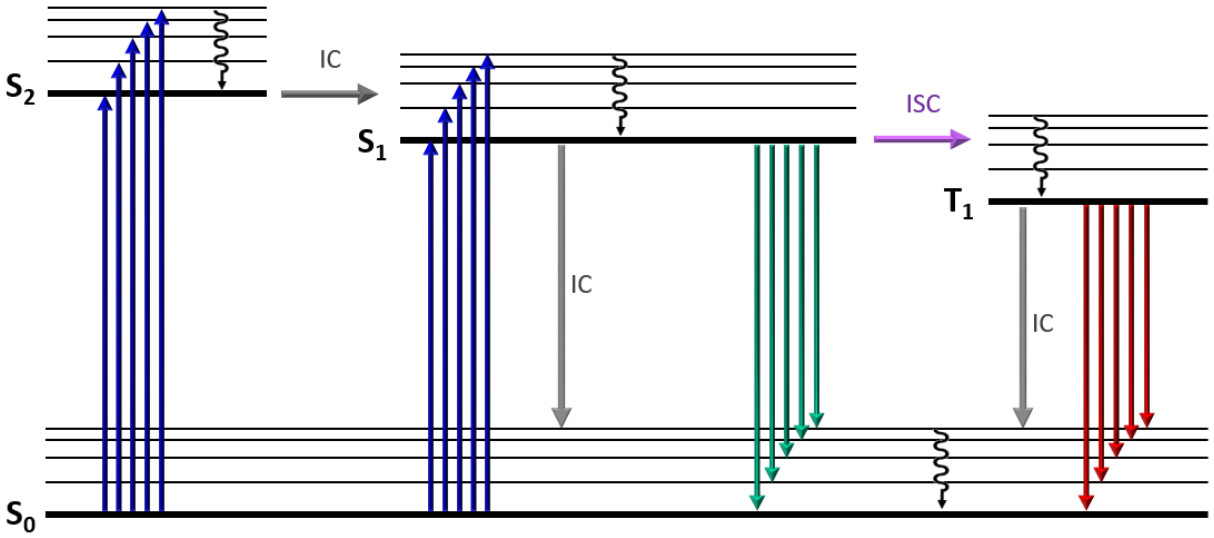

Figure 1. Scheme of the Jablonski diagram. The blue arrows indicate the absorption of light, the green arrows indicate the fluorescence emission, and the red arrows indicate the phosphorescence relaxation. The black arrows indicate the vibrational relaxation. IC represents the internal conversion and ISC represents the intersystem crossing. Adapted from references.[3; 4]

At room temperature, thermal energy alone is not enough to populate the excited vibrational states. Thus, the fluorophores are mostly excited from their lowest vibrational energy level, the ground state (S_0). Upon light absorption, the molecule is excited to higher excited singlet states, S_1 or S_2. Subsequently, in general the molecules relax to the lowest vibrational level from the first excited singlet state (S_1), by a non-radiative vibrational relaxation process, in a time scale of about 10^{-12} s.[3] At this point, at the lowest vibrational level of S_1, the molecule can relax to S_0 by different pathways. The depopulation of the state S_1 to a vibrational level of the ground state S_0 is a radiative spontaneous process, characterized by the emission of a fluorescence photon, occurring in about 10^{-9} to 10^{-7} s.[3]

The relaxation to the ground state may also take place *via* a non-radiative process, named internal conversion (IC). This transition of the same multiplicity ($S_1 \rightarrow S_0$) occurs typically on a timescale of 10^{-7} to 10^{-6} s.[3]

Molecules may also depopulate the S_1 state *via* a relaxation to the first triplet state (T_1), termed intersystem crossing (ISC). The radiative decay of the transition $T_1 \rightarrow S_0$, called phosphorescence, is a less probable process because it is spin-forbidden.[4] Hence, the rate constants for triplet emission are much smaller than those for fluorescence, presenting a timescale of 10^{-3} to 100 s.[5]

2 FLUORESCENCE MICROSCOPY

Fluorescence microscopy has been one of the most useful techniques utilized nowadays, since it has the potentiality to investigate several systems, with the advantages of its unique combination of high-sensitivity in detection, high specificity, and relative non-invasiveness.[6; 7; 8] Recent developments have allowed single-molecule detection, which provide an accurate study of biological events[9] and dynamics of polymeric systems.[8]

Fluorescence microscopy can be performed according to the necessity of the system studied. The most widely used fluorescence microscopy modes are the confocal and the wide field. Taking into account the confocal microscopy from an instrumentation point of view, the objective lens focuses the collimated laser beam to a diffraction-limited spot at the sample plane. The fluorescence emission originated by a dye molecule that passes through the confocal volume, as well as the backscattered laser light, are collected by the same objective and pass through the dichroic beam splitter. Subsequently, the fluorescence light passes by appropriate filters and it is focused through a pinhole aperture. This is the key advantage of the confocal microscopy, because the fluorescence background and out-of-focal-plane light are rejected, improving the axial resolution. After passing through a pinhole, the fluorescence emission of the dye can be imaged by a point detector, like an avalanche photodiode (APD).[8; 10] The confocal microscopy has enabled the collection and reconstruction of three-dimensional data, which is useful for the study of living systems.[11] It is worth mentioning that the confocal approach is used for fluorescence correlation spectroscopy (FCS) experiments. A schematic illustration of the confocal microscopy is shown in Figure 2.

Opposite to the confocal approach, the wide field microscopy is a technique that may provide both topographical and dynamic information. In this mode, a large extension of the sample (several microns in diameter) may be simultaneously illuminated, as illustrated in Figure 2. Using appropriate filters and optical systems, the excitation light is neglected and the fluorescence emission of the dyes near to the objective focal plane is imaged in a two-dimensional array detector, usually a CCD.[10] The advantages of the wide field mode are the possibility to image single fluorophores simultaneously, as well as the possibility to monitor their positions.[10] Moreover, wide field microscopes allow working with total internal reflection illumination, as documented *a posteriori*.

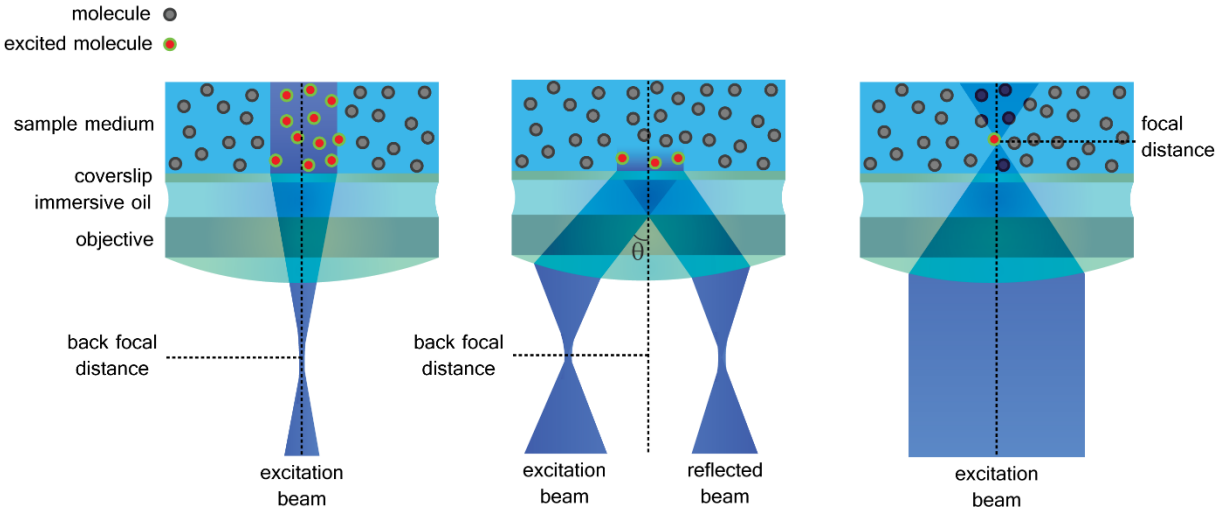

Figure 2. Comparative schematic illustration of the excitation modes of wide field (left), wide field in TIRF mode (middle), and confocal (right) microscopies. The red spots represent the excited dye molecules and the grey spots represent the ensemble dye molecules in the sample.[12]

2.1 Total internal reflexion fluorescence microscopy (TIRFM)

The wide field microscopy has the disadvantage of illuminating fluorescent molecules with a broad cone of light. Thus, the limited spatial resolution, mainly along the optical axis, makes it difficult to differentiate between the individual sample details, intensified by background fluorescence from outside the focal plane. Therefore, if the out-of-focus signal is eliminated, the signal-to-background ratio is greatly improved, and consequently, the spatial resolution of the structures of interest.[13; 14]

To overcome this disadvantage, one can make use of the technique called Total Internal Reflection Fluorescence Microscopy (TIRFM), which employs the unique properties of an induced evanescent wave to selectively illuminate and excite fluorophores in a restricted region immediately adjacent to the interface between the coverslip and the sample media (typically 100 nm).[1; 14] Another advantage of TIRFM is the reduction of the photodamage, since the excitation beam is reflected and does not cross the whole sample. This technique is commonly used for the study of cell signalling events, membrane-associated molecules, and even for imaging of individual fluorescent molecules.[1] A scheme of this microscopy mode is depicted in Figure 2.

The physical concept of TIRFM is based on Snell's Law. When a light beam propagating through a medium of refractive index n_1 (e.g. glass coverslip) meets an interface with a

second medium of refractive index $n_2 < n_1$ (e.g. a sample attached to the surface), beams are totally internally reflected back into the first medium at all angles of incidence θ which are greater than a critical angle θc.[1] The critical angle of incidence is obtained from:

$$n_1 \sin \theta_1 = n_2 \sin \theta_2 \quad (2)$$

The angles θ are the angles subtended by the incident and transmitted rays relative to the normal at the interface. Considering two transparent media, where n1 > n2, if the transmitted ray is 90°, the ray travels along the interface. Then, the critical angle can be calculated setting the angle θ_2 in the second medium to 90°, as follows:

$$\theta c = \sin^{-1}(n_2/n_1) \quad (3)$$

Therefore, at angles smaller than θc, rays are refracted and enter the second medium and at angles greater than θc, rays experience total internal reflection.[1] However, it is necessary taking into account the Fresnel coefficients, which determines the amount of radiation that is transmitted and reflected in the optical interface as a function of the state of polarization (s- and p-polarizations) of the excitation beam, as well as the angle of incidence.

Despite being totally reflected under TIR conditions, the incident beam establishes an evanescent wave at the interface. The electric field of this evanescent wave penetrates into the second medium and decays exponentially with the distance z from the interface. The intensity of the evanescent wave at a depth z, I_z, from the interface is:[1]

$$I_z = I_0 \, e^{-(z/d)} \quad (4)$$

Where I_0 and I_z are the light intensities at the coverslip surface at a perpendicular distance z. In this equation, d is the penetration depth, which depends on the refractive indices of the two media, the critical angle of incident light beam, and the wavelength as follows:

$$d = (\lambda/4\pi) \, (\sin^2 \theta - \sin^2 \theta c)^{-1/2} \quad (5)$$

As a result, utilizing this mode of illumination for fluorescence microscopy, only the fluorophores placed within about 100 nm from the coverslip surface can be excited by that field and emit photons into the second medium.[1] Because of such principle, the fluorescence images provided by TIRFM present a better resolution and contrast, when compared with those obtained from confocal and wide field modes.

Due to the aforementioned advantages of the TIRF microscopy, such as the minimization of the background fluorescence, this fluorescence microscopy configuration has been suitable

for the detection of emission from single molecules. Therefore, TIRFM was vastly employed in this research for the super-resolution purposes described in Chapter 3.

2.2 Super-resolution in fluorescence microscopy

One of the challenges involved with fluorescence microscopy techniques is the light diffraction limit, which provides a low spatial resolution. Abbe has postulated that optical microscopes can not resolve species that are closer together than approximately half the wavelength of the light (~λ/2),[15] therefore, the limit resolution for visible light is around 200 to 300 nm in lateral dimensions and in the range of 500 to 700 nm in axial direction.[3; 7] The optical resolution limit can be treated in terms of the point-spreading function (PSF), which takes into account the response of an imaging system to a point emitter.[3] In other words, focusing light by a microscope objective, the rays are not converted to a sharp focal point. Instead, they form a blurred focal spot, with finite dimensions, due to the immutable wave character of light. Due to the diffraction of light, the fluorescent signal of the emitter generates an Airy pattern in the image plane,[3] which can be defined by a brighter central spot surrounded by a series of diffraction rings.[1] The size of the blurred spot depends on the wavelength (λ) as well as on the numerical aperture (NA) of the objective. In a good approximation, the width of the spot is defined to approximately 0.6λ/NA.[9] Considering the PSF definition, if two emitters are place in a distance lower than the width of the PSF, they will be imaged as a single object, and hence, the two objects are unresolvable from each other.

Such spatial resolution does not allow, for instance, the distinction between two close fluorophores, and the resolution of cellular components. However, several recent advances have overcome the diffraction limit, providing spatial resolutions of about tens of nanometres, such as 20 to 30 nm in lateral and 50 to 60 nm in axial dimensions.[16] The set of methods that promote the breaking through the diffraction barrier are named super-resolution techniques. They operate by introducing nonlinear effects to sharpen the point-spread function,[7] such as the *Stimulated-Emission Depletion* (STED),[17] or localizing single fluorescent molecules based on their photoswitching or photoactivation properties,[6] such as *Photoactivation Localization Microscopy* (PALM),[18] *Fluorescence Photoactivation Localization Microscopy* (fPALM),[19] and *Stochastic Optical Reconstruction Microscopy* (STORM).[20]

2.2.1 Stimulated emission depletion

The stimulated-emission depletion microscopy was firstly published by Hell and co-workers in 1994.[17] In this technique, two lasers illuminating the focus are used, one for excitation and another for stimulated depletion. Firstly, a laser pulse (Airy mode) with a duration of picoseconds or less excites the sample molecules. Then, the second laser, operating in a special toroid module (donut), irradiates the same region, introducing the stimulated emission of the dye molecules placed in the toroid region, not of those situated in the centre of the focus. This effect occurs because of the distribution of the donut laser intensity.

Thus, there is a suppression of the fluorescence emission from the molecules placed in the donut region, which results in the signal acquisition of a region with dimensions under the diffraction limit. The generated images have a higher resolution in comparison to confocal microscopy, achieving a resolution of a few tens of nanometres.[6; 7]

2.2.2 Single-molecule localization microscopy

Single-molecule localization techniques take into account the precise position determination of fluorophores in a sample. In conventional wide field images, the main reason for the limitation of spatial resolution is the overlap of the fluorescent spots on the camera.[21] Thus, for achieving a sub-diffraction resolution image, it is necessary to separate the fluorophore emission in time. This can be performed if the population of molecules between the fluorescent and the non-fluorescent states is controlled over time.[6] Because of that, the fluorophores employed in such technique should have photoswitchable or photoactivatable character. The photoswitchable emitters can populate both the fluorescent (on) and non-fluorescent (off) states and the interconversion between the states can be reversibly controlled by light. Another condition to control this interconversion is the nano environment of the fluorophore. In contrast, the photoactivatable fluorophores are initially in the non-fluorescent state, but they can be converted to the fluorescent state upon excitation with an appropriate source of light.[3; 6]

To perform single-molecule localization microscopies, a structure of interest is densely labelled with fluorophores containing the photoactivatable or the photoswitchable character, and are initially in the non-fluorescent state. The sample is then weakly irradiated, so that only a sparse subset of molecules are allowed to fluoresce at any time. At this stage, it is necessary to ensure that each fluorophore is optically resolvable from the other. The emitting molecules are imaged, until they deactivate by photoswitching or by photobleaching

processes. Then, the positions of the fluorophores are precisely determined, and their locations are precisely determined. Subsequently, a unique subset of stochastically activated fluorophores is imaged and localized. This kind of cycle is recursively repeated and the ensemble of localized positions of the molecules can reconstruct a super-resolution image.[3; 6; 22]

The data are commonly acquired by an electron multiplying charge-coupled device, EMCCD camera, from a wide field setup operating in TIRF mode, in which the fluorescence emission is confined to a 100 nm region from the interface, eliminating background signals along the z-axis. The localization of the single molecules is performed by fitting the PSF to a Gaussian function. To this end, the PSF is represented in 2D and 3D diagrams. Then, the single-molecule localizations are determined by the centroid of the Gaussian profile, as illustrated in Figure 3.[1; 22]

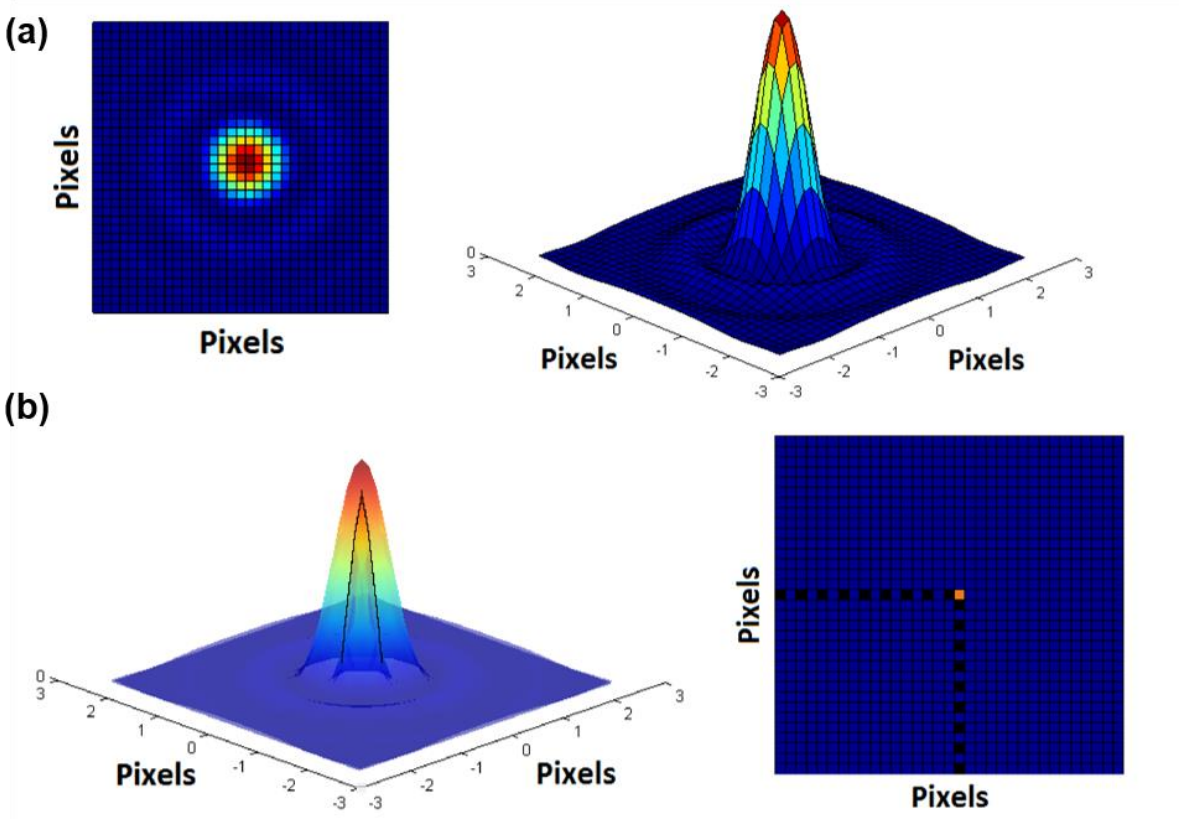

Figure 3. Schematic illustration of data analysis for single-molecule localization microscopy. In (a), the PSF of a single emitter is represented in a 2D and in a 3D diagram. Scheme (b) shows the 3D Gaussian representation of the data captured by an EM-CCD and the localized position of a single emitter established by the centroid of the Gaussian profile.[12]

This principle of single fluorescent molecules localization based on the stochastic activation of photoswitchable and photoactivatable fluorophores is used for the following related techniques.

2.2.2.1 Photoactivation localization microscopy (PALM)

This technique was pioneered by Betzig and co-workers in 2006,[18] using photoactivatable fluorescent proteins (PA-FP). In this work, the authors reported the visualization of intracellular structures, such as sections of lysosomes and mitochondria, and vinculin and actin in fixed whole cells.[18] Some photoactivatable fluorescent protein variants are the monomeric and dimeric Eos, mEos, and tdEos, Drompa fluorescent protein, PA-GFP, and PA-mCherry1.[1] The related technique Fluorescence Photoactivation Localization Microscopy (fPALM) was also introduced in 2006, by Hess and co-workers. The method reported the localization of PA-GFP single molecules.[19] Another technique is called PALMIRA, an acronym for PALM with Independently Running Acquisition. This approach, performed in 2007 by Egner and co-workers,[23] shows the advantage of super-resolution imaging at fast recording speeds. In this case, the camera runs without synchronization of the activation laser or the switching cycles of the fluorescent probes, also PA-FPs.[1] This the method reduced the background, which allowed the visualization of the interior of intact cells.[23]

2.2.2.2 Stochastic optical reconstruction microscopy (STORM)

This method concerns to the use of organic photoswitchable dyes. Zhuang and co-workers firstly reported the STORM method in 2006, using the photoswitchable cyanine pair Cy3-Cy5 for double-stranded DNA labelling, reaching an image resolution of 20 nm.[20] The pair Cy3-Cy5 is a cyanine switch. Initially, Cy5 molecules populate the non-fluorescent state. However, dark Cy5 can be activated with 532 nm light, when it is close to Cy3, which converts Cy5 to the fluorescent state. When Cy5 is in the fluorescent form, it can be excited with 633 nm, 647 nm, or 657 nm light sources.[1] In the original report, the linear double-stranded DNA was surface-immobilized and poorly labelled, so that the single switches could be resolvable. The switches were placed in a well-defined position of 135 base pairs from one another, which corresponds to the length of 46 nm along the DNA contour. The switches were turned on and off using the excitation by green and red lasers and the molecule Cy5 was excited at 633 nm. The periodical cycles of stochastically excitation of a small subset of

molecules, return to the off state, and localization provided images in quantitative agreement with the distance between the fluorophores along the DNA molecule. Such results opened the doors to the use of the STORM method as a valuable tool for biological imaging, like for fluorescence *in situ* hybridization and immunofluorescence imaging.[20]

Heilemann and co-workers introduced a related technique in 2008,[16] in which photoswitchable fluorophores, such as Cy5, Alexa 647, and Atto-dyes,[1] can be interconverted between the fluorescent and the non-fluorescent states without the use of an activator fluorophore, as in the case of the pair Cy3-Cy5.[16] In the technique, termed Direct Stochastic Optical Reconstruction Microscopy (dSTORM), the reversible interconversion between the on and off states occurs by irradiation with a single laser, in the presence of reducing reagents.[1] The standard fluorophores, which mostly belong to the class of rhodamine and oxazine dyes, are photoreduced upon irradiation in the presence of electron donor molecules, such as aromatic amines and thiols, for instance β-mercaptoethylamine (MEA).[24] The photoswitching character is also improved under conditions of oxygen depletion, thus, the application of an enzymatic oxygen scavenger system is convenient for this methodology.[24]

3 BIOLOGICAL EXTENT

3.1 DNA structure

Deoxyribonucleic acid (DNA) is a polymeric biomolecule composed of building blocks termed nucleotides. These monomeric units contain three primary components, a phosphate group, a pentose (deoxyribose), and a nitrogenous base derivative from the pyrimidine class, cytosine (C) and thymine (T), or from the purine class, adenine (A) and guanine (G). The structures and the numbering convention of the nitrogenous bases as well as the sugar-phosphate backbone are represented in Figure 4.[25]

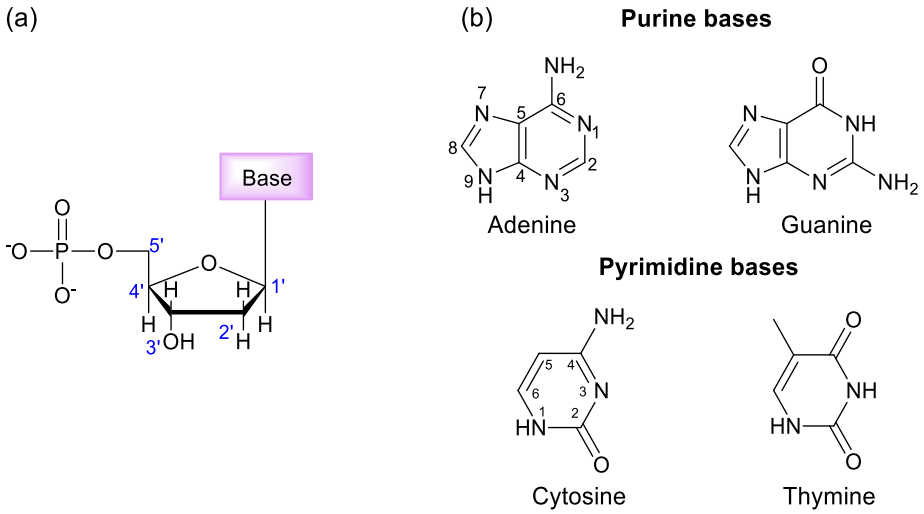

Figure 4. (a) General structure of a nucleotide containing the numbering convention for the pentose. (b) Structure and numbering convention for the purine and pyrimidine bases. Adapted from reference.[25]

The nucleotide unit is joined by an *N*-β-glycosyl covalent bond between the C1' of the pentose and the N1 of pyrimidines or N9 of purines. The phosphate group is esterified to the C5' of the pentose. Successive nucleotides are propagated by a covalent phosphodiester linkage, which joins the 5'- phosphate group of one nucleotide unit to the 3'- hydroxyl group of the next nucleotide unit.[25]

The chemical properties of the purines and pyrimidines are crucial for the establishment of the nucleic acids structure. They are weakly basic and highly conjugated. Furthermore, the resonance in the rings result in double bond characteristics. As a result, the pyrimidines are planar and the purines are nearly planar. These features in combination with the hydrophobicity in water, privilege the base-stacking interactions, as illustrated in Figure 5, and are governed by the van der Waals and dipole-dipole interactions. Besides, the stacking interactions between the bases minimizes the contact with water and stabilizes the three-dimensional DNA structure.[25]

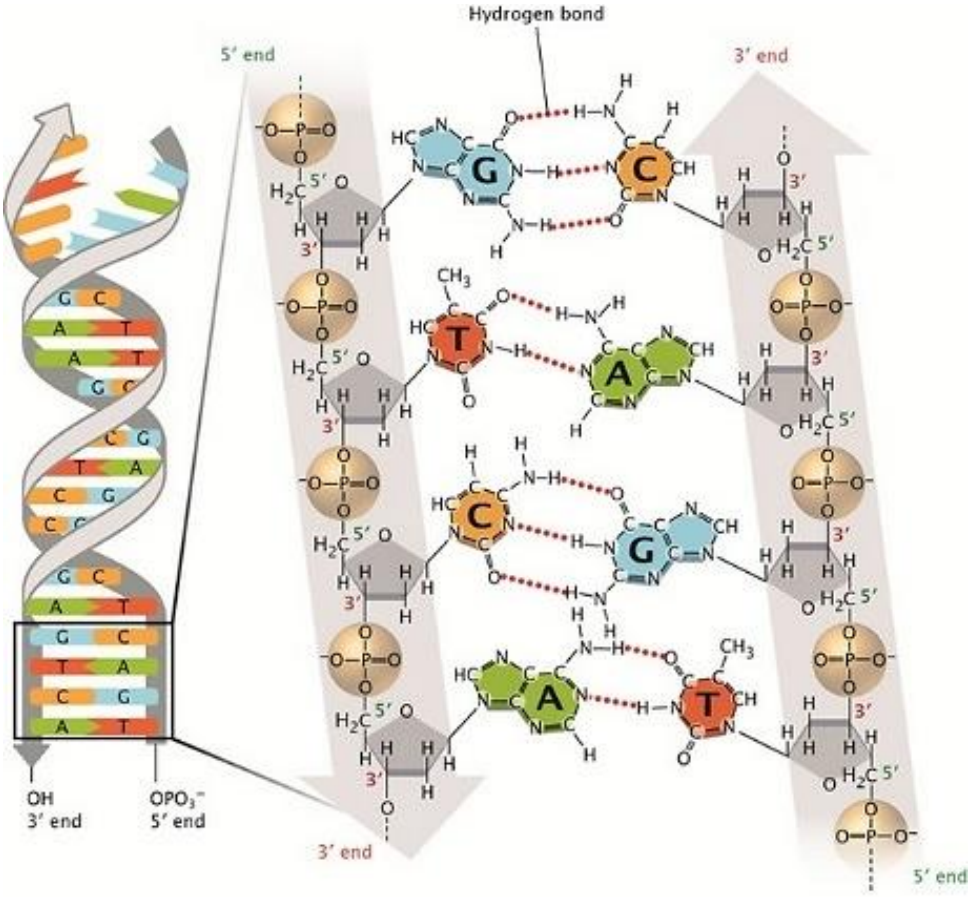

Figure 5. Scheme of the three-dimensional structure of DNA. The zoomed detail shows the base pairing, occurring two hydrogen bonds to associate the bases T and A, and three hydrogen bonds to associate G and C. The sugar-phosphate backbone are represented in grey. Illustration reproduced from the literature.[26]

Watson and Crick reported in 1953 important hydrogen-bonding patterns between the nitrogenous bases, which allow the complementary association of two strands of nucleic acid. In this study, the authors defined that the base adenine specifically bonds to the base thymine, while guanine specifically bonds to cytosine.[27] The three-dimensional structure of DNA was described as two helical chains coiled round the same axis, where the chains are composed by the sugar and the phosphate groups.[27] The resulting hydrophilic backbone is oriented to the outside of the double helix and the purine and pyrimidine bases of both strands are stacked inside the double helix, perpendicular to the long axis. The pairing of both strands causes a major and a minor groove on the nucleic acid surface.[25] The 3D DNA structure is represented in Figure 5. Additionally, the x-ray diffraction works of Franklin[28] and Wilkins[29] corroborated to the Watson and Crick's model. According to them, DNA molecules are helical and show two periodicities, the primary one of 3.4 Å, which represents the

distance between two adjacent base pairs in a single strand, and the secondary one of 34 Å, or 10 base pairs, which represents a complete turn of the DNA helix.[25]

3.2 DNA labelling

The rich structure of the DNA molecule allows the fluorescent labelling by different manners. There are the non-covalent interactions, such as major and minor groove binding, intercalation, and electrostatic interactions with the sugar-phosphate backbone, as well as the labelling performed by covalent bonds, which can take place at the nitrogenous bases or at the phosphate groups.

The groove binders do not promote large conformational changes to the double helix structure of the DNA. Such binders are usually crescent-shaped molecules that bind to the minor groove of DNA.[30] The minor groove binding is stabilized by a combination of electrostatic, van der Waals, and hydrogen bonding interactions, mainly near regions containing the base pair AT. On the other hand, the major groove binding is mostly stabilized by electrostatic interactions.[31] Some classic minor groove dyes are the indoles and imidazoles, such as the Hoechst dyes. Another example is the dye DAPI, which also associates with the minor groove, preferentially binding to AT regions.[32]

The intercalation binding is characterized by the insertion of a planar molecule between the adjacent base pairs of the DNA double helix.[30] The stabilization of this binding is performed by non-covalent π-stacking interactions between the intercalating molecule and the adjacent base pair. Often, hydrogen bonding also provides extra stabilization.[31] In general, the intercalation agents are molecules containing fused bi- or tricyclic ring structures and are positively charged. Thus, an additional stabilization originates from the ionic interaction between the agent and the negatively charged phosphate DNA backbone.[31; 33]

The intercalation induces a conformational change in the DNA so that it can generate an intercalation cavity. A model for intercalation binding was proposed by Chaires.[34] Briefly, in a first step, DNA base pairs separate to form a cavity in which the intercalating dye will be fitted. Subsequently, the intercalator migrates from the solution to the intercalation site, which is a hydrophobic transfer process. Finally, several molecular interactions may occur to stabilize the DNA-intercalator complex.[34]

The phenanthridines and acridines are classic intercalating dyes. Some examples are ethidium bromide, propidium iodide, and acridine orange.[32] Moreover, a class of compounds

that has attracted a great deal of attention are the cyanine dimer dyes, because they present a high sensitivity for nucleic acid staining. Some examples are YOYO-1, TOTO-1, POPO-1, YOYO-3, TOTO-3.[32] The remarkable properties of these dyes for DNA labelling have allowed several studies at the single-molecule level.

One of the most used dimeric cyanine dye for DNA staining is YOYO-1. Its structure is illustrated in Figure 6. This dye is commercially available and has a quantum yield of 0.52 and molar extinction coefficient, ε_{491}, of 98900 $M^{-1}cm^{-1}$ (when bound to dsDNA).[32] In solution, the fluorescence emission of YOYO-1 is quenched by the internal rotational motion. However, upon intercalation into the DNA duplex, the chromophores are immobilized and the fluorescence is greatly enhanced, with an 800-fold increase of the quantum yield,[35] and a 460-fold increase of brightness.[36] The dynamics and binding modes of YOYO-1 in DNA are reported in the literature.[33] Figure 6 (a-d) shows a scheme of the binding states of YOYO-1 in DNA.

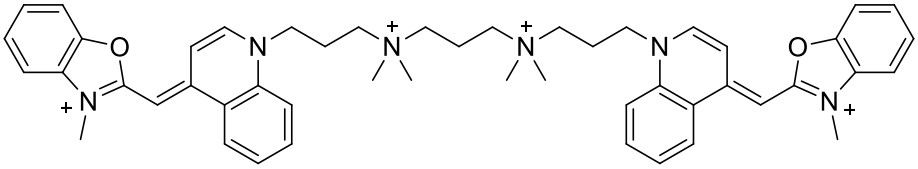

YOYO-1

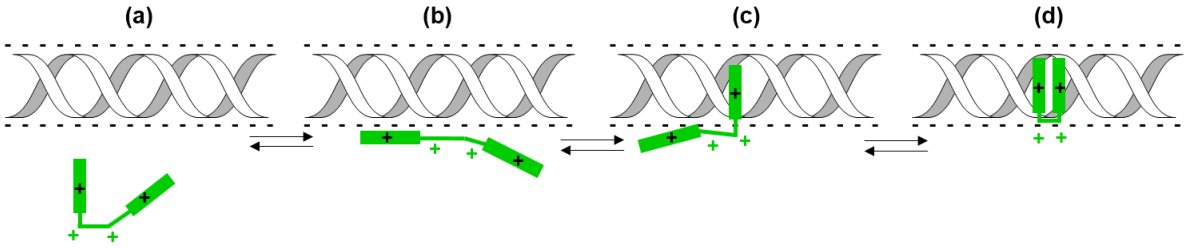

Figure 6. Structure of the YOYO-1 dye and schematic illustration of the binding states of YOYO-1 in the double-stranded DNA. The YOYO-1 molecule may be free (a) or bound to DNA. When it is bound, the positively charged dye can electrostatically interact with the negatively charged DNA backbone (b), it can be mono-intercalated in the DNA duplex (c), or bis-intercalated (d). Scheme adapted from reference.[33]

The use of YOYO-1 dye has also been widely reported for super-resolution imaging based on single-molecule localization.[33; 35; 36; 37; 38; 39] YOYO-1 enables this kind of super-resolution approach, because it can form dark metastable states or exhibit photoblinking at moderate

excitation powers in the presence of a “switching buffer”, which contains a thiol, such as MEA, and/or oxygen scavenger system.[36] Studies have suggested that the blinking process occurs due to an electron transfer reaction to YOYO-1 from the reducing MEA, or by the guanosine bases in DNA.[37]

A valuable contribution was the development of an approach termed Binding-Activated Localization Microscopy (BALM) that was reported by Vogel and co-workers.[35] This study is based on the single-molecule localization microscopy principles, in which YOYO-1 molecules are switched on upon binding to the target DNA. Then, taking into account the dynamic binding properties of YOYO-1 into the DNA duplex, repeated cycles of binding, localization, and bleaching allow the optical reconstruction of the DNA structure under investigation.

In the scope of binding methods to achieve subdiffraction imaging, it is important mentioning the approach introduced in 2006 by Hochstrasser, named Point Accumulation for Imaging in Nanoscale Topography (PAINT). In this case, the structure to be imaged is continuously targeted by fluorescent probes diffusing in solution. Upon the binding of a probe to the structure, it is immobilized and generates a fluorescent spot that can be treated as a PSF of a single molecule. Consequently, the PSF can be fitted as a Gaussian profile to evaluate the precise localization of the emitter on the structure.[40]

Thus, these principles based on the binding of fluorophores for localization of DNA molecules constitute the basis of the optical super-resolution experiments performed in this thesis.

One of the strategies for fluorescent covalent labelling at the DNA nitrogenous bases is making use of the unique ability of DNA methyltransferases to transfer chemical moieties from AdoMet analogues to specific sites of the DNA double helix. The approach was the basis of the fluorescent labelling studies described in Chapter 3. In the next section, a brief review about DNA methyltransferases is presented.

3.3 DNA methyltransferases

In nature, DNA methyltransferases (MTases) catalyse the transfer of a methyl group from the cofactor S-adenosyl-L-methionine (AdoMet) to an adenine or a cytosine base of the DNA duplex. The process of DNA methylation includes additional information to the DNA that is not encoded in the sequence. This is termed epigenetic information and it develops many important biological functions.[41] In prokaryotes, the most important role of the DNA methylation is the protection of host DNA against degradation by restriction enzymes.

Besides that, it corrects errors in the DNA replication through mismatch repair.[42] In eukaryotes, the DNA methylation contributes to the control of several cellular processes, such as gene expression, gene regulation, differentiation, parental imprinting, and protection of the genome.[41; 42]

The DNA methyltransferases sequence-specifically modify the DNA, usually at palindromic recognition sites. This process does not interfere in the pairing of the adenine and cytosine bases, but the additional methyl group is then positioned in the major groove of the DNA. The MTases are subdivided in three major classes, according to the nature of the modification introduced, i.e. the methylation target site. The methylation may take place at three different target sites, which are the exocyclic N6 of adenine, the exocyclic N4 of cytosine, or the C5 of cytosine. The methylation process performed by each class of MTase is schematized in Figure 7.[41]

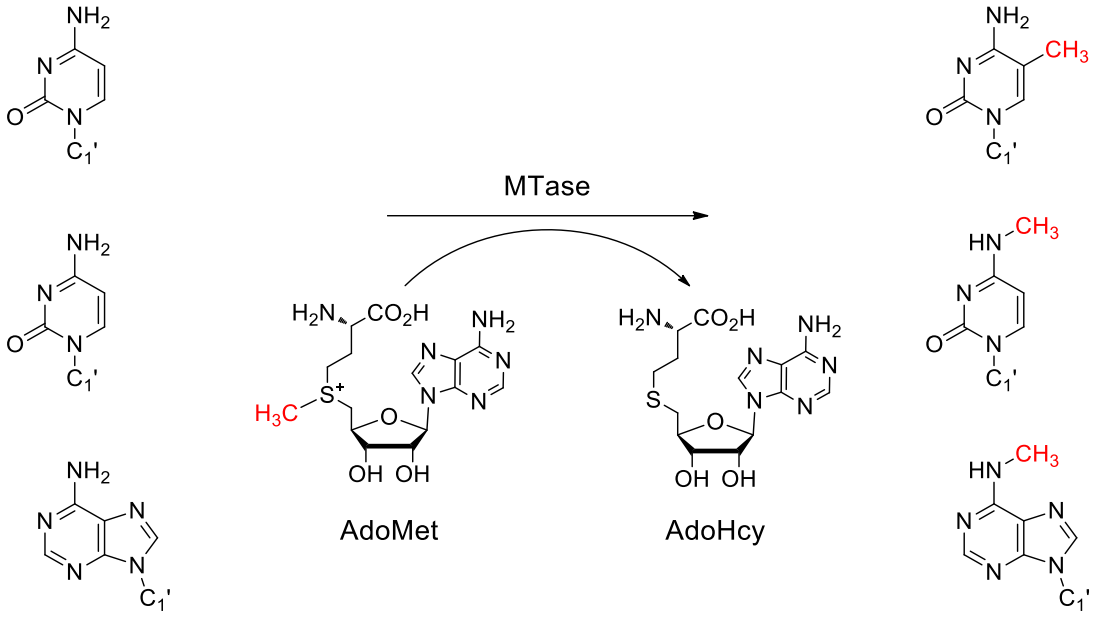

Figure 7. DNA methylation process performed for the target sites C5 of cytosine, exocyclic N4 of cytosine, and exocyclic N6 of adenine, respectively, by MTases. In this process, the activated methyl group is transferred from the AdoMet cofactor to the respective nitrogenous base, generating the S-adenosine-L-homocysteine (AdoHcy). Adapted from reference.[42]

Some examples of methyltransferases are M.HhaI, M.EcoRV, M.PvuII, and M.TaqI. The latter, M.TaqI, is part of the restriction-modification system of the thermophilic bacteria *Thermus aquaticus* and it is an integrant of the MTases class that catalyses the transfer of

the activated methyl group from AdoMet to the exocyclic amino group (N6) of adenine, within the double-stranded 5'- TCGA -3' palindromic target sequence.[43; 44] In this work, this enzyme was vastly used for sequence-specific DNA modification not only with methyl groups, but also with extended functionalised alkyl groups,[45] as described *a posteriori* in Chapter 3.

The catalytic mechanism by which the N-MTases proceed to modify the exocyclic amino group of adenine (N6) or cytosine (N4) is a nucleophilic substitution type S_N2, characterized by an inversion of the configuration of the methyl group.[41] A remarkable structural and mechanistic feature of the DNA MTases was studied by analysing the crystal structure of the complex DNA-MTase. The crystal structure of the M.TaqI in complex with specific DNA and a non-reactive AdoMet analogue was reported by Goedecke and co-workers in 2001.[44] To catalyse the reaction, the enzyme completely rotate the target nucleoside (adenine) out of the DNA helix. The enzyme therefore binds with the nucleoside in a hydrophobic domain of the enzyme, creating an active site for the methyl group transfer.[41; 44] This process generates an "orphan" nucleoside that is the thymine pair of the flipped adenine. Consequently, the π-π-stacking interaction of the non-flipped base is discontinued and the thymine needs to be positioned to stabilize the DNA duplex. Thus, the thymine forms an interstrand π- π-stacking interaction with the guanine base at position 5' neighbouring the target adenine.[44]

3.4 Bioorthogonal reactions

The advances in the fluorescence microscopy techniques have allowed the visualization of biological processes at even smaller scales. However, to follow these advances, a new very important task appears in this context, namely the labelling of biomolecules without damaging the biomolecule and its environment.

The term bioorthogonal chemistry relies on the strategies to modify biomolecules with a functional group, in which another specie can selectively conjugate without perturbing the biological system.[46; 47; 48] Finding the best manner to label a target biomolecule is a difficult issue, because the biological medium is full of reactive groups that can interfere in the desirable reaction. Furthermore, the bioorthogonal probes must be stable in aqueous environments and the chemistries must be nontoxic.[46] Herein, some of the bioorthogonal chemistry utilized in this thesis is presented.

3.4.1 Copper-catalysed azide-alkyne cycloaddition (CuAAC)

The 1,3-dipolar cycloaddition is a classic reaction in organic chemistry, which allows the synthesis of several five-membered heterocycles.[49] This reaction is an exergonic process, constituted by the addition of a 1,3-dipole to a dipolarophile, such as an alkene or an alkyne. The 1,3-dipole molecules contain one or more heteroatoms and at least one resonance structure that represents a charged dipole.[50] The pioneer to introduce the 1,3-dipolar cycloadditions to the scope of organic synthesis was the chemist Rolf Huisgen with his studies in the 1960s.[49; 51] For this reason, this kind of reactions are also known as Huisgen 1,3-dipolar cycloadditions.

To form stable triazoles, azides are used as the 1,3-dipole that can react with dipolarophiles such as terminal alkynes. However, this cycloaddition may require an elevated temperature, or elevated pressure, to overcome the activation barrier necessary to deform the alkyne's bond angle, 180°, and hence to form the triazole (120° angle).[52; 53] Theoretically, this reaction produces a mixture of the 1,4- and 1,5-regioisomers, in a 1:1 ratio, as illustrated in Figure 8.[50]

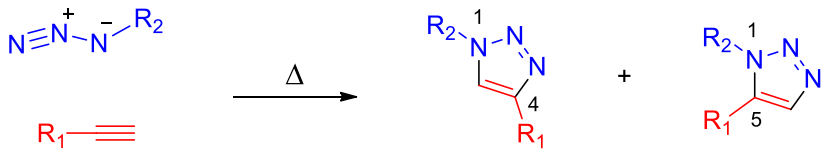

Figure 8. Scheme of the azide-alkyne 1,3-dipolar cycloaddition. Adapted from reference.[50]

These conditions of high temperatures or pressures are not compatible with reaction conditions in living systems. In 2002, Sharpless and co-workers[50] and Meldal and co-workers[54] independently developed an alternative to accelerate the rate of the cycloaddition between azides and alkynes obtaining high yields of product at mild conditions, by using Cu(I) as a catalyst.[53] This approach enabled the production of 1,4-disubstituted 1,2,3-triazoles, with near-complete regioselectivity, at room temperature. It is also possible to performed this cycloaddition in aqueous media and in a pH range from 4 to 12.[50]

The catalyst can be prepared *in situ* by reduction of Cu(II) salts.[50] The most common conditions are the use of $CuSO_4$ and a reducing agent, such as ascorbic acid, in aqueous media. Several reaction conditions are reported in the literature.[55] This robust methodology is known as the Cu-catalysed azide-alkyne cycloaddition (CuAAC). Due to CuAAC being high-yielding, selective, and having good reaction kinetics, it was also defined as a click reaction.[53]

Moreover, some authors consider the Cu-catalysed click reaction orthogonal, since their components are inert to the biological environment.[53; 55]

The vast application of CuAAC ranges from material to life sciences. In this thesis, such chemical transformation methodology is applied to biomolecules. The advent of the click chemistry has led some researchers to use CuAAC towards the nucleic acids field mainly because of its high efficiency. There is an increasing demand to label nucleic acids with fluorescent labels for optical sequencing and *in vivo* visualization[56; 57]. The use of the Cu-catalysed click reaction to this purpose has been well documented in the literature.[56; 57; 58; 59; 60; 61; 62; 63] The main use of this approach is towards the efficient incorporation of multiple labels into oligonucleotides.

The CuAAC has been chosen as an alternative to nucleic acids labelling, due to the following reasons. Azides and alkynes can be attached to nucleic acids without disturbing their biophysical properties; azides and unactivated alkynes are almost unreactive towards the functional groups normally encountered in biological environment; and the triazole unit formed is extremely stable to reactive conditions, e.g. oxidation, reduction and hydrolysis, and it is not toxic.[55; 57] Nevertheless, it is important to mention the recommendation of using Cu(I)-stabilizing ligands to protect the DNA from damage.[57]

Another important development in this field was the method of DNA labelling in vivo, which allowed the detection of DNA synthesis in proliferating cells.[64] This method used 5-ethynyl-2'-deoxyuridine (EdU) which is a thymidine analogue containing a terminal alkyne, and was incorporated into cellular DNA. The detection was possible thanks to the ligation of fluorescent azides to the terminal alkyne via CuAAC. However, the reaction conditions led to cell death. This research draws attention to the primary disadvantage of the copper-catalysed click reaction, which is the cellular toxicity of the metal catalyst.[52]

3.4.2 Strain-promoted azide-alkyne cycloaddition (SPAAC)

As the cytotoxicity of the metal catalyst is a noteworthy limitation of the use of CuAAC in living systems, research was conducted to discover a pathway to increase the rate of the azide-terminal alkyne cycloaddition, without the use of the catalyst. An alternative to activate the alkyne was the use of highly strained ring, for instance the use of an eight-membered cycloalkyne, which has 18 kcal/mol of ring strain, released in the transition state upon cycloaddition with an azide.[65] Therefore, click chemistry in the absence of the Cu(I) catalyst appears as an elegant approach, involving the reaction of azides with cyclooctyne derivatives

to provide regioisomeric mixtures of triazoles at ambient temperatures and pressures, with no apparent cytotoxicity, as reported by the pioneer work from Bertozzi *et al* in 2004.[66]

This methodology is called strain-promoted azide-alkyne cycloaddition (SPAAC) and is based on the initial work of Wittig and Krebs, whom reported that cyclooctyne is the smallest stable ring to react with azides.[67] However, the rate of SPAAC reactions with the first generation of cyclooctyne molecules was relatively slow compared to the corresponding CuAAC reactions.[68] The first generation cyclooctyne (**1**, **2**) was synthesized and further coupled to a biotin analogue.[66]

Bertozzi and co-workers further circumvented such disadvantage, enhancing the cycloaddition rate by installing propargylic fluorine atoms. The fluorine substitution causes an increase of the frontier molecular orbital interaction energies.[69] This action tends to decrease the energy of the lowest unoccupied molecular level (LUMO), hence increasing its interaction energy with the highest occupied molecular level (HOMO) of the azide. The monofluorinated compounds (**3**), also termed second generation, moderately improved the reaction rate.[70] In contrast, the third generation difluorinated cyclooctynes termed “DIFO” reacted with azides at a rate comparable to that of Cu-catalysed click chemistry (**4** - **6**).[71] Afterwards, a novel set of DIFO reagents was created, in which the bioorthogonality and the reaction kinetics were preserved, but their synthesis process was greatly simplified.[72] Under those conditions, the SPAAC reaction is then reported to occur in 1 h at room temperature.[68]

After the development of the DIFO cyclooctynes and the success of the copper-free click chemistry for labelling biological systems, a vast collection of cyclooctyne derivatives has been investigated, which makes SPAAC a more accessible methodology. The Figure 9 shows some derivatives to perform SPAAC. The synthesis of compound **7**, an azacyclooctyne, was proposed to obtain a more water-soluble product.[73] The dibenzocyclooctyn-ol compound, **8**, was reported by Boons and co-workers. This compound is also suitable for SPAAC with applications in living systems, non-toxic, and when reacted with azides it produces the corresponding triazoles in high yield and with a high reaction rate.[65] Nowadays, several dibenzocyclooctyne derivatives can be easily found commercially. Another kind of derivative was proposed containing an amide within the ring, the biarylazacyclooctynone “BARAC” (**9**). This molecule was reported to have better solubility and pharmacokinetic properties.[74] For review purposes, the publication of Schubert and co-authors brings valuable information about copper-free click chemistries.[68]

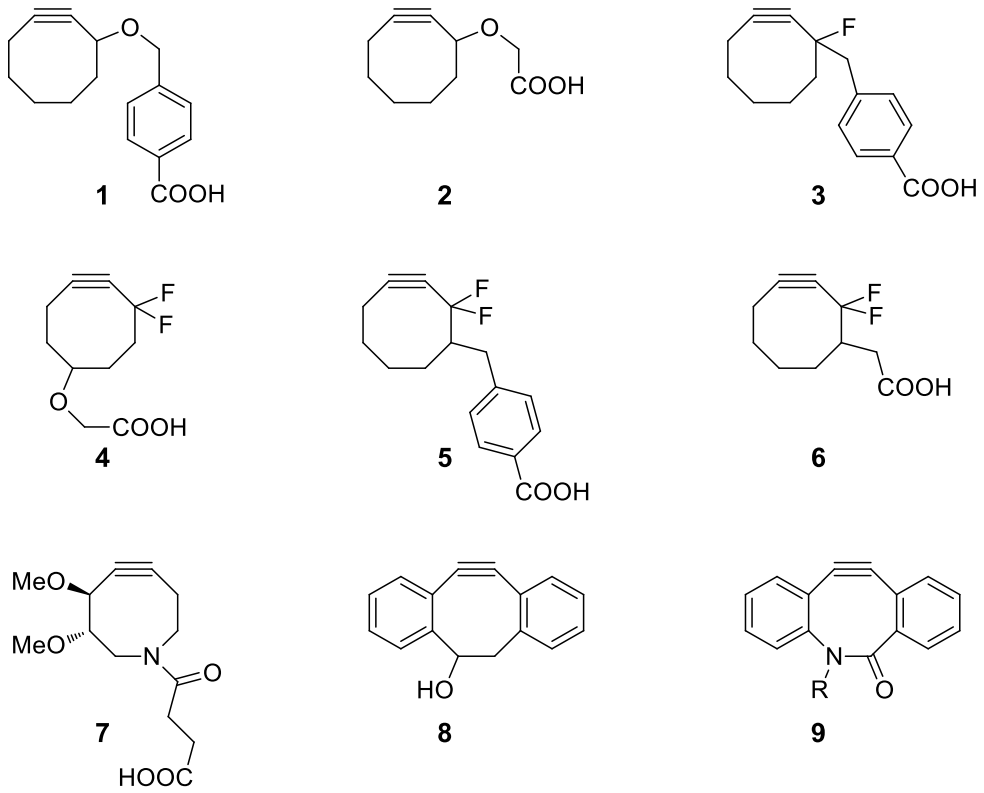

Figure 9. Cyclooctyne derivatives prepared for copper-free click reactions. Adapted from reference.[48]

The SPAAC reactions have demonstrated their high potential to be applied in different biological systems, such as for *in vivo* imaging of cells,[71] *C. elegans*,[75] and glycoconjugates of living zebra fish embryos.[76] This approach has also been utilized in the nucleic acids field. Several reports have applied fast copper-free click reactions to label oligonucleotides[61; 77; 78; 79; 80] and to perform DNA crosslinking.[81]

CHAPTER 2

Photophysical and confocal microscopy studies of maleic anhydride and maleimide derivatives

1 INTRODUCTION

The study of new dyes has been a topic of interest, towards the understanding of the fundamental electronic structure, as well as for potential applications in fluorescence microscopy, due to the advent of advanced optical microscopy techniques.[4] Among the types of fluorescent labels one can find the natural fluorophores, organic dyes, nano- and microspheres, and nanocrystals.[3]

The use of organic dyes is preferable for *in vitro* labelling because of their small size, compared to fluorescent proteins and quantum dots. Moreover, they enable to perform specific labelling to biomolecules. There are several classes of organic dyes, such as coumarin, xanthene, rhodamine, fluorescein, cyanine, BODIPY, and perylene derivatives.[3] Organic fluorophores are also used for single-molecule detection. However, they should fulfil some requirements like possessing a high extinction coefficient, a high fluorescence quantum yield, a large Stokes shift, and a high photostability. In this scope, the dyes that can be successfully applied for such purpose are the currently commercially available Atto- and Alexa Fluor-dyes.[3]

Among the organic fluorophores, one can also cite a type of probes that have been receiving special attention, namely the natural products derivatives. For that, many efforts have been practiced in organic synthesis for obtaining the fluorescent analogues,[82; 83; 84] which can be used for biological processes signalling, for instance, intracellular trafficking and membrane association.[82; 83] Thus, information provided by the basic photophysical study of such analogues is of great importance.

1.1 Push-pull dyes

Another notable group of fluorescent probes are the molecules with the so-called push-pull effect. These probes should contain a π-conjugated framework end-capped by electron-accepting and electron-donating groups. Typical electron donors (D) can be exemplified by the substituents OH, NH_2, OR and NR_2, heterocyclic moieties such as thiophene, and some metallocenes. In contrast, the substituents NO_2, CN, CHO, and electron deficient heterocycles, such as benzothiazole, and imidazole, represent the typical electron acceptor (A) moieties.[85] Some classical compounds that show the push-pull character are the cyanostilbenes, polyenes, merocyanines and cyanines.[86; 87]

The interaction between the donor and acceptor groups is termed intramolecular charge-transfer (ICT), which is responsible for the polarization of the push-pull molecule and hence the formation of a molecular dipole.[85] The push-pull molecules can exhibit a negative solvatochromic shift when the ground state dipole moment is larger than the excited state dipole moment, as a consequence, the excited state energies are lower in nonpolar solvents. However, when the excited state dipole moment is larger than the ground state dipole moment, the compound shows a positive solvatochromic shift. This effect is more pronounced for fluorescence, because the solvent relaxation can stabilize the excited state and destabilize the ground state.[86]

Therefore, when a fluorophore shows a charge shift in the excited state, it can be used as a valuable probe to monitor micro and nanostructures in biological systems,[88; 89] polymers,[90] and colloids.[91; 92] In this process, a partial charge shift can occur in different parts of the molecule, which contains electron-donating and electron-accepting groups.[4; 93] In the excited state, an increase of the charge separation can take place. Then, the immediate environment, such as solvent polarity, pH, and viscosity, may modulate the electronic transitions and the excited state properties.[4]

Besides the solvatochromic property, the tuneable structure and unique properties make the push-pull molecules also a widespread target for application in optoelectronics,[94; 95] organic solar cells,[96] and chromophores with non-linear optical properties.[85]

1.2 Polycitrin-inspired fluorophores

A class of compounds that have demonstrated great potential to be applied as optical sensing and as microenvironment probes are the imides. The photophysical properties of the indolylmaleimides,[97; 98; 99; 100; 101; 102] monoimides,[103] and polyimides,[104] have been well documented. Arylated maleic anhydrides and maleimides are described in the literature as compounds exhibiting fluorescence,[105; 106] and their syntheses is also well-documented.[106; 107; 108]

In this extent, the fluorescent bisaryl-substituted maleimides present the advantage of being a precursor of the natural product polycitrin A and B, isolated from the marine ascidian *Polycitor* sp., known as a source of active secondary metabolites with biomedical potential. The structural elucidation of such natural products were conducted by Kashman and co-workers in 1994.[109] Although the structure of these compounds has already been known

since then, the fluorescent properties of the polycitrin derivatives have not been explored until now.

In this chapter, the photophysical study of several derivatives synthesized by the Heck-Matsuda reaction is presented.[110; 111] Among the potential fluorescent probes, the bisarylated maleic anhydride and maleimide derivatives were investigated, as well as the compounds with condensed rings, termed phenanthrene derivatives.

2 OBJECTIVES

The second chapter of this thesis describes the photophysical study of a series of bisarylated maleic anhydrides and maleimide derivatives, all of them synthesized by the Heck-Matsuda arylation reaction.

- Steady-state and time-resolved photophysical characterization of the bisarylated maleic anhydride and maleimide derivatives;
- Solvent effect study of the maleimides by the Lippert-Mataga approach;
- Basic photophysical characterization in solution by confocal microscopy and imaging in a polymeric matrix.

3 METHODOLOGY

3.1 Synthesis of maleic anhydride derivatives

In this section, the synthesis scheme of the maleic anhydride derivatives used in this research is presented. Briefly, a direct methodology to obtain bisarylated maleic anhydrides using the Heck arylation with arenediazonium tetrafluoroborates was developed by Correia and co-workers in 2006.[110] However, an improved methodology is being applied, in which fumaric acid (**1**) is used as a substrate for the Heck-Matsuda reaction, followed by a one-pot cyclization.[111] The details of the synthesis can be found in the literature.[112]

The bisarylated maleic anhydrides (**4a**-**e**) were prepared by a second Heck-Matsuda reaction. From these compounds, one can obtain the bisarylated maleic anhydrides substituted with bromide ions, also denominated as prepolycitrin A and B (**6a**-**b**), the bisarylated maleimides (**5a**-**d**) and the cyclized compounds, are called phenanthrene derivatives (**7a**-**b**, **8a**-**b**). For their preparation, the bisarylated Heck adduct (compound **4a** from Figure 10) was dissolved in benzene and elementary iodine, then exposed to a photochemical reactor operating with an immersion lamp Hanovia (450 W) for 12 h.

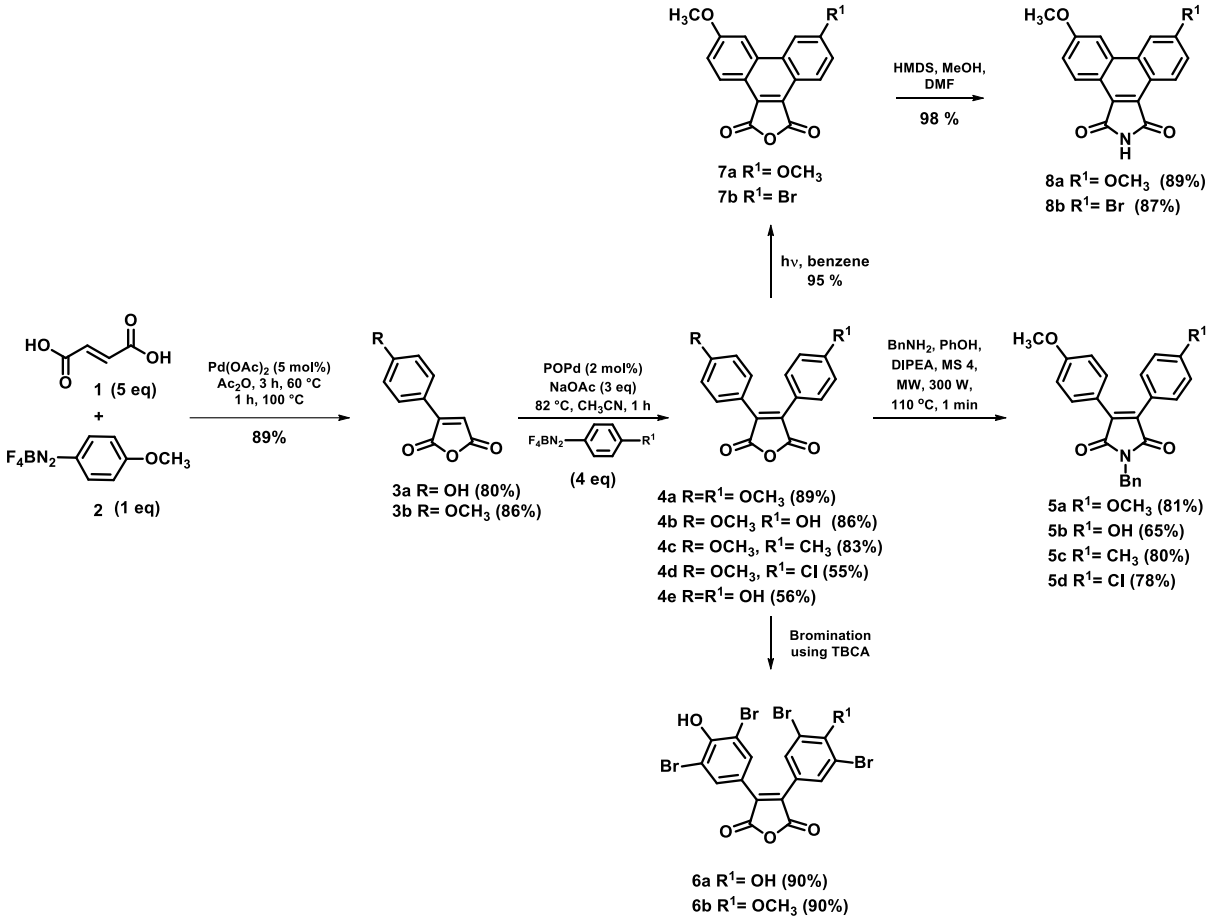

Figure 10. Scheme of the synthesis of maleic anhydride derivatives by the Heck-Matsuda route.

3.2 Stationary measurements

The stationary measurements were performed to characterize the compounds and to determine the fluorescence quantum yields. The UV-visible absorption and the emission spectra were acquired using the spectrophotometers Jasco V-630 or Shimadzu RF-5301 PC, and Hitachi F-4500 or Shimadzu UV-1800, respectively, using a quartz cuvette, with 1 cm optical path.

The fluorescence quantum yields were determined using 9,10-diphenylanthracene (ϕ = 0.9 in cyclohexane) or quinine sulphate (ϕ = 0.577 in H_2SO_4 0.1 M) as standards. The measurements of the samples and standards were performed at the same conditions and the absorbance was kept under 0.05 AU's. For the quantum yield evaluation eq. (6) was employed, which used a correction by refraction index.[4]

$$\phi = \phi_r \frac{I}{I_r} \frac{A_r}{A} \frac{n^2}{n_r^2} \quad (6)$$

Where: ϕ is the quantum yield of the sample, I is the integrated fluorescence intensity, A is the absorbance of the sample and n is the refractive index. The subscript r refers to the reference fluorophore of known quantum yield. All solvents were of HPLC or spectroscopic grade and were dried on 4 Å molecular sieves prior to use. 1,4-dioxane was previously distilled.

3.3 Time-resolved measurements

In order to explore the excited state dynamics, fluorescence decays were acquired by a time-correlated single-photon counting (TCSPC) technique using the system depicted in Figure 11. This instrumentation was previously described in the literature.[112; 113] For the measurements, laser pulses at 395 nm were generated by frequency doubling the 150 fs laser pulse of a Ti-Sapphire Mira 900 laser pumped by Verdi 5 W (Coherent). The fluorescence decays were collected in magic angle mode (54.7°) using Glan-Laser polarizers (Newport), with 0.5 or 1x10^4 peak counts and time increment of 20 – 100 ps per channel and the photon detector was a Peltier cooled MCP-PMT (Hamamatsu R3809U-50). The instrument response function (irf) was typically 40 ps at fwhm.[91; 112; 113; 114]

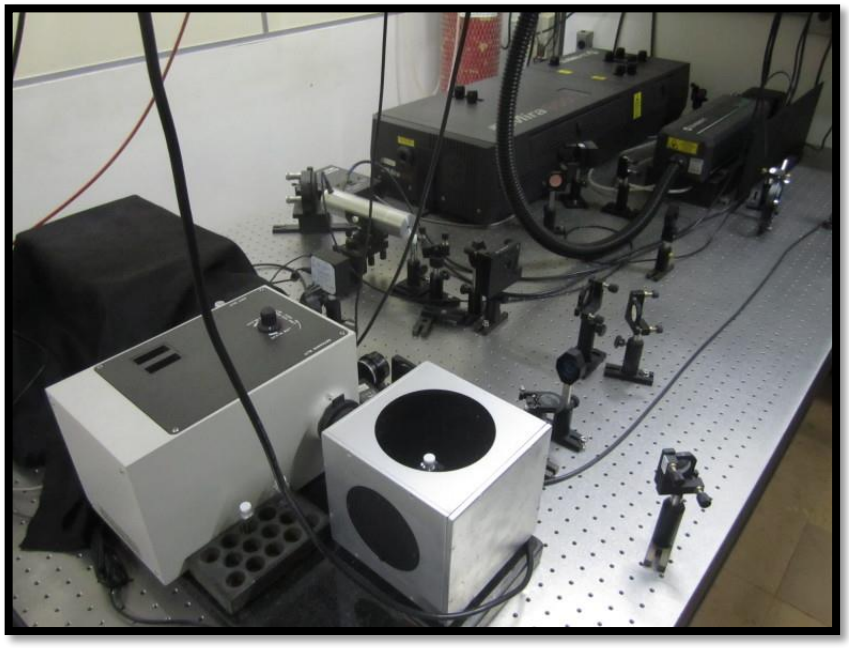

Figure 11. Laser system (Verdi 5 W / Mira 900) utilized for time-resolved experiments. This system is available in the Molecular Fluorescence Laboratory – IQSC/USP.[12]

All of the samples were analysed with an absorbance below 0.5 AU's. Decays were recorded with the TC900 counting board and software from Edinburgh Instruments. Lifetimes were evaluated by the reconvolution procedure with multiexponential decay models, according to equation (7).

$$I(t) = \sum_i b_i \, exp\left(\frac{-t}{\tau_i}\right) \qquad (7)$$

In equation (7), τ_i and b_i are the decay time and its pre-exponential factor of the i^{th} component, respectively. Decays from compounds **4a**, **5a**, **7** e **8** were also studied by the global analysis method, in which it assumed that decay times are independent of the wavelength, which results in a higher probability of recovering the most representative values.[4] Global analysis was employed for five wavelengths spaced 15 nm from the emission maxima with linked-lifetimes. The decays were analysed using FAST software from Edinburgh Instruments.[112; 113]

3.4 Confocal microscopy

The confocal fluorescence microscopy system from Molecular Fluorescence Laboratory, at IQSC-USP, is based on an inverted microscope (Olympus IX71) with a digital piezoelectric stage (PI, E-710.3CD e P-517.3CD) for nanometric sample scanning. This system was used to obtain three kinds of experimental data: imaging; emission spectra, with excitation performed by coherent light sources operating in the continuous regime; and fluorescence decays, with pulsed excitation mode. This confocal microscopy instrumentation has already been described in the literature.[113]

3.4.1 Imaging

The samples were excited by a CW laser at 405 nm (Coherent Cube), operating with an output power adjustable between 1 and 40 mW. The excitation light was converted into a circularly polarized laser beam using zero-order quarter (Del Mar Photonics) and focused on the sample with an oil objective (Olympus, UPLSAPO 60XO 60x NA = 1.35), or an air objective (Olympus, UPLFLN 40XPH 40x NA = 0.75). The measurements were performed in air, thus the used numerical aperture of the first mentioned objective was 0.89. The emission signal was separated from the laser excitation beam using a dichroic cube (Chroma, z405lp)

and a notch filter (Semrock, NF02-405U-25). The detector used for this system was an avalanche photodiode point detector (Perkin Elmer, SPCMAQR-14) aligned with a 50 μm pinhole in the confocal line. This detector shows a dark count of about < 100 counting per second and a spectral response in the region of 430-850 nm.[113]

The confocal images were generated due to the control and synchronization of the piezoelectric system with two electrical boards from National Instruments, PCI-GPIB NI-488.2 and PCI-6601, applied to the acquisition of transistor-transistor logic (TTL) detector signals. The signals were transferred to a computer for 2D plotting using a scanning control program written in LabView 8.5, developed in the Molecular Fluorescence Laboratory. The images obtained by this program were imported and treated using a Matlab code, also developed by the group from IQSC-USP. Fluorescence images covering a region of 60 x 60 μm, with pixel size of ~λ/2, were recorded using false-colour mapping, where the colours were assigned according to the difference in intensity of the fluorescence signal.[113]

3.4.2 Spectra

The emission spectra were obtained from a spectrometer Maya 2000 Pro – Ocean Optics that was coupled to the lateral port of the Olympus IX71 microscope, using an optical fiber QP400-2-UV-VIS from Ocean Optics, with a core diameter of 400 μm. A long pass filter (Thorlabs, cut-off wavelength of 450 nm) was used to block the scattering light from the excitation. This setup is pictured in the Figure 12.[113]

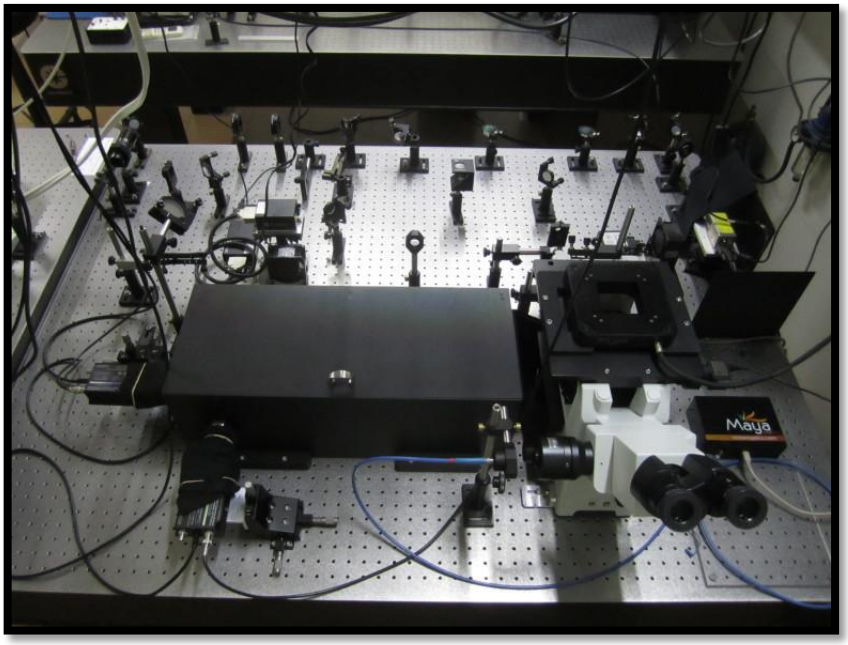

Figure 12. Confocal microscopy setup. Microscope IX71 containing two APD detectors and piezoelectric PI controller. The Maya 2000 Pro spectrometer is laterally coupled to the microscope. This system is placed in the Molecular Fluorescence Laboratory – IQSC/USP.[12]

3.4.3 Fluorescence decays

For the fluorescence decay measurements, the samples were excited with pulses at ~400 nm, provided by the frequency doubled light pulses from a Ti:Sapphire laser (Mira 900, Coherent). The pulses had width of 150 fs and frequency of 76 MHz. A pulse picker (Conoptics) kept the excitation pulse frequencies at 4 MHz. Fluorescence decays were acquired according to the TCSPC technique using a counting board (Becker&Hickel, 140) with start laser pulses triggered by a photodiode (PicoQuant TDA 200). Decays were analysed with exponential models without deconvolution using the FAST software (Edinburgh Instruments). The scheme of the instrumentation for confocal microscopy measurements is depicted in Figure 13.[113]

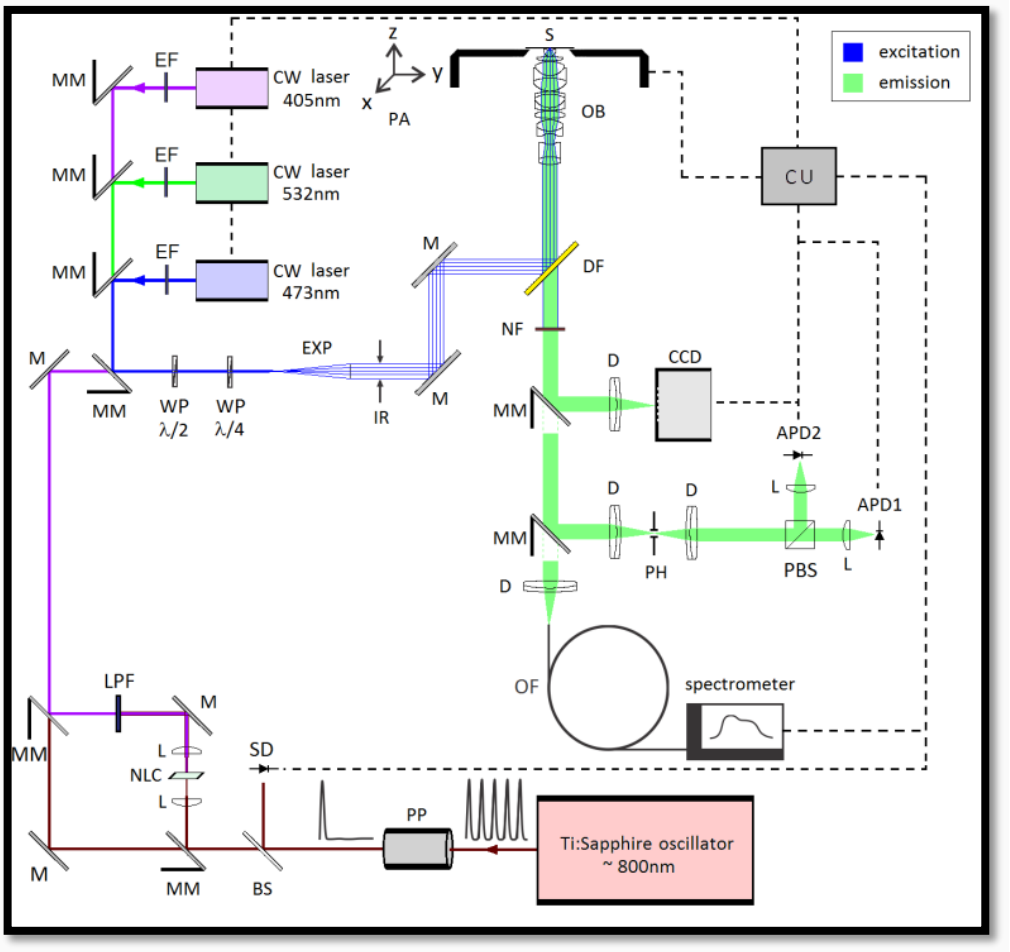

Figure 13. Scheme of the fluorescence confocal microscopy instrumentation available in the Molecular Fluorescence Laboratory – IQSC/USP. APD: avalanche photodiode; BS: beam splitter; CU: control unit; DF: dichroic filter; EXP: beam expander; IR: iris; L: lens; LPF low-pass filter; M: mirror; MM: mobile mirror; NF: notch filter; NLC: non-linear crystal; OB: objective; OF: optical fibre; Pbs: prism beam splitter; PA: piezoelectric; PH: pinhole; PP: pulse picker; S: sample; SD: silicon detector; WP: wave plate. Illustration available in the literature.[12]

3.5 Theoretical calculations

Theoretical calculations were performed in order to evaluate the Onsager radius, that is the radius of the cavity in which the fluorophore resides,[4] and the ground state dipole moment of each molecule. These parameters are required to determine the excited state dipole moment by the Lippert-Mataga equation.[115; 116] All the structures were optimized before calculations. We used the density functional theory (DFT) method, using Gaussian 03 software,[117] with the implementation B3LYP associated to the 6-311G basis, with two polarization functions and two diffuse functions (2d, 2p).[112] The calculations were performed in collaboration with the Quantum Chemistry Group, at Institute of Chemistry of São Carlos – USP, Brazil.

4 RESULTS AND DISCUSSION

4.1 Photophysical study of the bisarylated maleic anhydride derivatives

4.1.1 Steady-state analysis of the maleic anhydride derivatives

Some maleic anhydride derivatives were not stable in solution because of thermo- and photo-hydrolysis, generating the correspondent dicarboxylic acid, which impairs the fluorescence emission in the visible region. Thus, these derivatives were used in dried solvents. Most part of the maleic anhydride derivatives did not show emission in solvents such as DMF and DMSO. However, compound **4a** was stable in solution, which allowed the study in DMF and DMSO.

Changes in absorption spectra as a function of the solvent polarity were negligible. Nevertheless, the positions of the broad emission bands changes with the solvent polarity, promoting solvatochromic shifts in the range from 511 nm to 557 nm. The compounds **4a** and **4e** exhibited a double absorption band, while the compounds **6a** and **6b** showed a single absorption band at the UV region. The absorption spectra of compound **4a** in 1,4-dioxane and in DMSO can be found in Appendices 1. The stationary data are exposed in Table 1.

Compound **4a** was the most stable among this group of derivatives. Its emission bands exhibited a red shift with the increase of the solvent polarity. The increase of 46 nm of the spectral shift from 1,4-dioxane to DMSO is attributed to the reorganization of the polar solvent around the molecule in the excited state, decreasing its energy level.[4] The fluorescence quantum yields also decreased with the increase of the solvent polarity, from 0.47 in 1,4-dioxane to 0.05 in DMSO. This behaviour may suggest an excited state charge shift between the electron donor, 4-methoxyphenyl, and the acceptor group, carbonyl.

Table 1. Stationary parameters from maleic anhydride derivatives.

Compound		Solvent	λ_{abs} (nm)[a]	λ_{em} (nm)[b]	E_{0-0} (eV)[c]	$\Delta\nu$ (cm^{-1})[d]	ϕ_F[e]
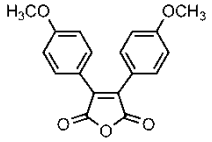	**4a**	1,4-dioxane	392	511	2.71	5941	0.47
		THF	395	517	2.68	5974	0.45
		DMSO	397	557	2.60	7236	0.05
		DMF	396	547	2.60	6971	0.18
		Acetonitrile	396	544	2.63	6870	0.22
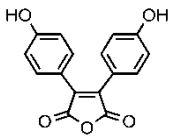	**4e**	1,4-dioxane	395	515	2.69	5899	0.31
		THF	402	525	2.63	5828	0.14
		Acetonitrile	399	546	2.61	6748	0.06
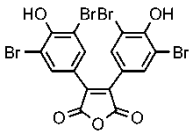	**6a**	1,4-dioxane	388	510	2.73	6165	0.26
		THF	389	517	2.70	6365	0.05
		Acetonitrile	386	532	2.69	7110	0.05
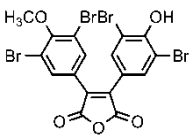	**6b**	1,4-dioxane	377	505	2.84	6723	0.12
		THF	375	515	2.78	7249	0.01
		Acetonitrile	372	529	2.77	7249	0.01

[a] Maximum absorption wavelength. [b] Maximum emission wavelength. [c] 0-0 energy transition. [d] Stokes shift. [e] Fluorescence quantum yield.

4.1.2 Time-resolved analysis of the maleic anhydride derivatives

Time-resolved experiments are crucial to characterize new fluorophores and investigate their dynamic processes in the singlet-excited state. Compound **4e** showed a monoexponential behavior in all the solvents studied and the shortest decay time (2.37 ns) was determined in acetonitrile. Typical fluorescence profiles are plotted in Figure 14. On the other hand, in 1,4-dioxane and in THF, the fluorescence lifetimes were 8.86 ns and 8.46 ns, respectively. Such behavior can be ascribed to the solvent stabilization of the polar excited state of **4e**. Compound **6a** exhibited a similar decay times in THF and in acetonitrile (1.83 ns and 1.97 ns respectively), while in 1,4-dioxane a longer lifetime was evaluated (6.19 ns). This result suggest that the excited state of **6a** is better stabilized in THF and acetonitrile than in 1,4-dioxane, which leads to a fast relaxation to ground state. The compound **6b** showed a

peculiar behavior, namely a fast monoexponential decay in acetonitrile (389 ps), but a biexponential decay in 1,4-dioxane (τ_1 = 0.93 ns and τ_2 = 5.17 ns).

For **4a**, global analysis was performed because this method improves the resolution of the surface fluorescence decay analyzed.[4] The time-resolved parameters are summarized in Table 2. All decays, shown in Figure 14, followed a biexponential model. The shorter decay component was observed in 1,4-dioxane with a value of 1.50 ns, and its contribution corresponds to only 2% of the entire decay. Most notable was the excited state dynamics of **4a** in DMSO. This solvent provided the smallest values among the decay components (τ_1 = 0.70 ns and τ_2 = 2.48 ns), probably due to the formation of a complex between the compound and the solvent, according to the proposed model by Chandross and co-workers.[118]

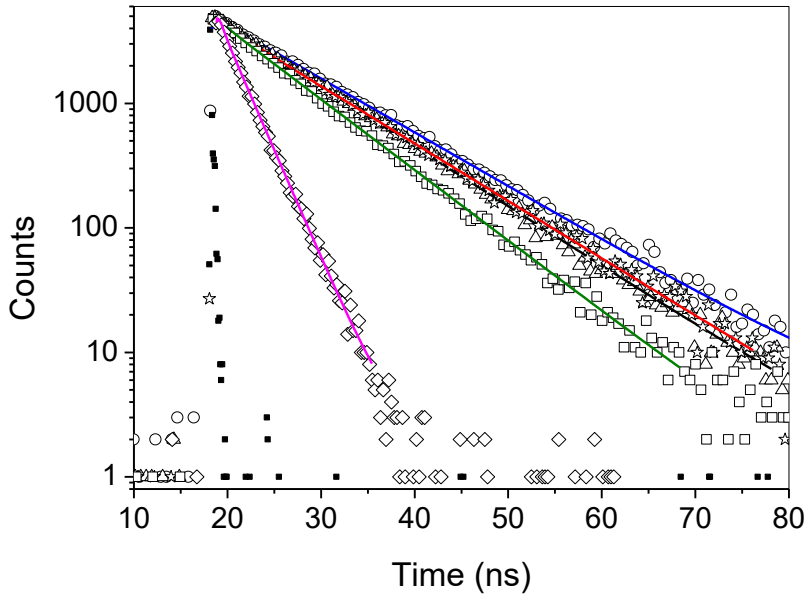

Figure 14. Fluorescence decay of compound **4a** in: acetonitrile (○) decay with λ_{em}= 544 nm; 1,4-dioxane (Δ) λ_{em}= 511 nm; THF (☆) λ_{em}= 519 nm; DMF (□) λ_{em}= 547 nm; DMSO (◇) λ_{em}= 555 nm; (■) irf. λ_{exc}= 395 nm.

Table 2. Time-resolved data of compound **4a**.

Compound	Solvent	Δf [a]	τ_1 (ns)	τ_2 (ns)	b_1 [b]	b_2	χ^2_g [c]
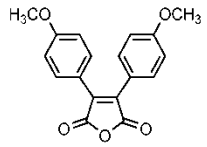 **4a**	1,4-dioxane	0.021	1.50	8.97	0.09	0.91	1.05
	THF	0.209	1.37	9.36	0.12	0.88	1.09
	DMSO	0.265	0.70	2.48	0.15	0.85	1.14
	DMF	0.275	0.73	7.62	0.13	0.87	1.12
	Acetonitrile	0.306	0.71	10.05	0.13	0.87	1.05

[a] Δf = orientation polarizability (equation 10). [b] $b_i = b_i = B_i / \Sigma B_i$, B_i is the pre-exponential factor in the model for the exponential components. [c] χ^2_g = chi-square value of the global decay fit.

4.2 Photophysical study of the bisarylated maleimide derivatives

4.2.1 Steady-state analysis of the maleimide derivatives

The absorption spectra of the maleimide derivatives presented non-structured bands centred around 389 nm, which did not promote significant alterations with the change of the solvent polarity. The absorption spectrum of compound **5a** in 1,4-dioxane can be found in Appendices 1. In contrast, the emission spectra presented broad bands with maxima emission between 550 nm and 568 nm, and a pronounced solvatochromic effect of about 960 cm^{-1}, as illustrated by the positive solvatochromic shift of compound **5a** in Figure 15. In this Figure, it is possible to observe the red shift of the emission bands with the increase of the solvent polarity (from 1,4-dioxane to DMSO) of about 757 cm^{-1}, because of the stabilization of the excited state by the solvent.[4] The compounds **5b**, **5c**, and **5d** showed similar trends.[112]

Moreover, the evaluated Stokes shift is in the range of 6075 – 7292 cm^{-1}, which is an indication that the dipole moment of these dyes is greater in the excited state than in the ground state. The spectral parameters determined under different conditions of solvent polarity are presented in Table 3. In general, the emissive behaviour can be related to the push-pull effect, in which a significant charge shift occurs.[86; 112] Some typical push-pull dyes are the merocyanines, cyanostilbenes,[86] and *p*-dimethylamino-4-nitro-stilbene (DMANS),[87] whose behaviour is in good agreement with that observed for the compounds related here.

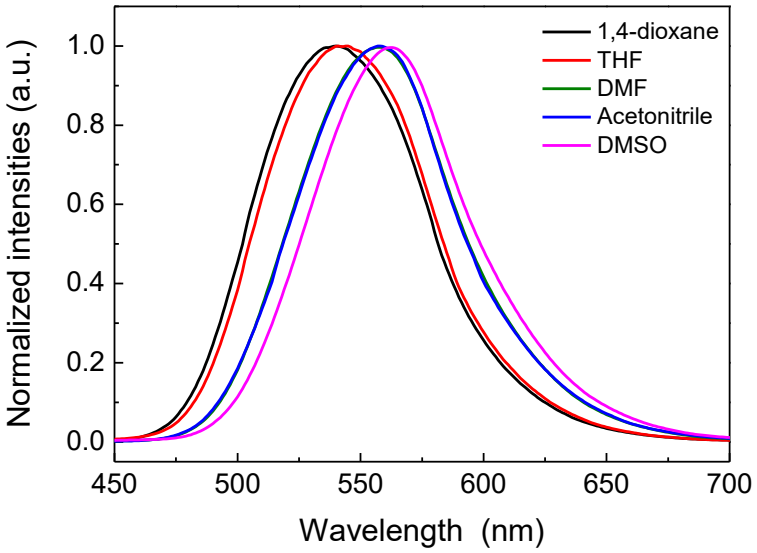

Figure 15. Solvatochromic shift of emission spectra of compound **5a**.[112]

Concerning the Stokes shifts, the highest values were related to the compounds in acetonitrile, and the smallest values to the compounds in THF. The fluorescence quantum yields were higher for nonpolar solvents, such as 1,4-dioxane and THF (0.24 – 0.71), which indicates that the excited states deactivation is less effective in nonpolar solvents.

The smallest Stokes shift was observed for compound **5b**, which contains the 4-hydroxyphenyl group. In this compound, a solvent assisted proton transfer may occur, when using polar solvents such as DMSO or DMF. This process will decrease the fluorescence quantum yield, since the excited state phenolate formed can decrease the emission efficiency. Evidence of this process can be verified by the quantum yield values (between 0.04 and 0.38), which were smaller for the polar solvents.

Compound **5d**, which contains a chloride substituent, showed the highest value for the quantum yield among all analysed maleimides (0.71 in 1,4-dioxane). Contrary, compound **5b** showed a value of 0.24 for the same solvent. This difference can depend substitution of the hydroxyl group for the chloride, which impairs the solvent assisted proton transfer process. The results from the bisaryl maleimides exposed in this section are comparable to the data reported in the literature for the bisindolylmaleimides,[97; 98; 99; 100; 101; 102] in which an impressive, but not complete, charge shift in excited state occurs.

Table 3. Stationary data from the bisarylated maleimide derivatives.[112]

Compound		Solvent	λ_{abs} (nm)	λ_{em} (nm)	E_{0-0} (eV)	$\Delta\nu$ (cm^{-1})	ϕ_F
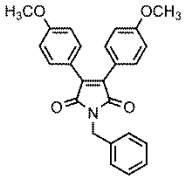	**5a**	1,4-dioxane	402	540	2.60	6954	0.39
		THF	406	544	2.59	6248	0.43
		DMSO	406	563	2.52	6869	0.24
		DMF	404	556	2.54	6767	0.27
		Acetonitrile	400	558	2.57	7079	0.24
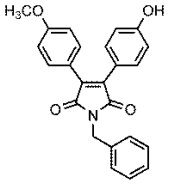	**5b**	1,4-dioxane	404	540	2.59	6234	0.24
		THF	410	546	2.57	6075	0.38
		DMSO	413	568	2.49	6607	0.04
		DMF	411	564	2.51	6600	0.11
		Acetonitrile	401	558	2.56	7017	0.23
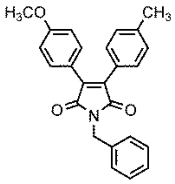	**5c**	1,4-dioxane	393	526	2.68	6434	0.32
		THF	394	526	2.66	6369	0.53
		DMSO	396	554	2.59	7202	0.34
		DMF	394	545	2.61	7032	0.36
		Acetonitrile	390	545	2.66	7292	0.35
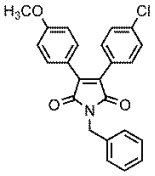	**5d**	1,4-dioxane	392	526	2.68	6499	0.71
		THF	394	529	2.67	6477	0.35
		DMSO	394	550	2.60	7199	0.24
		DMF	392	548	2.62	7262	0.36
		Acetonitrile	389	543	2.66	7291	0.39

4.2.2 Time-resolved analysis of the maleimide derivatives

Global analysis was performed for compound **5a** in five solvents. In polar solvents, the fluorescence decays exhibited short (1.34 ns– 7.55 ns) and long lived components (11.52 ns – 13.55 ns). In contrast, the decays followed a monoexponential trend, when acquired in nonpolar solvents, such as 1,4-dioxane and THF. The lifetimes were very similar to the long-

lived components found in polar solvents. The fluorescence decays are depicted in Figure 16 and the complete set of decay parameters are summarized in Table 4.

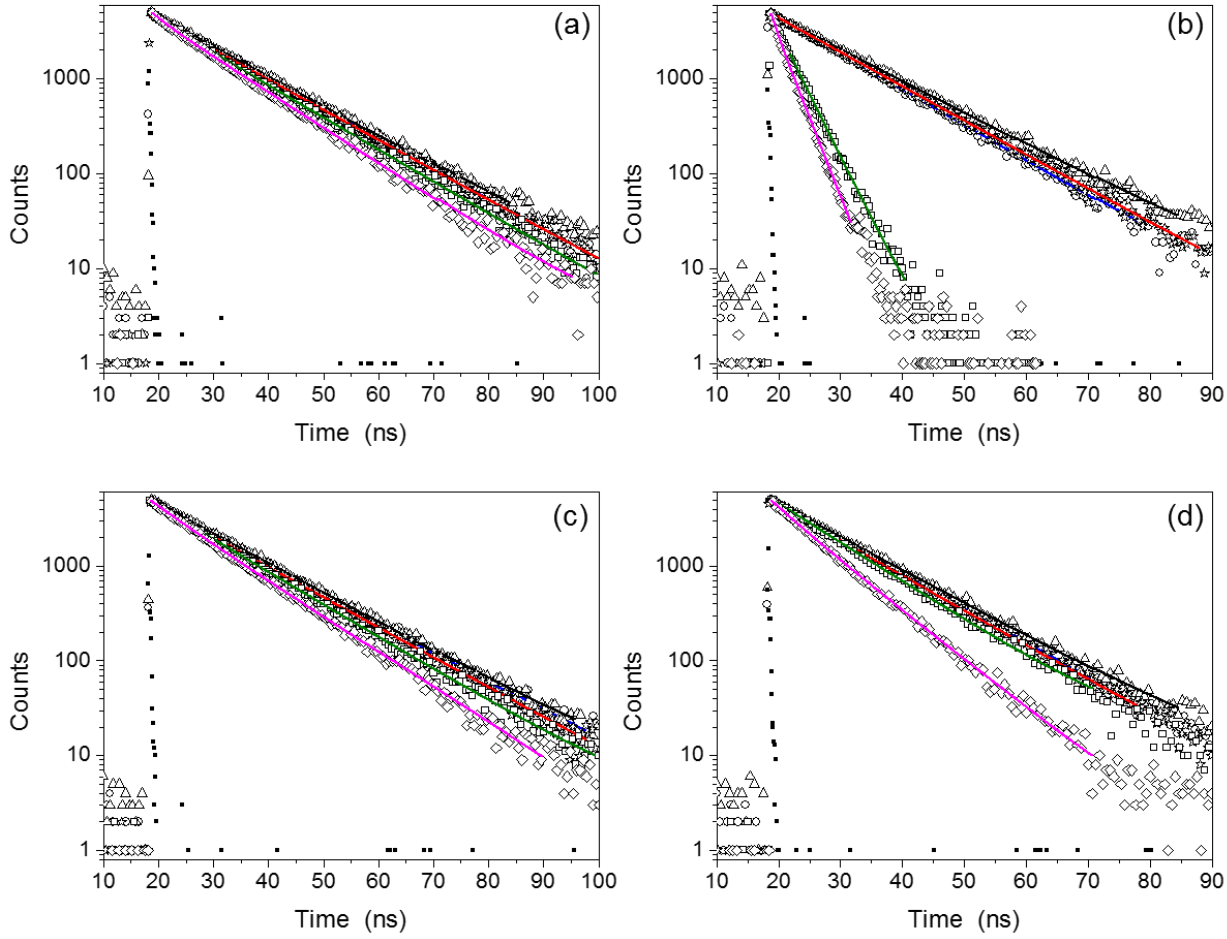

Figure 16. Fluorescence decays of compounds **5a** (a), **5b** (b), **5c** (c), and **5d** (d), in the respective solvents: acetonitrile (○); 1,4-dioxane (Δ); THF (☆); DMF (□); DMSO (◇). The decays were acquired in the maximum λ_{em} of each sample in its respective solvent. (■) irf; λ_{exc}= 395 nm.[112]

Table 4. Time-resolved data from the bisarylated maleimide derivatives.[112]

Compound	Solvente	τ_1 (ns)	τ_2 (ns)	b_1	b_2	χ^2
5a	1,4-dioxane	-	13.79	-	1.00	1.05
	THF	-	13.52	-	1.00	1.07
	DMSO	2.18	11.52	0.17	0.83	1.09
	DMF	7.55	13.45	0.24	0.76	1.07
	Acetonitrile	1.34	13.55	0.08	0.92	1.07
5b	1,4-dioxane	-	12.86	-	1.00	1.05
	THF	-	12.01	-	1.00	1.05
	DMSO	0.83	2.65	0.11	0.89	1.12
	DMF	0.99	3.28	0.11	0.89	1.14
	Acetonitrile	-	11.48	-	1.00	1.12
5c	1,4-dioxane	-	13.88	-	1.00	1.11
	THF	3.77	13.66	0.08	0.92	1.00
	DMSO	7.20	11.97	0.24	0.76	1.17
	DMF	5.58	12.67	0.07	0.93	1.18
	Acetonitrile	1.44	13.75	0.05	0.95	1.12
5d	1,4-dioxane	-	12.39	-	1.00	1.05
	THF	-	11.55	-	1.00	1.07
	DMSO	5.22	8.62	0.25	0.75	1.23
	DMF	-	10.51	-	1.00	1.19
	Acetonitrile	1.77	12.00	0.06	0.94	1.11

Compound **5b** showed an interesting behaviour due to its 4-hydroxyphenyl substituent. In the presence of the solvents DMSO and DMF, this compound exhibited biexponential dynamics, with the short components smaller than 1 ns. The fluorescence decays are shown in Figure 16. This phenomenon can be ascribed to the compound being deprotonated when exposed to proton acceptor solvents, as mentioned in paragraph 4.2.1. Consequently, the emission originated from the formed phenolate ion can take place. This evidence was confirmed by literature data reporting values for the second decay of **5b** in DMSO and DMF in agreement with the fluorescence lifetime of the phenolate anion.[112; 119]

Then, taking into account that the solvent assisted excited state proton transfer may occur in this compound, if we utilize **5a** as a model compound, its comparison with **5b** enable us to evaluate the rate constant of proton transfer (k_{pt}). Using an approximation of a very fast excited state intramolecular charge shift, we have the following equation.[112]

$$k_{pt} = \left(\frac{1}{\tau_1}\right)_{5b} - \left(\frac{1}{\tau_1}\right)_{5a} \quad (8)$$

By utilizing equation (8), the k_{pt} values in DMSO and DMF were determined to be 1.3 10^9 s^{-1} and 0.9 10^9 s^{-1}, respectively. This result suggests that the excited state deactivation rate *via* deprotonation occurs in a rate similar to that verified in the solvent assisted proton transfer studied by Kasha and coworkers.[112; 120]

Compound **5c** followed the same trend as **5a**, but only in 1,4-dioxane the behavior was monoexponential, while for the other solvents the best model fitted was biexponential. To explain such biexponential behavior, it is possible to make use of the model proposed by Chandross and coworkers for intramolecular exciplex systems,[118] characterized by high dipole moments and fluorescence quantum yields that decrease with the increase in solvent polarity. Therefore, the short components can be ascribed to a weak 1:1 complex between the compound and the solvent, while the long-lived components can be ascribed to a specific interaction between the excited state with push-pull character and the electron donor solvent.[112] A similar behavior was identified for compound **4a**, and is discussed in paragraph 4.1.2.

Compound **5d** has a 4-chlorophenyl substituent, which is an electron acceptor. However, this moiety did not interfere in the dynamical and spectral properties in respect of compounds **5a** and **5c**. It can indicate that the charge shift, from the donor 4-methoxyphenyl group to the acceptor carbonyl, is operating at the charge shift process. In addition, the presence of the second aryl group with the chloride substituent did not promote any significant effect in the global charge shift process.[112]

4.2.3 Dipole moment analysis

Fluorophores with the ability to shift the position of their emission bands according to the solvent polarity, solvatochromic shift, constitute valuable probes to monitor micropolarity of their immediate surroundings.[121; 122] This effect can be investigated by the Lippert-Mataga

approach,[115; 116] which correlates the solvent polarity effect with the Stokes shift,[4; 93] using the following equations:

$$\nu_A - \nu_F = \frac{2}{hca^3}\Delta f(\mu_E - \mu_G)^2 + C \quad (9)$$

$$\Delta f = \frac{\varepsilon - 1}{2\varepsilon + 1} - \frac{n^2 - 1}{2n^2 + 1} \quad (10)$$

In equation (9), $\nu_A - \nu_F$ is the Stokes shift (cm^{-1}), a is the radius of the Onsager cavity, h is the Planck constant, c is the speed of light, C is a constant, and μ_E and μ_G are the dipole moments in the excited state and in the ground state, respectively. In equation (10), Δf is a parameter named orientation polarizability that is evaluated from the dielectric constant ε and the refraction index n of the solvent. The Lippert-Mataga plot of compound **5a** is exhibited in Figure 17.[112]

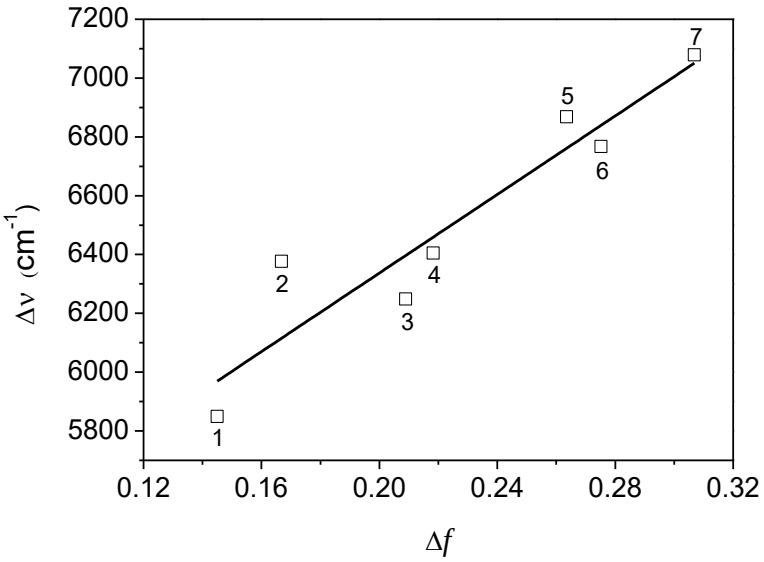

Figure 17. Lippert-Mataga plot of the compound **5a**. 1: Di-*n*-propyl ether, 2: diethyl ether, 3: THF, 4: CH_2Cl_2, 5: DMSO, 6: DMF, 7: acetonitrile. The linear correlation coefficient, r, is 0.85.[112]

By using equation (9), a positive slope of 6681 cm^{-1} was obtained. For the other compounds, **5c** and **5d**, reasonable linear coefficients were found, which did not indicate the presence of strong specific effects of the solvent. From the difference in dipole moments according to equation (10) and utilizing the values of the ground state dipole moments evaluated by theoretical computations (DFT), the excited state dipole moments of the maleimide

derivatives could be evaluated and the values are summarized in Table 5. The optimized geometry of these molecules and the contribution of each axis for the dipole moment are exhibited in Appendices 2.

Table 5. Theoretical parameters and evaluated excited state dipole moments.[112]

Compound	a_0 (Å)	μ_G (D)	Δμ (D)	μ_E (D)
4a	5.5	8.7	10.6	19.3
5a	6.0	4.3	11.9	16.2
5c	5.9	4.2	12.5	16.7
5d	5.7	3.0	12.6	15.6

The differences between the excites state and the ground state dipole moments were determined in the range of 11 and 13 D, which suggests the contribution of a excited state charge shift.[123; 124] Compound **5b** did not provide a good linear correlation, probably due to interactions with solvents, like the deprotonation process in polar solvents, as previously discussed. The dipole moments of compound **4a** were also reported in this section, because it was the only maleic anhydride derivative with these properties evaluated.

4.3 Photophysical study of the phenanthrene derivatives

4.3.1 Steady-state analysis of the maleic anhydride derivatives

The phenanthrene derivatives, those originating from the maleic anhydride cyclization, as well as those derived by the maleimide cyclization, showed good thermo- and photochemical stability. These molecules are structurally advantageous, so they present lower non-radiative energy loss, because the molecules previously studied have more rotational freedom degrees.

Two pairs of analogue compounds were analysed, the pair **7a** and **8a** and the pair **7b** and **8b**. The absorption spectra of compound **7a** showed three bands, as can be seen in Figure 18, which is characteristic from compounds containing condensed rings. The position of these bands depends on the solvent polarity, and a change of 17 nm from 1,4-dioxane to DMSO was observed. The emission spectra exhibited broad bands with the maximum emission wavelengths centred between 464 nm and 505 nm. There was a large Stokes shift

of about 98 nm in acetonitrile and in DMF. This compound also showed a considerable solvatochromic shift to the red region, of about 41 nm. The steady-state spectral data are available in Table 6.

Table 6. Stationary data of the phenanthrene derivatives.

Compound		Solvent	λ_{abs} (nm)	λ_{em} (nm)	$\Delta\nu$ (cm^{-1})	ϕ_F
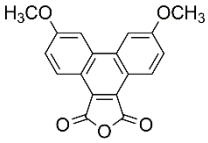	**7a**	1,4-dioxane	391	464	4024	0.52
		THF	396	468	3885	0.72
		DMSO	408	505	4707	0.09
		DMF	401	499	4898	0.32
		Acetonitrile	408	496	4964	0.56
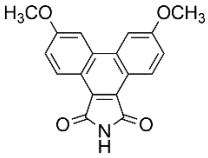	**8a**	1,4-dioxane	397	488	4697	0.92
		THF	398	477	4161	0.69
		DMSO	402	504	5034	0.57
		DMF	408	500	4510	0.46
		Acetonitrile	402	501	4916	0.54
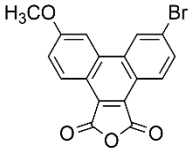	**7b**	1,4-dioxane	385	454	3948	0.42
		THF	388	463	4178	0.30
		DMSO	392	499	5470	0.02
		DMF	391	495	5373	0.08
		Acetonitrile	390	487	5107	0.62
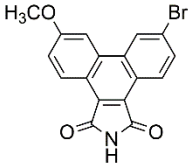	**8b**	1,4-dioxane	388	462	4128	0.70
		THF	388	463	4175	0.77
		DMSO	394	495	5179	0.45
		DMF	392	486	4934	0.56
		Acetonitrile	391	489	5126	0.45

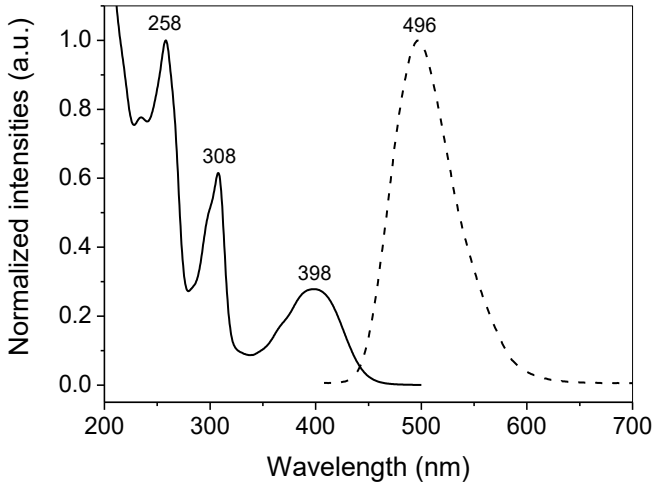

Figure 18. Normalized absorption and emission spectra of compound **7a** in acetonitrile.

For compound **8a**, the absorption spectra also showed three bands, with the low energy absorption band centred around 397 nm for 1,4-dioxane, and around 408 nm for DMF. In this case, the spectral shift with the solvent polarity was smaller (by 11 nm) than the corresponding spectral shift found for the compound **7a**. The Stokes shifts were of a similar magnitude, 102 nm for DMSO and 79 nm for THF. For this compound, the solvatochromic shift was much lower (27 nm). There is not a large difference regarding the band position as a function of the solvent polarity, especially for solvents of intermediate polarity, such as DMF, acetonitrile, and DMSO, as illustrated in Figure 19. For the analogue pair **7b** and **8b**, which contains the bromide substituent, similar trends were observed.

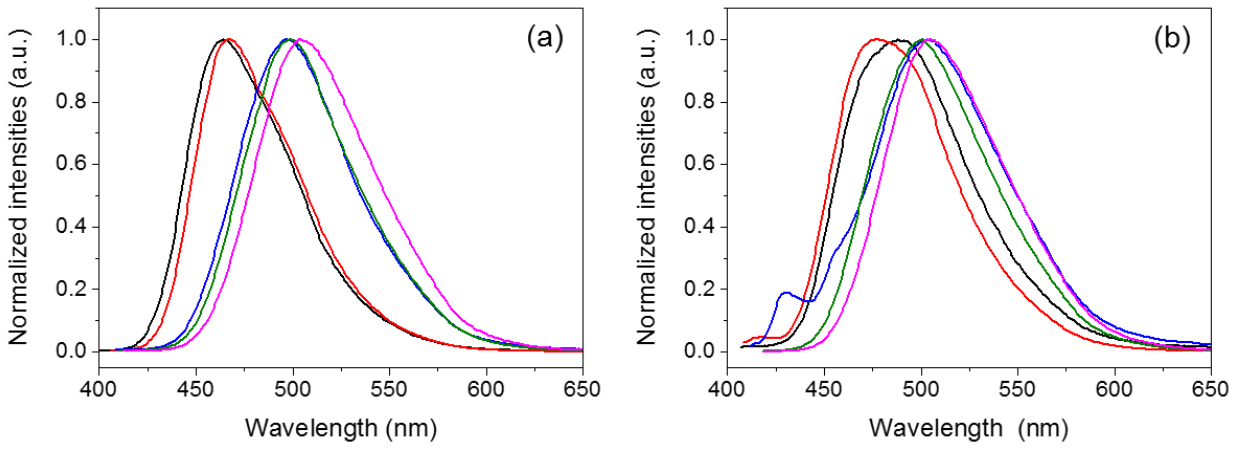

Figure 19. Solvatochromic shift of emission spectra of compound **7a** (a) and compound **8a** (b) in 1,4-dioxane (black), THF (red), acetonitrile (blue), DMF (green), and DMSO (magenta).

The quantum yield enhancement of the phenanthrene derivatives is remarkable in comparison with the other derivatives. This occurs due to the decrease of structural flexibility upon the rings condensation, which decreases the loss of fluorescence efficiency by internal conversion. The most notable quantum yield was found for compound **8a** in 1,4-dioxane being 0.92.

4.3.2 Time-resolved analysis of the phenanthrene derivatives

The fluorescence decays showed a biexponential behaviour in general. Additionally, the contribution of the short-lived component of the intensity of the entire decay is always reduced. It is important to mention that fluorescence decays of phenenthrene derivatives were analysed by the global approach. The fluorescence decays are shown in Figure 20 and the parameters extracted from the time-resolved experiments are reported in Table 7.

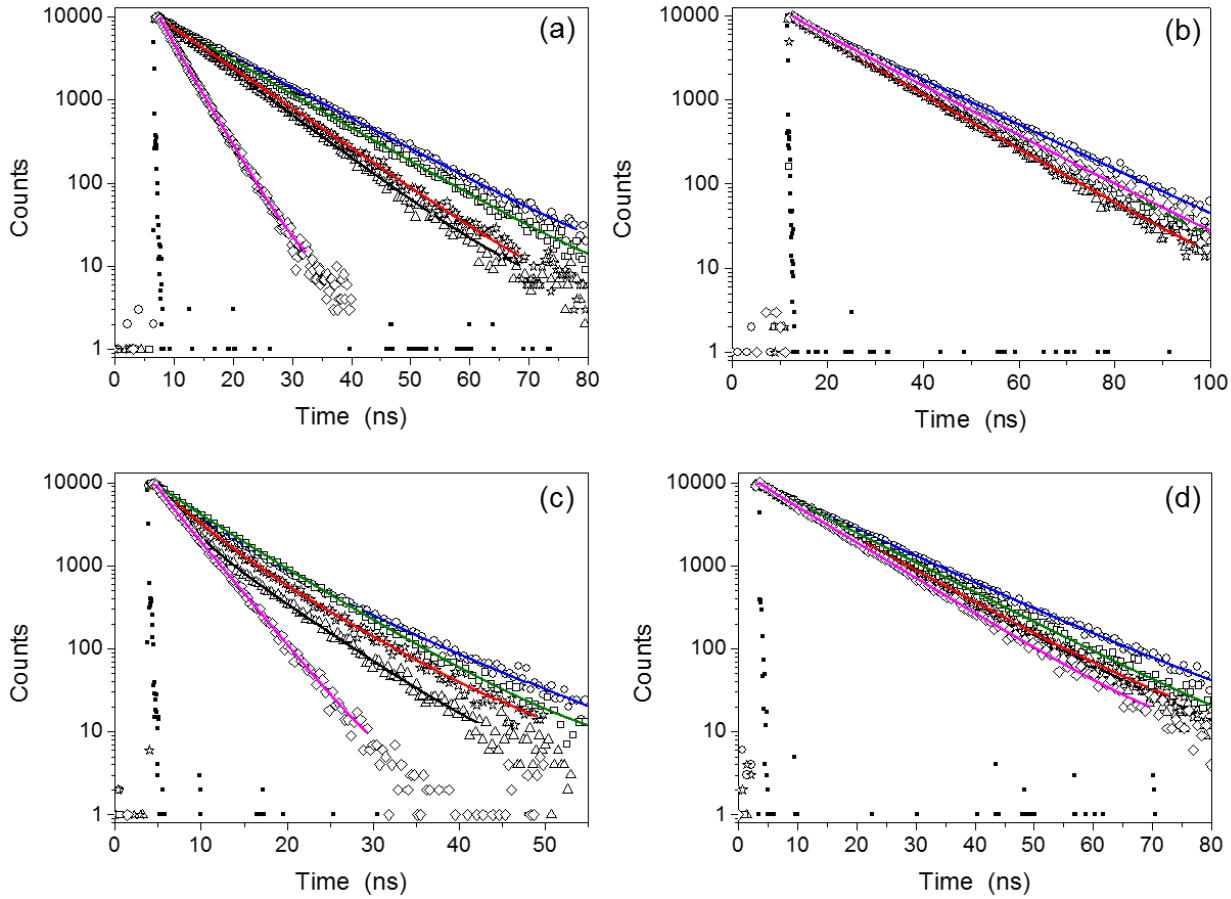

Figure 20. Fluorescence decays of compounds **7a** (a), **8a** (b), **7b** (c), and **8b** (d), in the respective solvents: acetonitrile (○); 1,4-dioxane (Δ); THF (☆); DMF (□); DMSO (◇). The decays were acquired in the maximum λ_{em} of each sample in its respective solvent. (■) irf; λ_{exc}= 400 nm.

Table 7. Time-resolved data of the phenanthrene derivatives.

Compound	Solvent	τ_1 (ns)	τ_2 (ns)	b_1	b_2	χ^2_g
7a	1,4-dioxane	0.94	8.45	0.05	0.95	1.15
	THF	1.17	9.03	0.05	0.95	1.18
	DMSO	0.88	3.60	0.13	0.87	1.35
	DMF	1.59	10.73	0.06	0.94	1.09
	Acetonitrile	1.45	11.75	0.06	0.94	1.09
8a	1,4-dioxane	-	12.98	-	1	1.25
	THF	1.10	13.24	0.15	0.85	1.18
	DMSO	1.84	14.70	0.08	0.92	1.11
	DMF	1.65	14.43	0.06	0.94	1.15
	Acetonitrile	1.34	16.29	0.05	0.95	1.13
7b	1,4-dioxane	2.26	6.34	0.66	0.34	1.13
	THF	3.70	7.80	0.68	0.32	1.15
	DMSO	1.06	3.52	0.14	0.86	1.28
	DMF	5.55	8.49	0.69	0.31	1.09
	Acetonitrile	4.72	9.82	0.72	0.28	1.14
8b	1,4-dioxane	6.31	11.41	0.13	0.87	1.19
	THF	6.79	11.43	0.12	0.88	1.19
	DMSO	4.50	10.20	0.05	0.95	1.26
	DMF	7.70	12.28	0.09	0.91	1.20
	Acetonitrile	7.54	13.56	0.08	0.92	1.23

Similarly to the compound **4a** and to some maleimide derivatives, the excited state dynamics of these phenanthrene derivatives may be related to the charge delocalization and push-pull effect in the excited state,[86] the fast components of the biexponential model may be related to a weak complex between the compound and the solvent, as proposed by Chandross *et al*.[118] This effect can be observed mainly for the maleic anhydrides **7a** and **7b** in DMSO, which exhibited short lifetimes, as well as the precursor **4a**. Moreover, this effect can be supported by the quantum yields values reported in Table 6. It is notable that the quantum yield of the phenanthrene derivatives **7a** and **7b** were lower in more polar solvents, like DMSO and DMF, than those of the maleimide-based analogues **8a** and **8b** under the same

conditions. Comparing the analogue compounds **4a** and **7a**, the quantum yields were slightly enhanced, from 0.05 for **4a** to 0.09 for **7a**, due to the decrease in the number of the rotational degrees of freedom.

4.3.3 Photophysical study and imaging by confocal microscopy

The phenanthrene derivatives showed good photochemical stability when exposed to a laser beam, i.e., the dye did not suffer a spontaneous photobleaching after laser exposure, as verified for compound **4a**, which was completely bleached. To examine the potential of these compounds for use as fluorescent probes for optical microscopy, bulk experiments were performed, by means of confocal microscopy.

Emission spectra as well as fluorescence decays were carried out in acetonitrile solutions and in a polyvinylpyrrolidone (PVP) matrix. Imaging was performed in a PVP matrix containing such dyes. The images are related to regions of the polymeric layer where the dye molecules tend to be more concentrated. The maxima of the emission bands showed a red shift and are centred around 525 nm, as observed in Figure 21 (a).

The decays in solution of acetonitrile followed a biexponential behaviour and the lifetimes were very similar to those determined by the conventional technique, as described in section 4.3.1. It is important to mention that by the microscopic technique the decays were not deconvoluted with the instrumental response function (irf). Therefore, some differences may be observed in the fitting parameters, mainly for the fast components. The decay of compound **7a** is illustrated in Figure 21 (b). However, for the decays obtained for the sample prepared in the PVP matrix, the long-lived components ranged from 4.90 ns to 8.71 ns.

In polymeric matrices, the dye molecules tend to concentrate in micro domains formed by the polymer chains, which allows the acquisition of fluorescence maps of such regions. An example can be visualized in Figure 21 (c) and corresponds to a fluorescence map of compound **7a** concentrated in a micro region of the PVP layer. The colour scale is related to the fluorescence intensity, and the highest intensity is represented by the colour red.

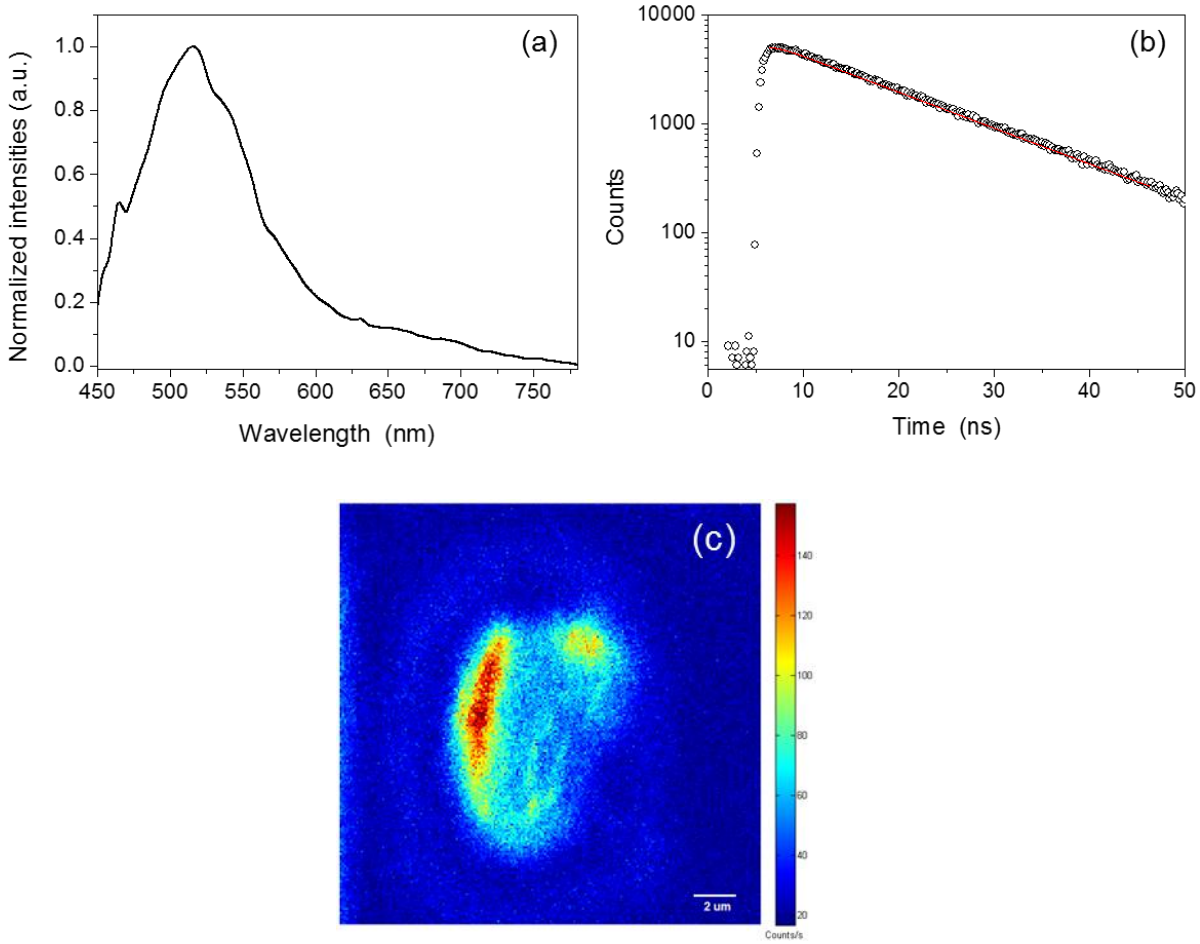

Figure 21. Normalized emission spectrum (a) and fluorescence decay (b) of compound **7a** in acetonitrile. (c) Confocal microscopy image of compound **7a** 1.0 x 10^{-7} M, concentrated in a region of the PVP matrix.

5 CONCLUSIONS

In summary, the photophysical study of a series of natural products-inspired maleic anhydride and maleimide derivatives was performed. The fluorescent properties of these compounds were modulated by the type of solvent and by the substituents effect. All the compounds showed a positive solvatochromic shift and a notable charge shift in the excited state, which can be attributed to the push-pull effect. Specifically, the bisarylated maleimides presented a difference between the excited and ground state dipole moments of about 12 D, which supports this conclusion.

In particular, the phenanthrene derivatives, mainly the maleimide-containing molecules, have the advantage of being structurally more rigid than the bisarylated compounds. When applied to confocal microscopy experiments, we were able to study the local solvent properties, affecting the fluorescence relaxation dynamics in different condensed media.

Therefore, based on the photophysical properties, one can infer that the most stable maleimides, such as **5a**, **5c**, **5d**, and **8**, are potential solvatochromic probes. Additionally, these molecules open the door for the synthesis of derivatives containing a spacer and a functional group, which allow for the specific and covalent *in vitro* labelling to a target material.

CHAPTER 3

Investigation of DNA fluorescent labelling strategies by super-resolution optical microscopy and atomic force microscopy

1 INTRODUCTION

The methyltransferase enzymes catalyse the transfer of a methyl-group from their natural cofactor S-adenosyl-L-methionine (AdoMet) in a targeted fashion to DNA, RNA and proteins, as previously documented in section 3.3 from Chapter 1. However, multiple studies pioneered by the Klimasauskas and Weinhold groups[125] have reported that these enzymes are catalytically active with a range of AdoMet analogues, hence they are capable of transferring much more complex chemical moieties to DNA. For instance, extended moieties containing functional groups[126; 127; 128; 129; 130] or fluorescent probes[45; 131; 132; 133] instead of the methyl group can be transferred in a specific and covalent transfer. This technology was named methyltransferase-directed Transfer of Activated Groups (mTAG).

Thus, when using AdoMet analogues containing functional groups, the mTAG approach enables fluorescent labelling of DNA using a two-step procedure, as schematized in Figure 22. The first one consists of a specific DNA modification with an alkyne, an azide, or an amine group using methyltransferase as a catalyst. The enzyme M.TaqI catalyses the S_N2 nucleophilic substitution of the exocyclic N6 of adenine from the target sequence 5'- TCGA - 3' onto the sulphonium-bound extended chain of the AdoMet analogues. Subsequently, the fluorophore attachment is performed by a suitable bioorthogonal reaction.[46; 47; 48]

Another methodology enabled by the mTAG approach is the direct coupling of a fluorophore to the DNA using a one-step reaction. The direct single-step labelling was firstly reported by Weinhold and co-workers using fluorescent aziridine-based cofactors.[131] A recent work of the Klimasauskas group has also reported the use of this strategy to label RNA duplexes using the HEN1 MTase.[133] Additionally, another recent work from Weinhold's group reports on the synthesis of the 7-deazaadenosylaziridine cofactor modified with a biotin or dansyl fluorophore, which was efficiently used by the M.HhaI MTase to label a duplex DNA in a one-step reaction.[134]

According to the methodology adopted in this research, the direct one-step reaction is effected firstly by coupling a dye to a target cofactor and then, labelling the DNA using MTaqI as a catalyst, as schematized in Figure 23.

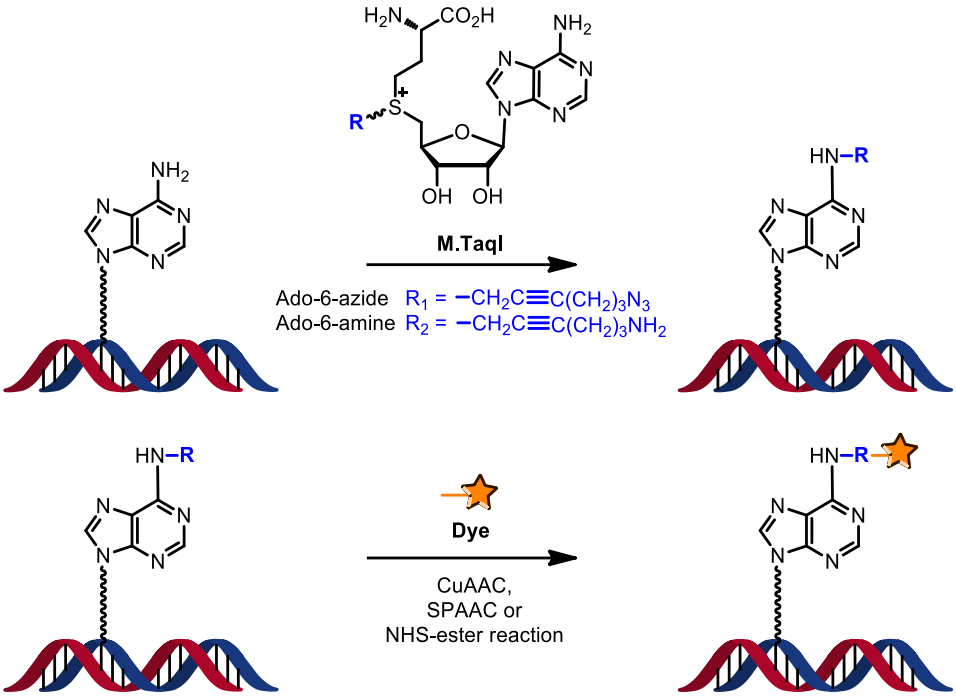

Figure 22. General scheme of the two-step sequence-specific fluorescent labelling of pUC19 plasmids.

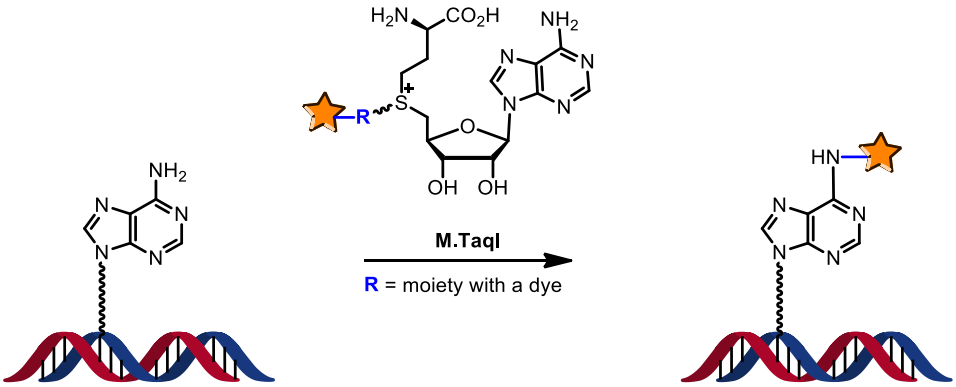

Figure 23. General scheme of the direct one-step sequence-specific fluorescent labelling of pUC19 plasmids.

The mTAG technology has been successfully implemented for nucleic acid sequence-specific fluorescent labelling directed towards different applications. The advantage of the fluorescent labelling in well-known sequences of the DNA favours the use of such technology to DNA sequencing purposes. For instance, genomic DNA was fluorescently labelled by the mTAG approach using the DNA MTase M.HhaI for optical mapping, achieving a resolution of less than 20 bases.[135] The two-step methodology was also used to label DNA using the CuAAC click reaction to couple fluorophores. The study then reported the super-resolution

map of DNA sequence.[63] The mTAG approach also opens the doors to be employed in techniques where sequence-specific labelling is pivotal, such as super-resolution fluorescence *in situ* hybridization.[136]

In this research, the plasmid pUC19 was covalently labelled with fluorophores in sequence-specific regions by enzymatic transfer using synthetic cofactors. All the strategies were investigated by super-resolution experiments and by AFM measurements. Furthermore, AFM imaging was used to verify the DNA topology after the fluorescent labelling reactions. The retention of the ability to encode genetic information, despite the fact that they carry fluorophores in the DNA sequences encoding genes, was also examined by transfection experiments into mammalian cells using the methylase-functionalized plasmids.

2 OBJECTIVES

The main purpose of this chapter is to study the strategies of sequence-specific DNA fluorescent labelling using super-resolution fluorescence microscopy. To determine the optimal methodology for DNA labelling, the following specific objectives were established:

- Optimization of the bioorthogonal reactions for the fluorophore coupling to the DNA. These are: Click reactions catalysed by copper or not and the primary amine-to-NHS-ester coupling;
- Evaluation of the number of fluorophores covalently attached to single plasmids by super-resolution microscopy experiments;
- Investigation of the morphology of the plasmids after fluorescent labelling by atomic force microscopy (AFM) imaging.

With the knowledge concerning the fluorescent labelling optimizations, we propose the following actions:

- Application of plasmids labelled by an optimal methodology to mammalian cells;
- Application of the fluorescent labelling technology to FISH probes.

3 METHODOLOGY

3.1 Materials

pUC19 plasmid (1µg/µL), NEBuffer 4, CutSmart® buffer, TaqI methyltransferase and proteinase K were purchased from New England Biolabs. TaqI methyltransferase was purified prior to use. Atto-647-N-propargylamide and Atto-647N-NHS-ester (Atto-Tec) were diluted in DMSO to a final concentration of 20 mM and stored at -20 °C. A stock solution of YOYO-1 (Invitrogen), 5 µM, was prepared in DMSO and kept at -20 °C. Ethanol spectroscopic grade was purchased from Merck. All other reagents (PLL 0.1% w/V in H_2O, Tris, EDTA, sodium chloride, sodium ascorbate, sodium bicarbonate, mercaptoethylamine - MEA, cupric sulphate, tris[(1-hydroxypropyl-1*H*-1,2,3-triazol-4-yl)methyl]amine - THPTA, DMSO, DMF, D-(+)-glucose, catalase C-1345 and glucose oxidase G-7141) were purchased from Sigma-Aldrich and used as received.

For the Cu-catalysed reaction, a 50 mM solution of sodium ascorbate was freshly prepared. The purification of plasmids was also performed by silica-based spin columns from Zymo Research, code D4004. For optical microscopy experiments, an imaging buffer 10x was prepared using 500 mM Tris/HCl, 500 mM NaCl and 10 mM EDTA, pH = 7.70. For biological experiments Fugene 6 (Roche), DMEM (Dulbecco's Modified Eagle's Medium, Invitrogen), FBS (Fetal Bovine Serum, Sigma-Aldrich) and DiI (1,1′-dioctadecyl-3,3,3′,3′-tetramethylindocarbocyanine perchlorate, Molecular Probes) were used.

3.2 Cu-catalysed azide-alkyne cycloaddition (CuAAC)

3.2.1 Preparation of sequence-specific modified plasmid DNA using the azide cofactor and M.TaqI for CuAAC

This reaction produces the modified DNA with an azide group. For that, 5 µg of pUC19 DNA was functionalized in a 100 µL reaction composed of 10 mM Tris, 1 mM NaCl, 0.5 mM EDTA, 0.1 mg/ml BSA, and 0.01% Triton X-100 using 120 µM AdoMet analogue cofactor functionalized with an azide group (Ado-6-azide),[128] 2.5 µL of purified TaqI methyltransferase. The reaction was incubated at 60 °C for 2 h. Subsequently, 1 µL of proteinase K was added to digest the methyltransferase. The system was gently mixed, and incubated at 55 °C for 1 h. The system was purified using silica-based column and the DNA

was eluted in 25 μL of the elution buffer (10 mM Tris-HCl, 0.1 mM EDTA, pH 8.5). The sample was stored at 4 °C.

3.2.2 Fluorophore coupling by CuAAC reaction

For the coupling of a fluorophore to the DNA by the Cu-catalysed click reaction, a mixture of 25% of DMSO, 200 μM Atto-647-N-propargylamide, 200 μM $CuSO_4$ and 2 mM THPTA was added to 100 μL of the azide labelled DNA (~ 0.86 μg DNA) previously prepared. Then, 5 mM of a fresh sodium ascorbate solution was added to the sample, which was incubated at room temperature for 30 minutes.

Afterwards, the purification was performed by ethanol precipitation or using silica-based spin columns. For ethanol precipitation, 15 μL of a 3 M NaCl and 495 μL of ethanol (100%) were added. Then, the mixture was centrifuged at 14000 G for 10 minutes. The supernatant was removed and the pellet of DNA was washed with 200 μL of 70% ethanol. The pellet was suspended by adding 20 μL of a buffer at pH = 8.4, composed of 10 mM Tris-Cl and 1 mM EDTA. The solution was incubated at 50 °C for 1 h. The process of ethanol precipitation was repeated following the respective proportions. After this process, the ligand THPTA was added at a final concentration of 1 mM, in order to prevent DNA damage caused by copper oxidation. The scheme of the two-step labelling is illustrated in Figure 24.

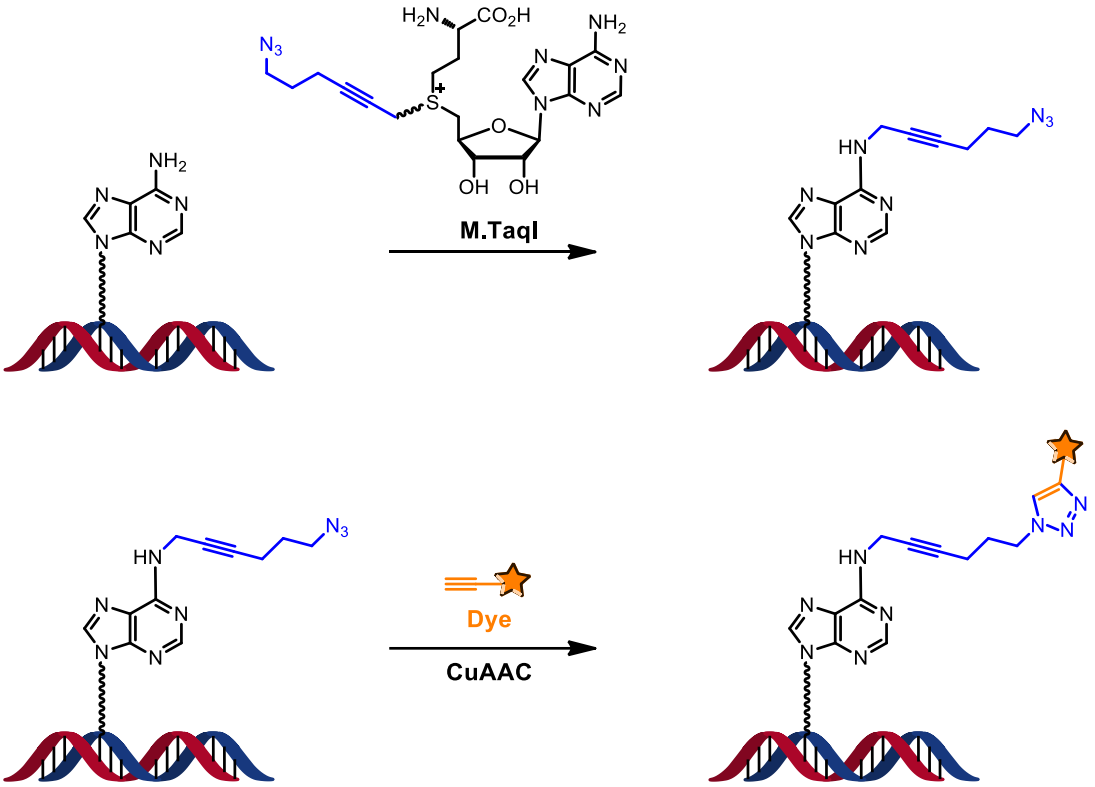

Figure 24. Scheme of the DNA labelling by the Cu-catalysed click reaction. In the first step, the plasmid was functionalized with an azide moiety. In the second step, the fluorophore containing an alkyne group was coupled to the modified DNA.

3.2.3 CuAAC reaction with ClickOx approach

The Cu-catalysed reaction was also performed in the presence of an enzymatic oxygen scavenger system, the ClickOx approach, as recently published.[137] The same procedure as mentioned in paragraph 3.2.1 was used to obtain the azide functionalized DNA. For a 100 µL reaction, 1% glycerol (stock solution of 10%), 1% glucose (stock solution of 10%), 2 U glucose oxidase and 40 U catalase (both from stock solutions 100x) were added to the same contents of the second step of the CuAAC reaction (paragraph 3.2.2). The enzymatic system (100x) contained 200 U/mL of glucose oxidase, 4000 U/mL of catalase, 25 mM KCl, 22 mM Tris/HCl (pH = 7) and 50% of glycerol. The purification was performed using silica-based columns.

3.3 Strain-promoted azide-alkyne cycloaddition (SPAAC)

3.3.1 Preparation of sequence-specific modified plasmid DNA using the azide cofactor and M.TaqI for Cu-free reaction

The methodology for the DNA functionalization with azide groups was slightly modified in comparison with the previous methodology presented in 3.1.1. In this case, for a final volume of 100 µL, NEBuffer™ 4 (10x), 10 µg pUC19 plasmid, 300 µM of the Ado-6-azide cofactor,[128] 2.5 µL of TaqI methyltransferase and Milli-Q water were mixed and incubated at 60 °C for 2 h. Subsequently, 1 µL of proteinase K was added, the system was kept at 55 °C for 1 h and purified using a silica-based column. For the subsequent copper-free reaction, the pellet was suspended in 20 µL of Milli-Q water.

3.3.2 Fluorophore coupling by SPAAC reaction

The click reaction in the absence of a copper catalyst was performed between the azide functionalized DNA and the dye rhodamine B containing a cyclooctyne group. This reaction was tested in different solvents to obtain the best reaction parameters. Figure 25 schematizes this methodology.

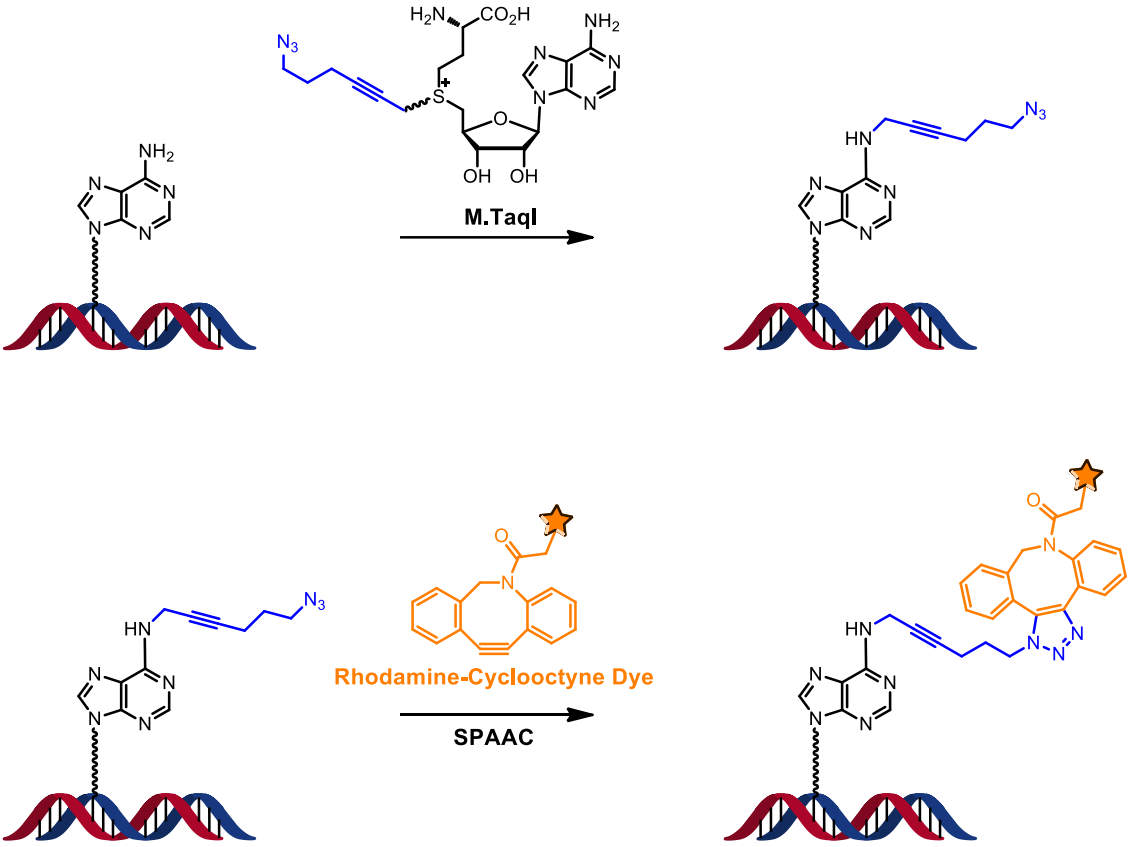

Figure 25. Scheme of the two-step labelling using the strain-promoted azide-alkyne cycloaddition for the fluorophore coupling to the DNA.

3.3.2.1 Effect of the solvent

To investigate in which solvent the SPAAC reaction has the best performance for coupling the fluorophore, this reaction was carried out in four solvents. For that, the sample of the azide functionalized and purified DNA (20 µL) (paragraph *3.2.1*) was divided in four parts, with ~1 µg of the azide coupled pUC19 DNA. The SPAAC reaction was performed in Milli-Q water, 60% ethanol, 50% DMSO and 30% DMF using 1 mM of the cyclooctyne-rhodamine B dye (final volume = 50 µL). The reactions were incubated overnight at room temperature and then purified by spin-columns. The resultant pellets were suspended in 20 µL of Milli-Q water.

3.3.2.2 Effect of the DMSO concentration

A similar procedure as reported in paragraph 3.3.2.1 was performed to investigate the effect of the DMSO concentration. The labelling reactions were carried out in 0%, 10%, 25%, 50% and 75% DMSO, using ~1 µg of the pUC19 plasmid functionalized with azide groups, and a final concentration of 1 mM of cyclooctyne-rhodamine B. The reactions were incubated overnight at room temperature and, subsequently, purified using silica-based columns.

3.4 Amine-to-NHS-ester coupling

3.4.1 Preparation of sequence-specific modified plasmid DNA using the amine cofactor and M.TaqI for NHS-ester reaction with primary amines

In this step, a moiety containing a primary amine group is linked to the plasmid. The reaction mixture with a final volume of 100 µL contained 10 µg of pUC19, CutSmart® buffer (10x), 120 µM of the Ado-6-amine cofactor,[128; 133] 2 µL of the enzyme M.TaqI, and Milli-Q water to complete the volume. This system was incubated for 2 h at 60 °C. After that, 1 µL of proteinase K was added and the system was incubated for 1 h at 55 °C. The purification was performed using silica-based columns and the elution procedure utilized 25 µL of Milli-Q water.

3.4.2 Fluorophore coupling using the amine-to-NHS-ester reaction

To determine the best condition to perform this step in terms of DMSO concentration, the reactions were carried out in different concentrations of this solvent. To a 50 µL reaction mixture containing, 0.89 µg of the DNA functionalized with an amine group, 0.01 M PBS buffer, 500 µM of the Atto-647N-NHS-ester dye and the volumes of DMSO corresponding to 5%, 10%, 25% and 30% were added. The systems were incubated for 2 h at room temperature and purified by silica-based columns. The fluorescently labelled DNA was eluted using the elution buffer provided by the manufacturer. The reaction is illustrated in Figure 26.

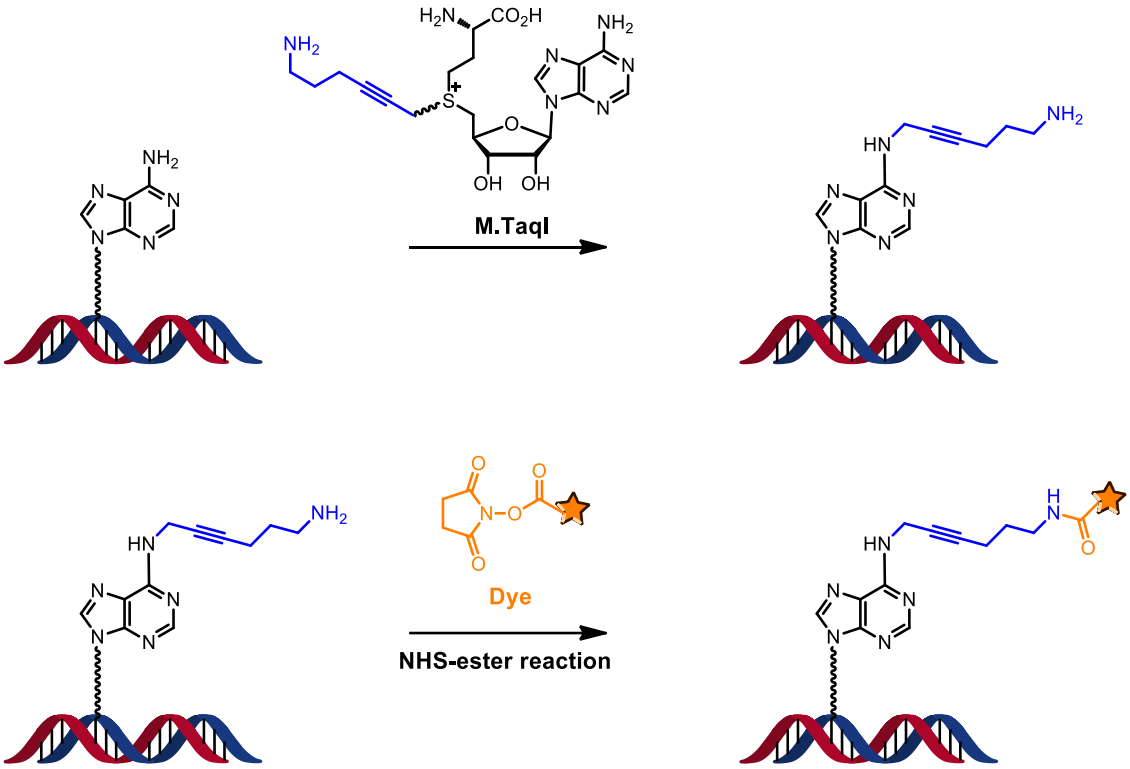

Figure 26. Scheme of the two-step labelling using the amine-to-NHS-ester coupling.

3.5 Direct one-step reaction

This approach involves only one-step, in which the fluorescent group is directly transferred from the cofactor to the DNA by the action of the methyltransferase. Firstly, the dye was coupled to an amine-functionalized cofactor. For that, in a 4 µL reaction, 25% DMSO, 0.01 M PBS buffer, 1 mM of the Ado-6-amine cofactor[128; 133] and 2.5 mM of the Atto-647-N-NHS ester were mixed and kept on ice for 10 minutes. Subsequently, 2 µL of the NEB CutSmart® buffer was added to quench the reaction. After 1 minute, 2 µg of the pUC19 plasmid, 0.5 µL of M.TaqI enzyme and 11.5 µL of Milli-Q water were added. The system was incubated at 60 °C for 1 h. After this time, 1 µL of proteinase K was added to the reaction mixture which was subsequently incubated at 55 °C for 1 h and purified using a silica-based column. This methodology is schematized in Figure 27.

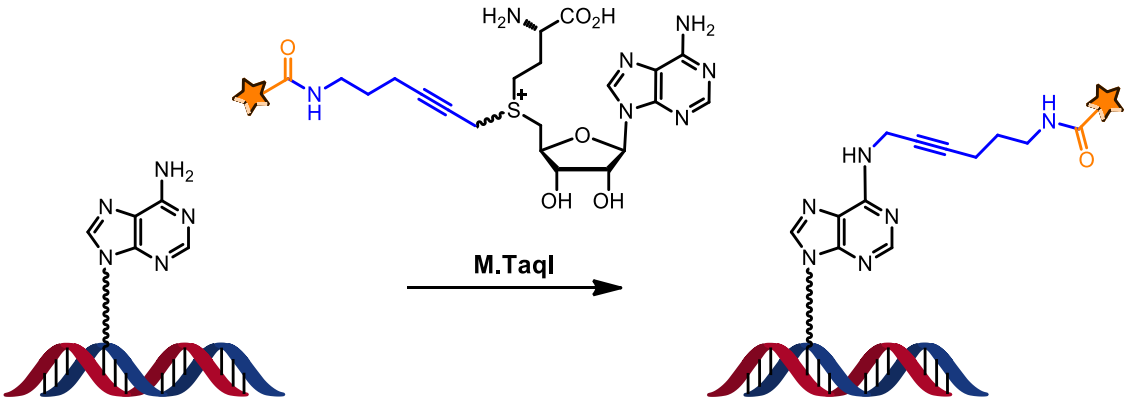

Figure 27. Scheme of the direct one-step labelling. In this methodology, the fluorophore is transferred from the cofactor to the plasmid.

3.6 Sample preparation for microscopy analysis

The coverslips used in this research (0.13 mm, 22 x 22 mm, VWR International) were cleaned according to the following procedure: rinsing thoroughly with Milli-Q water, drying with argon gas and overnight storing in a muffle at 450 °C. The coverslips as well as the DNA structures are negatively charged, therefore, it was necessary to deposit a positively charged polymeric layer onto the coverslip to enable the DNA deposition. The coverslips were coated by adsorption with a solution of the polymer poly-L-lysine (PLL) (0.01% w/v in H_2O) for 15 minutes, then rinsed with Milli-Q water and carefully dried with argon gas. Subsequently, 50 µL of a DNA solution (fluorescently labelled DNA at a final concentration of ~ 0.5 – 1 ng/µL, using the imaging buffer as a solvent) was spin-coated onto a PLL-coated slide at a rotation speed of 2500 min^{-1}. After that, the coverslip was rinsed with 5 mL of Milli-Q water, in a drop-wise fashion, at the same rotation speed and dried under a gentle flow of argon gas. This process stretches the DNA molecules and removes the unbound materials.

3.7 Fluorescence microscopy setup

The images were acquired using an inverted wide field microscope Olympus IX83 operating in Total Internal Reflection Fluorescence (TIRF) module. The objective used was a UAPON NA 1.45, with a magnification of 150x. The microscope was coupled to an EM-CCD digital camera Hamamatsu, model ImagEM, and to 405, 488, 561 and 640 nm solid-state diode laser lines, 150 mW (Spectra Physics).

3.8 BALM experiments

The basis of this research experiment is the Binding-Activated Localization Microscopy (BALM), reported by Vogel *et al.*, which is characterized by repeated cycles of binding, localization and bleaching, that enables the optical reconstruction of biological structures, like DNA molecules.[35]

For the BALM experiments, a perfusion chamber (8-9 mm diameter x 0.9 mm depth, Grace Bio-Labs) was sealed onto the DNA-coated coverslip. Then, 45 µL of a solution constituted of 5 nM YOYO-1, 50 mM MEA and the imaging buffer were introduced in the chamber. The measurements started immediately after this step. Figure 28 shows a scheme of the sample preparation for BALM experiments.

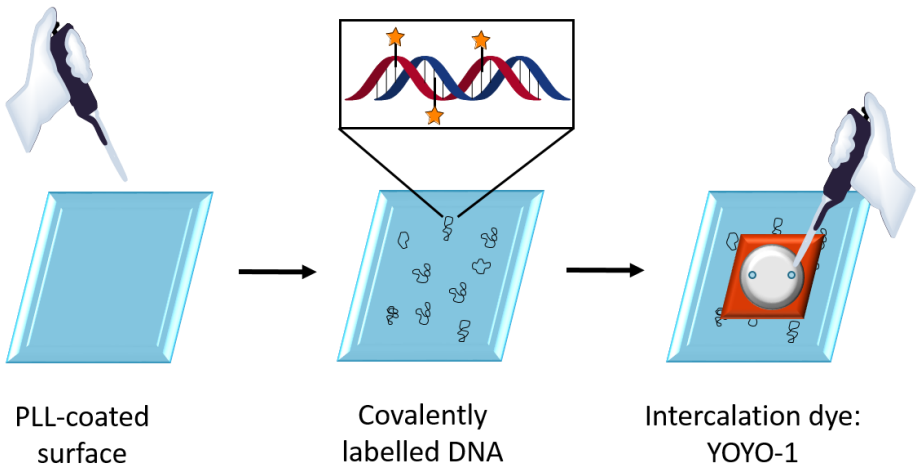

Figure 28. Scheme of the sample preparation for BALM measurements.

The system constitutes a two-colour-mapping experiment. For each system, five to ten movies were acquired in different parts of the same sample. At first, the so-called bleaching experiment was performed. 250 or 1000 frames were recorded to bleach the dyes covalently bonded to the plasmids. For the samples using the Atto-647N dye, they were illuminated with 640 nm laser at 100% or 30% power intensity and for the samples that were labelled with rhodamine-B dye, for example in Cu-free labelling, a 561 nm laser was employed at 50% laser power. The images were acquired until only a few individual molecules remained. After that, the 488 nm laser was switched on at full intensity and a delay time of 10 s was performed to bleach the YOYO-1 molecules. Then, 2000 frames were acquired at the same laser intensity. All sequences used an exposure time of 30 ms and an EM gain of 100. Each movie spent 2-3 minutes and the total number of frames was 2250 or 3000 per movie.

3.8.1 Data analysis

The data were analysed in two parts using the software *Localizer*.[138] Firstly, a bleaching fitting was performed to provide the number of labels that each plasmid is carrying. This procedure was previously described.[135] Taking into account that the process of photobleaching has a stochastic nature, a group of fluorophores photobleaches until only one remains.[24] Thus, the fluorescence emission of such fluorophores can be fitted as a 2D Gaussian. The procedure of analysis started from the last frame of the bleaching movie, where the appearing spots were fitted with a 2D Gaussian and subtracted from the previous images of the movie. Therefore, by the use of this strategy for all other frames of the movie, the emission of each fluorophore could be resolved.[135]

Secondly, the blinking images of the intercalating dye YOYO-1 provided data to create a high-resolution image of the plasmid structure, since several cycles of binding, localization and bleaching were established. The images were analysed by the software *Localizer*,[138] using the localization approach (PALM/STORM). For this analysis, the spot deviation was increased as a manner to compensate drift effects during the measurements.

To obtain a fluorescence map of the fluorescently labelled plasmids and to count the number of labels that each plasmid is carrying, it was necessary to overlap the images obtained by the both experiments: the image of the localization of the plasmids (from the YOYO-1 binding experiment) and the image of the fluorophores detected in the first part of the experiment (bleaching fitting). For that, a black and white image was created from the high-resolution YOYO-1 image. Then, spots were used to create an outline of the plasmid. This procedure was done using a home-developed program written in Matlab, termed *Counter*, developed by Dr Jochem Deen at KU Leuven.

We established some criteria to define an intact plasmid, accepted for data analysis. The corresponding image of an intact plasmid should have an area greater than 50 pixels^2, the circularity should be lower than the value of 1.7, where the circularity is defined by $c^2/4\pi A$. In this relation, c is the feature's perimeter and A the area. The plasmids with shapes different from these criteria were not analysed.

Subsequently, the plasmid outline was compared with the fitted 2D Gaussian to test if there were any localized emitters from the bleaching experiment fitted within the boundaries of the plasmid. Then, a histogram of all the labels was created containing 1, 2, 3, …, n labels from each experiment. The percentages of labels per plasmid were calculated. Figure 29 schematizes the procedure used for the data analysis. Typical data extracted from *Counter* can be found in the Appendices 4.

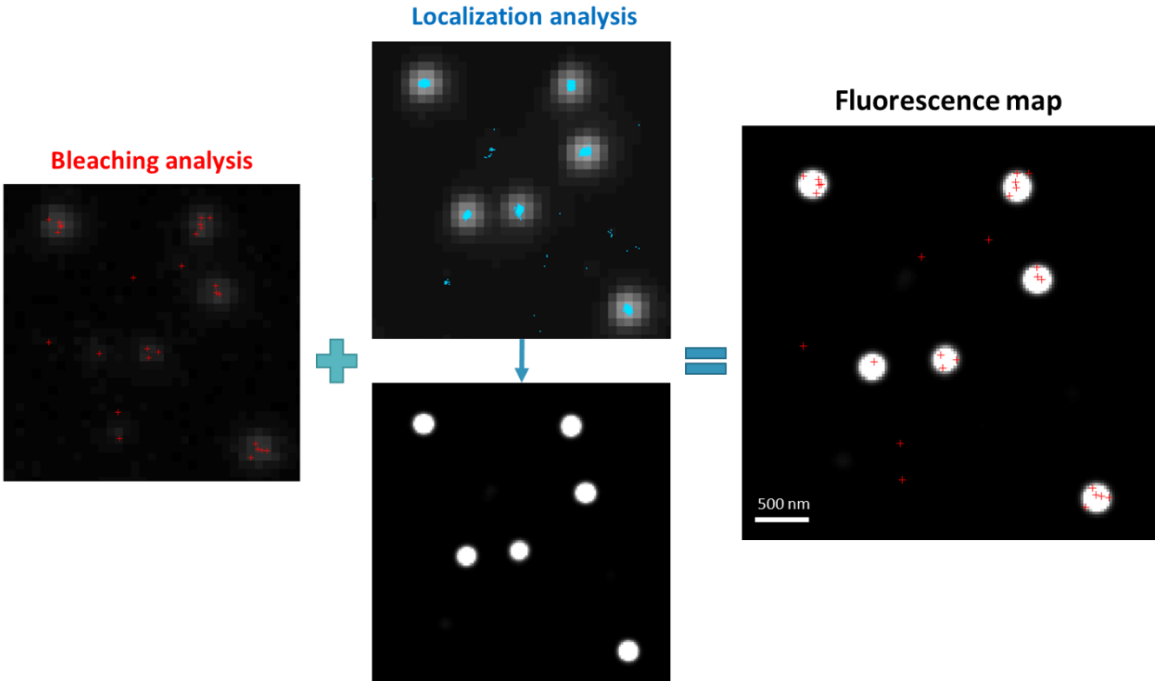

Figure 29. Scheme of the data analysis procedure. The images correspond to a region from the total frame. The sample utilized at this example originates from the pUC19 plasmids labelled with the Atto-647N dye, by the direct single-step reaction. In the bleaching analysis, the white forms are the wide field image. The red overlapped spots are the contributions of each emitter after the bleaching analysis. For the localization analysis, in the top image, the white forms are also the wide field images. The blue overlapped spots correspond to the scatter plot after the localization analysis. Then, the spots were saturated to result in an image of the reconstructed plasmid shape (bottom image). The fluorescence map was created from the overlap of both analysis: the white images correspond to the plasmids shape and the red markers to the dye molecules covalently coupled.

3.9 Atomic force microscopy experiments

For the atomic force experiments, a mica sheet substrate (SPI Supplies, mica grade V-I) was cleaved prior to use. Subsequently, the surface was coated with 20 µL of a 0.01% w/V PLL solution. The substrate was incubated for 30 s, washed with 50 mL of Milli-Q water in a drop-wise fashion and carefully dried with argon gas. The DNA samples were diluted to a final concentration of 0.5 ng/µL in a buffer containing 200 mM of sodium acetate and 10 mM of Tris-Cl (pH = 8.0). 10 µL of this solution was coated onto the coverslip and incubated for 30 s. It was rinsed using 20 mL of Milli-Q water in a drop-wise fashion and dried under a gentle flow of argon gas.

The samples were immediately analyzed in tapping air mode. The experiments were carried out using a multimode AFM with a Nanoscope VIII controller and a J-scanner (Brucker). The

system was equipped with silicon cantilevers (AC160TS, drive frequency of 300–350 kHz, Olympus). The images were acquired with 2-4 μm^2 (1024 x 1024 pixels).[139] In order to obtain a statistical population, around 150 plasmid molecules were recorded after every fluorescent labelling performed (as well as for the plasmids without any labelling). Each plasmid was analysed, by eye, and their morphology was classified based on the number of nodes, i.e., the number of overlaps of the DNA strands.[139]

3.10 Cell transfection

The vector that encodes for the Venus protein was labelled using the direct single-step reaction, following the same procedure as done for the plasmid pUC19. For the transfection preparation, 3 µL of Fugene 6 was mixed with 92 µL of DMEM. Subsequently, 5 µL of the labelled plasmid (~50 ng/µL) was added and mixed. This preparation was incubated for 15 minutes at room temperature.

For the imaging experiments, HeLa cells[140] were kept in DMEM supplemented with FBS and antibiotics at 37 °C and 5% CO_2 atmosphere. The cells (250 µL) were grown onto 35 mm bottom dishes with 1.15 mL of DMEM and 100 µL of the transfection preparation. This dish was stored in an incubator and the experiments were carried out after 3, 24 and 48 h.

Fluorescence imaging experiments were performed on a FV 1000-IX81 confocal laser scanning microscope (Olympus, Japan). Imaging was performed inside an incubator at 37 °C and 5% CO2 atmosphere, placed above the microscope.

4 RESULTS AND DISCUSSION

The super-resolution optical microscopy experiments are an important tool to investigate different methodologies of DNA fluorescent labelling. Using this approach, we were able to determine the number of fluorophores that was covalently associated to specific sequences of a single plasmid pUC19.

All the labelling strategies utilized the methyltransferase-directed Transfer of Activated Groups approach, in a typical two-step procedure. Briefly, in the first step, a functional group (azide or amine) is transferred to the plasmid DNA pUC19 using M.TaqI as a catalyst, and in the second step, the fluorophore is coupled by a suitable biorthogonal reaction.[46; 47] A one-step direct reaction was also developed.

It is important to mention that the plasmid pUC19 has four TaqI sites in the positions 400, 430, 906 and 2350, as depicted in Figure 30. However, these sites are palindromic and each one has the possibility to carry two fluorophores. Therefore, the pUC19 plasmid has in principle eight available sites for fluorophore coupling.

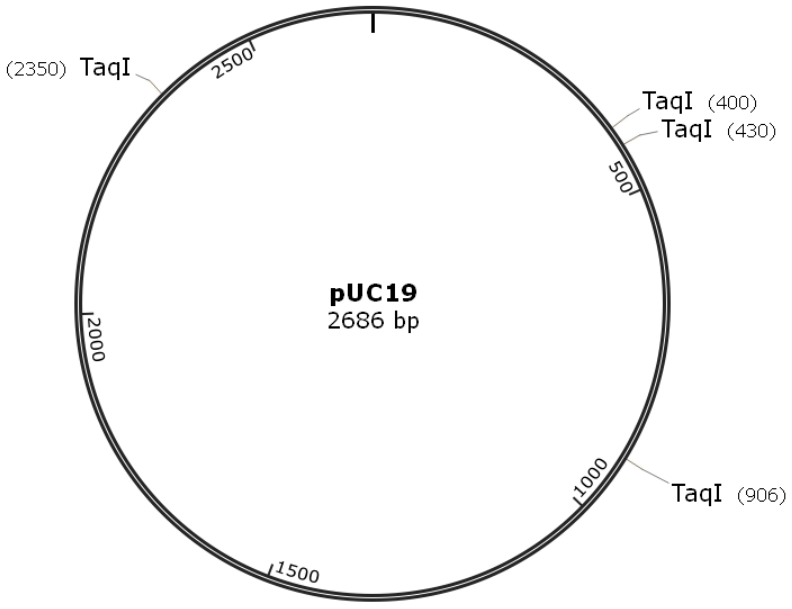

Figure 30. pUC19 plasmid DNA map indicating the position of the four TaqI sites for enzymatic modification, at 400, 430, 906 and 2350 bp.

In the next sections, each methodology used for labelling is discussed in terms of the super-resolution microscopy experiments and in terms of the DNA plasmids morphology, elucidated by AFM imaging. As a proof-of-concept, two applications of fluorescently labelled DNA by our approach were performed: one of them is the use of labelled DNA to cell transfection and the second one is the use of labelled DNA for fluorescence *in situ* hybridization (FISH) purposes.

4.1 DNA labelling by the Cu-catalysed azide-alkyne cycloaddition (CuAAC)

The remarkable efficiency of click chemistry and its wide versatility have attracted great attention from several fields, including the nucleic acids area. This reaction has been applied to label DNA structures with a vast range of reporter groups, like fluorophores, sugars and peptides. Moreover, it has an additional advantage, very important to the use in DNA systems: the moieties containing azide or alkyne groups can be attached to nucleic acids without causing perturbations in their biophysical structures.[57]

However, it is known that the system Cu/ascorbate is a potential generator of reactive oxygen species (ROS), which are responsible for damages to DNA, such as breaking single or double strands, releasing free nucleobases, chemical changes in nucleobases, and modification of sugar moieties.[141; 142] As an alternative to avoid the production of ROS species, the addition of Cu(I)-stabilizing ligands has been reported as an effective method. Besides, the ligands also increase the reaction rate.[56; 143] For this reason we used the triazole ligand tris[(1-hydroxypropyl-1*H*-1,2,3-triazol-4-yl)methyl]amine (THPTA) in a ratio tenfold concentrated relative to the amount of $CuSO_4$ utilized. Previous studies have shown that the THPTA ligand is more effective in DNA damage prevention than the triazole ligand tris(benzyltriazolylmethyl)-amine (TBTA).[63]

Even using a highly efficient reaction and an aminated-ligand, the BALM experiments showed that 66% of the plasmids labelled by the CuAAC methodology were carrying at least one fluorophore, as shown in Table 8. Furthermore, the plot of the fraction of population as a function of the number of fluorescent labels, Figure 31, shows a continuous decrease, which means that most of the labelled plasmids contains in average one or two fluorophores.

Table 8. DNA labelling using the copper-catalysed click reaction.

Labelling	Plasmids carrying at least 1 label (%)
CuAAC Standard	66
CuAAC ClickOx	64

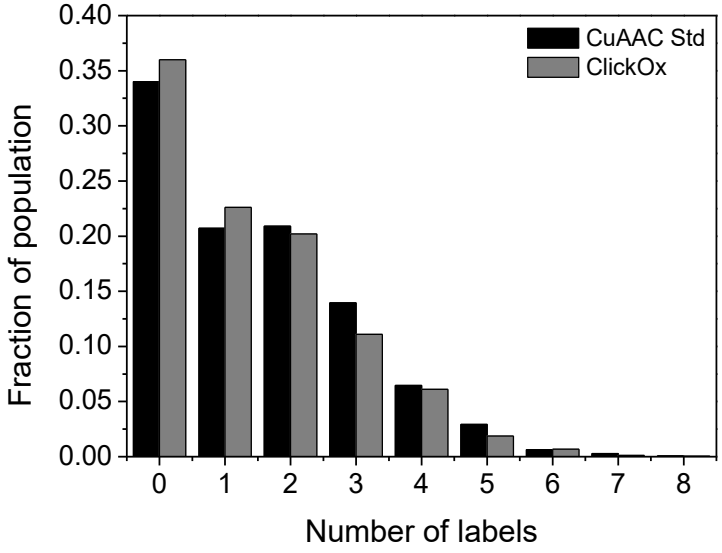

Figure 31. Comparison between the profiles of labelling using the standard copper-catalysed click reaction, in black, and the reaction in the presence of an oxygen scavenger system, in grey.

With the aim of investigating why the fluorophore coupling step was not complete, the same reaction was performed in the presence of an enzymatic oxygen scavenger system, termed ClickOx approach.[137] This method is known for its the oxygen removal ability and consequently the decrease of ROS associated damage, introduced by Cu(I)-mediated chemistry, for instance •OH production.[141] The oxygen-depletion system employed is composed of glucose, glucose oxidase and catalase. This system works according to two equations. In the first, glucose is oxidized by glucose oxidase, to gluconolactone. This product is hydrolysed to gluconic acid spontaneously. The first reaction produces hydrogen peroxide, which is decomposed by catalase in the second reaction.[144] This kind of oxygen scavenger system is commonly used in studies involving biomolecules, including those for single-molecule detection purposes.[137; 145]

As presented in the Table 8, 64% of the plasmids were labelled with at least one fluorophore. This value was very similar to that found for the CuAAC reaction without ClickOx, which indicated that the introduction of the enzymatic system did not interfere with labelling process. On the other hand, its addition did not promote the increase of the fraction of the labelled population, neither the increase of the number of labels per plasmid, as presented in Figure x. In an attempt to understand what is happening after the CuAAC labelling, the DNA morphology was investigated by AFM imaging and will be presented in later sections.

4.2 DNA labelling by strain-promoted azide-alkyne cycloaddition (SPAAC)

Besides the structural damage to DNA molecules cause by the Cu(I)-mediated reactions and inherent oxidative processes, this kind of reactions promotes another disadvantage, which is the potential toxicity of the metal catalyst to biomolecules.[68] This characteristic limits the use of CuAAC for imaging proceedings *in vivo*.[64; 143]

As an alternative to CuAAC, we used a variation of this click reaction for the fluorophore coupling step, but in the absence of a metal catalyst, the SPAAC. For that, it is necessary to use a cyclooctyne, because this kind of strained alkyne reacts selectively to form the triazole, without apparent cytotoxicity.[72] Herein, we performed the SPAAC reaction in different solvents and concentrations to investigate the optimal reaction conditions.

4.2.1 Effect of the solvent on the SPAAC reaction

The click reaction in the absence of copper was conducted in four different solvents: DMSO, H_2O, DMF, and ethanol. The results provided by the BALM experiments are reported in Table 9. The best performance of the SPAAC reaction was established to be in 50% DMSO, for which 90% of the total plasmids were labelled with at least one molecule of dye. This result can be ascribed to the outstanding solubility of the cyclooctyne in DMSO, which is a di-benzo-cyclooctyne functionalized with a rhodamine B dye.

Table 9. Effect of the solvents on the copper-free reaction.

Solvent	Plasmids carrying at least 1 label (%)
50% DMSO	90
H_2O	82
30% DMF	76
60% EtOH	59

In Figure 32, one can note a different behaviour of the SPAAC reaction in comparison with that of the CuAAC reaction. In this case, there is not a continuous decrease of the fraction of population with the increase in the number of labels per plasmid, but there is a curve with a maximum at about three fluorophores per plasmid. Therefore, the plasmids labelled by SPAAC showed a labelling density higher than the previous reaction. SPAAC showed a different behaviour for the experiment in ethanol, with a trend similar to the CuAAC result.

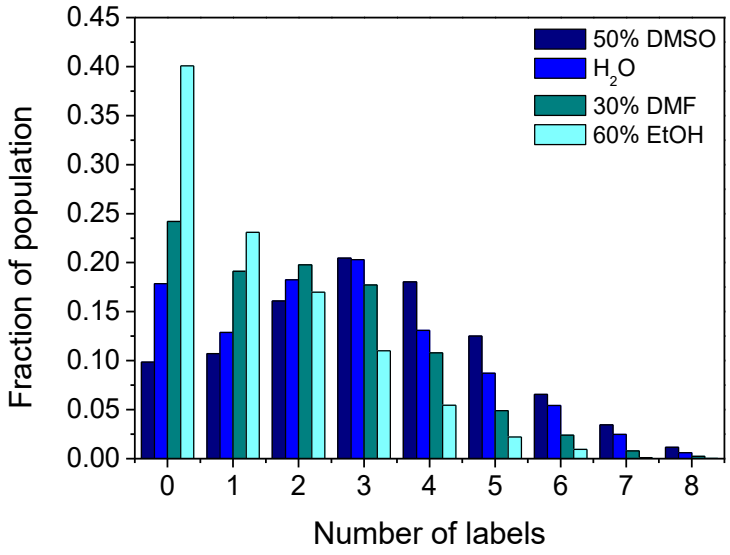

Figure 32. Effect of the solvents DMSO, H_2O, DMF, and ethanol on the copper-free click reaction.

4.2.2 Effect of the concentration of DMSO on the SPAAC reaction

The previous results have shown that DMSO in water (1:1) was the best solvent combination to perform the copper-free click reaction. In order to examine the optimal DMSO

concentration, new experiments were carried out. The results in Table 10 show that the reactions performed at 10 and 25% of DMSO in water provided the largest amount of plasmids labelled with at least one molecule of dye, of about 90%.

Table 10. Effect of the DMSO concentration on the copper-free reaction.

Concentration of DMSO (%)	**Plasmids carrying at least 1 label (%)**
0	76
10	84
25	90
50	71
75	80

Figure 33 shows that for the reactions performed at 10 and 25% DMSO, the majority of the plasmids contain on average two or three labels, which demonstrate that the density of labelling promoted by the SPAAC reaction is superior to that promoted by CuAAC. This satisfactory result is in agreement with previous studies reported by the literature, in which oligonucleotides were completely labelled *via* copper-free click chemistry.[79] Therefore, strain-promoted azide-alkyne cycloaddition has shown great potential to be applied to DNA plasmids fluorescent labelling, since in optimized solvents and concentration provided 90% of the plasmids got labelled with an improved labelling density. Moreover, SPAAC is biorthogonal and is not toxic towards biomolecules.

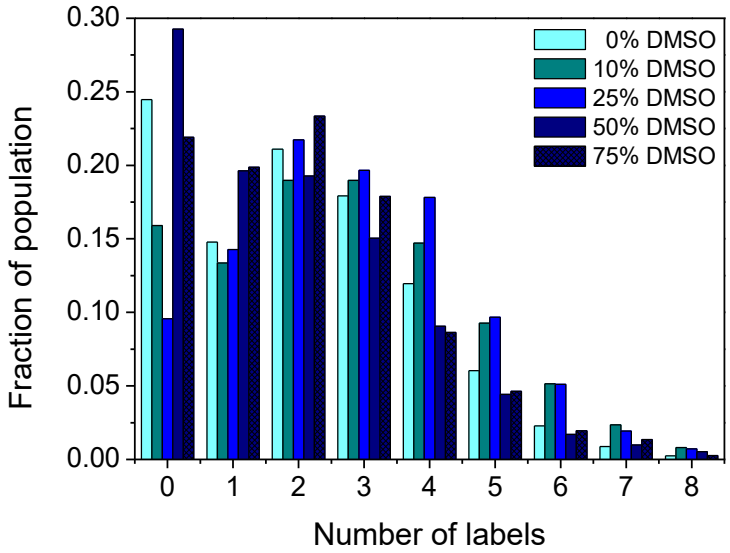

Figure 33. Effect of the DMSO concentration on the performance of the SPAAC reaction. The different shades of blue represent the different concentrations of DMSO.

4.3 DNA labelling using the amine-to-NHS-esters coupling

The use of NHS-ester reactions for conjugation with primary amine groups of biomolecules is very widespread, because of its orthogonality. This kind of reaction was also examined for the fluorophore-coupling step of the two-step methodology using MTase.

4.3.1 Effect of the DMSO concentration on the amine-to-NHS-ester coupling reaction

This reaction was also studied in terms of DMSO concentration and, according to the results reported in Table 11, it is noted that the coupling efficiency in the second-step of the reaction is improved with the increase of the DMSO concentration, which can be related to the solubility of the dye. The best solvent composition was found to be 30% DMSO, which resulted in 59% of all the plasmids labelled with at least one fluorophore. This result is expected considering the low efficiency of the amino-to-NHS-ester coupling reaction, when compared to the high efficiency of the click reactions.[63]

The graph of Figure 34 supports these findings and it shows a continuous attenuation of the fraction of population as a function of the number of labels per plasmid. Here, the majority of the plasmids was labelled with only one dye molecule. This scenario indicates the low density of labelling, similar as found for the CuAAC reaction.

Table 11. Effect of the DMSO concentration on the regular amine-to-NHS-ester coupling reaction.

Concentration of DMSO (%)	Plasmids carrying at least 1 label (%)
5	31
10	20
25	41
30	59

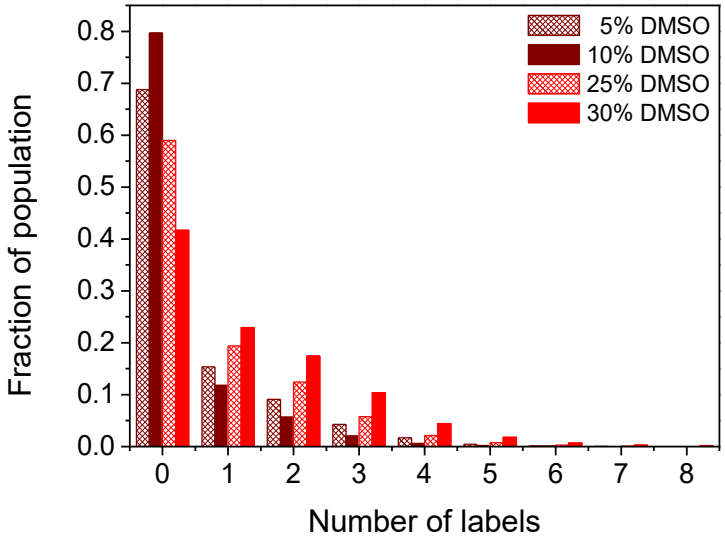

Figure 34. Effect of the DMSO concentration on the fluorophore coupling step performed by the regular amine-to-NHS ester coupling reaction. The different shades of red show that the increase in DMSO concentration improves the amount of fluorescently labelled plasmids.

4.4 DNA labelling by direct one-step reaction: an innovative method

In this extent of the research, a direct one-step approach, in which the fluorophore is part of the transferable moiety of the AdoMet analogue cofactor is introduced. Hence, the enzyme M.TaqI directly transfers the fluorophore group to the specific sequence in DNA. This reaction was already schematized in Figure 27.

A similar methodology has been previously proposed using aziridine based cofactors, containing the fluorophore.[146] However, in this approach we firstly couple the fluorophore to the Ado-6-amine cofactor,[128; 133] the reaction is quenched and subsequently, the fluorophore is transferred to the DNA by the MTase. We envisioned producing a better labelling efficiency by reducing the number of chemical steps.

4.4.1 Study of the direct one-step reaction using different dyes

This methodology was tested utilizing a 2.5 mM solution of two different dyes, Atto-647N-NHS-ester and Atto-565-NHS-ester. This reaction showed one of the best labelling performances amongst all methodologies already described in this work. According to the results reported in Table 12, the one-step methodology performed with the dye Atto-647N reached near-complete DNA labelling, where 96% of the plasmids were labelled with at least one fluorophore, while the reaction using Atto-565 provided 85% of plasmids labelled.

Table 12. Efficiency of the direct fluorophore-to-amine cofactor coupling using NHS-ester chemistry.

Dye	Plasmids carrying at least 1 label (%)
Atto-647N-NHS ester	96
Atto-565-NHS ester	85

The remarkable performance of the direct one-step reaction can also be observed in the labelling profiles shown in Figure 35. The graphs show that the majority of the plasmids labelled is carrying on average 3-4 labels. These results are similar to those provided by SPAAC and in contrast to those provided by the CuAAC and the amino-NHS-ester coupling. Therefore, we can infer that even with the best labelling reactions, the fluorophore coupling

to both target adenines in the 5'- TCGA -3' sequence is not frequent. As depicted in Figure 35, only a small fraction of population is carrying more than 5 fluorescent labels per plasmid.

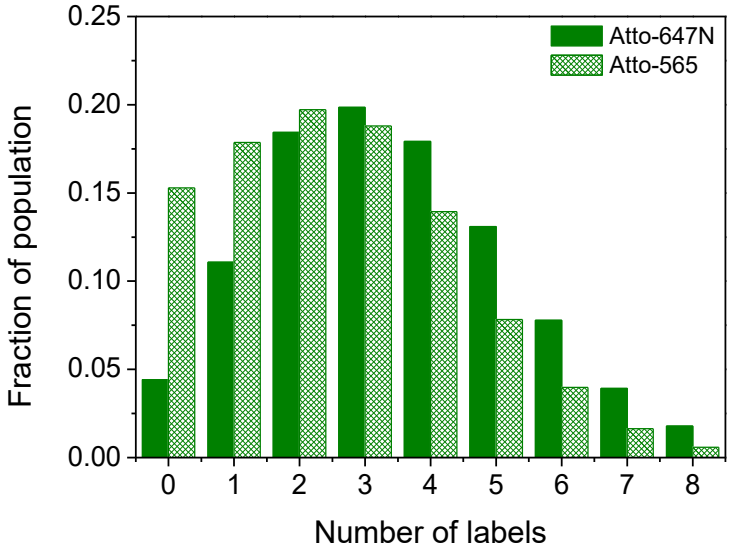

Figure 35. Histogram of the direct one-step NHS ester reaction using different dyes for coupling. The filled green bars exhibit the profile of the labelling performed using the Atto-647N dye, in which the major part of the fraction of population is labelled with 3 labels per plasmid. The hatched green bars show the reaction profile performed using the Atto-565 dye having a similar trend.

4.4.2 Effect of the DNA concentration

The direct reaction was also studied as a function of the DNA concentration. Furthermore, in this set of experiments, the concentration of the dye was increased from 2.5 mM to 4 mM to investigate whether a higher number of labelled plasmids could be reached. The results of these experiments are summarized in Table 13. It is possible to note that at the same DNA concentration as used in the previous experiment (100 ng/µL), the increase in concentration of the dye did not enhance the labelling ratio as would be expected. A small decrease down to 79% of the plasmids labelled with at least one fluorescent label was observed, in contrast to 96% provided using 2.5 mM of the dye. This unexpected effect can be related to the degradation of the cofactor over time.

Table 13. Effect of the DNA concentration on the direct one-step NHS ester labelling reaction.

DNA concentration	Plasmids carrying at least 1 label (%)
100	79
50	81
20	92
5	93

The Table 13 also shows that at low DNA concentrations the percentage of labelling is quite high. Nevertheless, from Figure 36 is possible to observe that at low concentrations of DNA, there is an increase in the fraction carrying a number of labels per plasmid above the number of Taq sites available in pUC19 (recognition until 8 sites). This lack of specificity observed at low concentrations of DNA is compatible with the star activity of enzymes, which normally appears in some conditions, such as a high enzyme concentration, the presence of organic solvents like DMSO, a prolonged reaction time, a high glycerol concentration, and a non-optimal buffer.[147; 148]

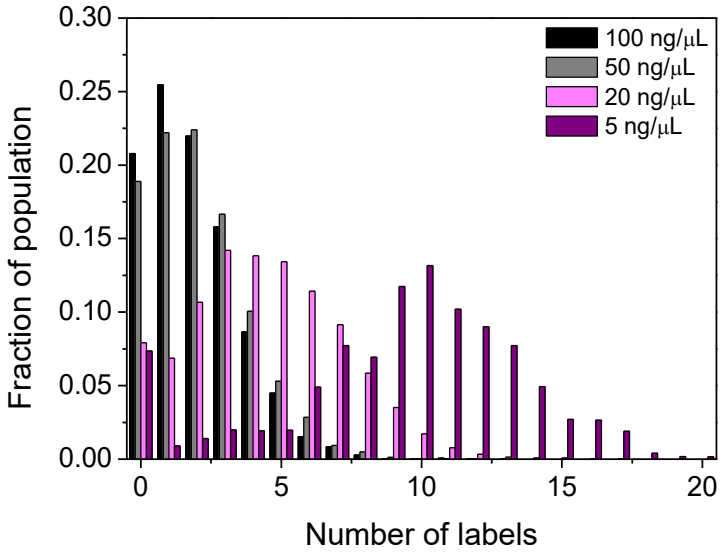

Figure 36. Behaviour of the direct one-step labelling reaction at different concentrations of DNA. The shades of purple denote the low concentrations of DNA in comparison with the concentration of the enzyme, in which appears a fraction of population labelled with more than the maximum of the eight available sites.

4.4.3 Effect of DMSO on the direct one-step reaction

The presence of DMSO is among the conditions to propitiate star activity. Therefore, some reactions were investigated in the absence of this solvent. The reactions at a standard concentration of DNA (100 ng/µL) as well as the reactions at low concentrations of DNA, in which the star activity was observed (20 and 5 ng/µL) were performed without additional DMSO. However, all reactions have a DMSO concentration of about 4%, since the dye was diluted in DMSO for solubility reasons.

The results of the reactions performed without the addition of DMSO are reported in Table 14. At 100 ng/µL of DNA, the absence of DMSO decreased the efficiency of labelling, from 79% to 59%. This result can be related to the lower solubility of the dye in water than in DMSO. For the concentrations of 20 ng/µL and 5 ng/µL, the problem of over-labelling was not completely prevented, as illustrated in Figure 37, since some plasmids still carried more than eight labels.

Table 14. Direct one-step NHS ester reactions performed in the absence of DMSO.

DNA concentration (ng/µL)	Plasmids carrying at least 1 label (%)
100	59
20	85
5	92

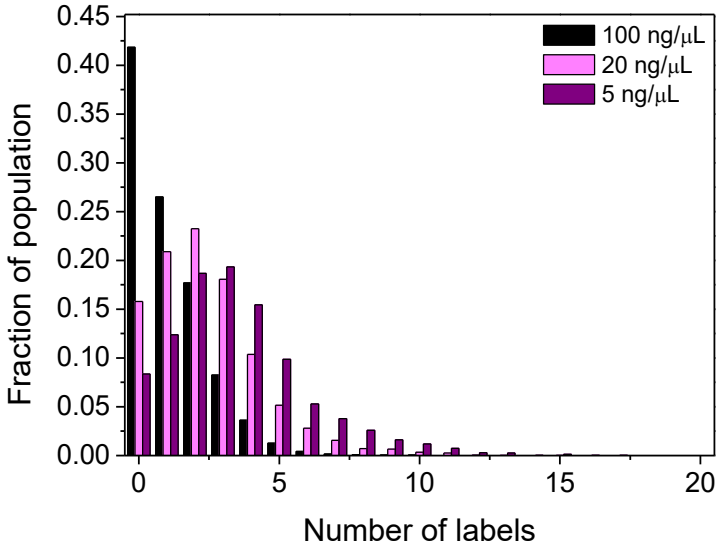

Figure 37. Behaviour of the direct one-step NHS ester reaction carried out in the absence of additional DMSO.

4.4.4 Control experiments

For an attestation of the method and because of the lack of specificity of the reactions at low DNA concentrations, some control experiments were performed, such as the direct one-step reaction using methylated DNA as well as the direct reaction in the absence of the enzyme M.TaqI.

4.4.4.1 Methylated DNA

For this investigation, firstly methyl groups were transferred to the available sites of the plasmids pUC19 using the cofactor S-adenosyl-L-methionine and the enzyme M.TaqI. Subsequently, the same procedure for the fluorescent labelling using the one-step reaction was applied to check if even with the sites unavailable, there is any fluorescent attachment.

At lower concentrations of DNA, in which the star activity was observed, one can note that there is still fluorescent labelling and it is more pronounced at the lowest DNA concentration, 5 ng/μL. This test proves that at low concentrations of DNA, and consequently a high ratio of enzyme, the star activity takes place and M.TaqI loses its specificity. Table 15 and Figure 38 show the data and corresponding plots of the methylated plasmid control experiment.

Table 15. NHS labelling using methylated DNA as a control.

Concentration of methylated DNA (ng/μL)	**Plasmids carrying at least 1 label (%)**
20	77
5	94

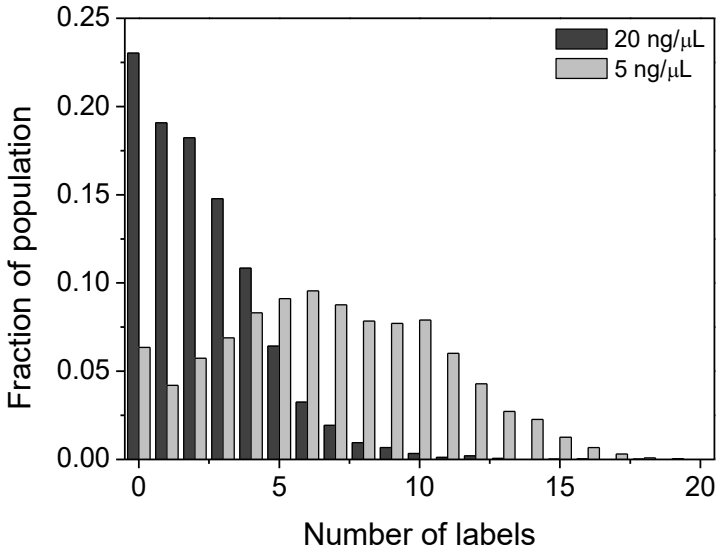

Figure 38. One-step NHS ester reactions behaviours using methylated DNA.

4.4.4.2 Absence of enzyme

The control experiment performed in the absence of the M.TaqI enzyme showed that no labelling is produced without enzyme. The Table 16 exhibits a value of 3% of plasmids carrying at least one label, which proves that the over-labelling found is not promoted by any external parameter, but only by the action of the enzyme.

Table 16. Direct one-step labelling performed in the absence of the enzyme M.TaqI as a control experiment.

DNA concentration (ng/μL)	Plasmids carrying at least 1 label (%)
100	3

4.5 Summary of fluorescent labelling strategies

In summary, this research presented an mTAG based direct single-step approach that was capable to reach near-complete fluorescent labelling of pUC19 plasmids. This reaction, under optimized conditions (100 ng/μL DNA and 2.5 mM dye) showed 96% of the plasmids fluorescently labelled with at least one label and the higher fraction of population has on average 3-4 labels per plasmid. However, some mTAG based two-step methodologies were also investigated. The strain-promoted azide-alkyne cycloaddition has also shown great potential, since less than 10% of the plasmids remained unlabelled.

The Cu-catalysed click chemistry provided 66% of the plasmids labelled with at least one molecule of dye, even in the presence of an enzymatic oxygen scavenger system. A comparable result was found for the DNA labelling performed by the amino-to-NHS-ester coupling. The use of this approach provided 59% of labelled plasmids under optimized conditions. However, such a low efficiency was expected for this kind of coupling reaction, in contrast to the click chemistry which is remarkably highly efficient.

The list of DNA fluorophore coupling reactions and their efficiencies at optimized conditions are summarized in Table 17 and illustrated in Figure 39. The distribution plots give evidence that the less efficient coupling reactions have a continuous attenuation of the fraction of population as a function of the number of labels per plasmid, whereas the best-case methodologies generate distributions of fluorescent labels per plasmid centered in 3-4 fluorophores per plasmid.

Table 17. Efficiencies of the different strategies of fluorescent labelling.

Reaction	Plasmids carrying at least 1 label (%)
Direct one-step Atto-647N	96
SPAAC	90
Direct one-step Atto-565	85
CuAAC	66
NHS-ester	59

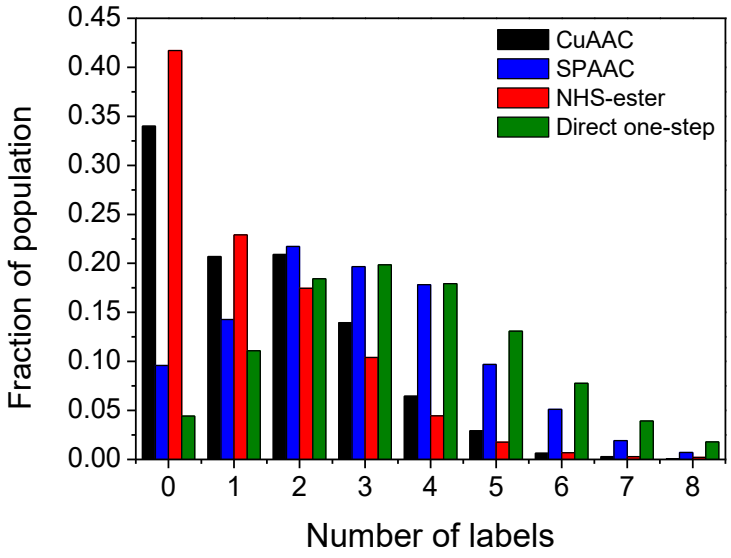

Figure 39. Profiles of the different strategies of DNA labelling performed on pUC19 plasmids as a function of the number of labels per plasmid. The standard CuAAC (black) as well as the amino-to-NHS ester coupling (red) reactions show a continuous decrease of the fraction of population fluorescently labelled with the increase of the number of labels. While the SPAAC (blue) and direct one-step (green) have most part of the population carrying, on average, 2-4 dye molecules per plasmid.

4.6 DNA morphology

One of the main issues attributed to DNA fluorescent labelling methodologies is related to the potential damage that can be introduced to the DNA molecules. Such damage is capable to prevent the normal biological processes performed by the DNA, like transcription. For this reason, it is crucial to analyse the DNA morphology after the fluorescent labelling. Herein, a statistical amount of DNA molecules were studied by AFM, which is a reliable technique to investigate DNA topology based on the number of crossovers on the plasmids deposited on the surface. The number of such overlaps was determined and the plasmid molecules were classified into supercoiled, nicked open-circular, and linear. The supercoiled conformation is the native structure of plasmids, and it is attributed to molecules containing more than 5 nodes. The molecules containing from 0 to 4 nodes were classified as open circular, which is a more relaxed conformation, caused by a nick in one of the strands. When both strands of the DNA molecules have been cut, the linear classification was applied.[139]

Firstly, a considerable amount of the pUC19 plasmid molecules, without any labelling, was imaged so that they can be used as a control set. In total, 224 molecules were analysed, of

which 88% show the native morphology, supercoiled, as can be seen by Figure 40 (a) and (b). Figure 40 (c) shows the distribution of the amount of molecules as a function of the number of nodes, and demonstrates the predominance of the supercoiled conformation. Here, this distribution is centred in seven overlaps per plasmid. It is common that a lower percentage of relaxed plasmids may be detected. Here, 12% of the plasmids were imaged at the open-circular conformation. No linear fragments were found in our samples. Table 18 exposes the amount of plasmids classified according to the number of nodes for each type of fluorescent labelling (CuAAC standard, CuAAC with ClickOx approach, SPAAC, and the direct one-step reaction) as well as for the control.

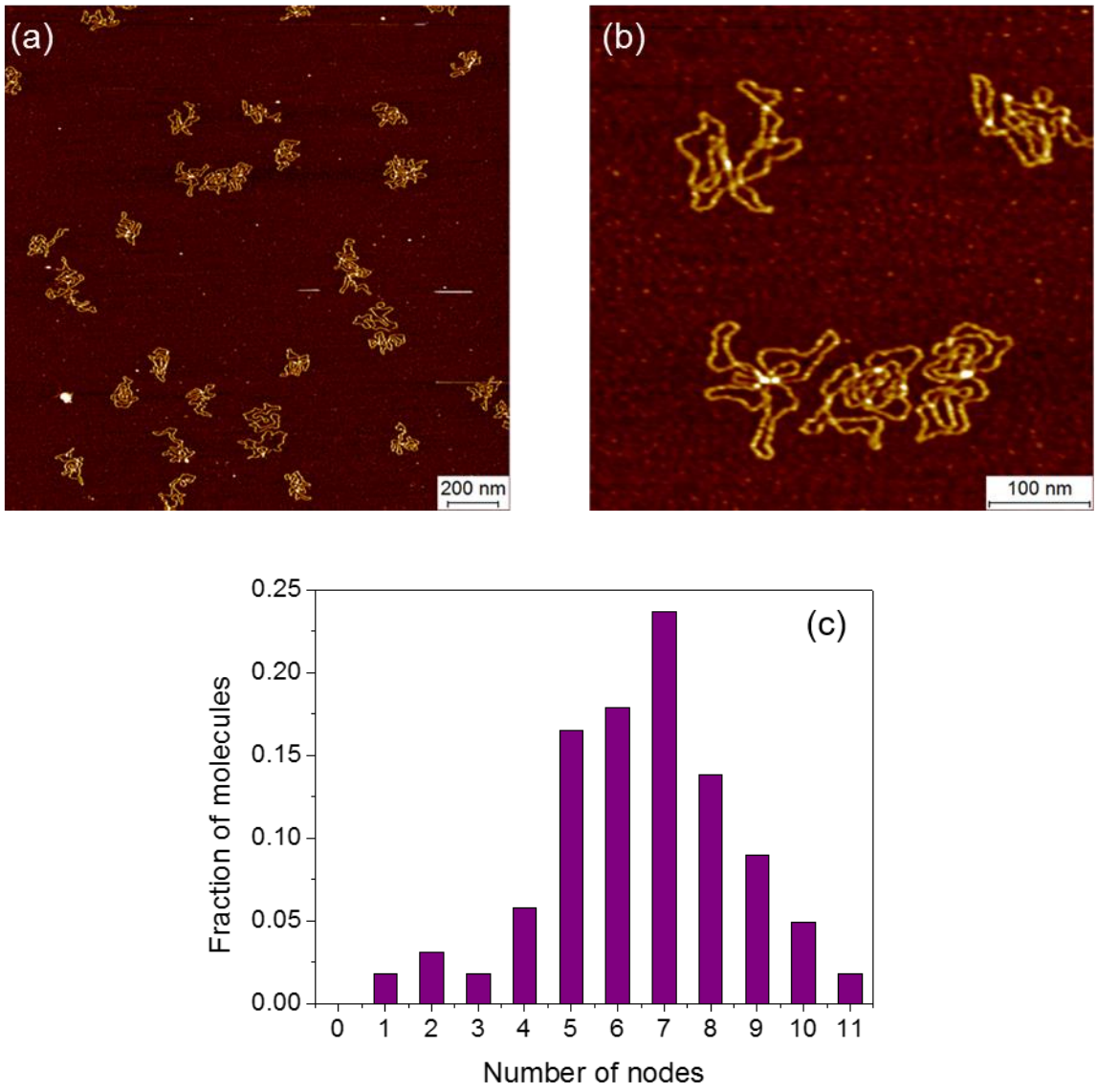

Figure 40. Typical AFM image of the pUC19 plasmids without fluorescent labelling (a) and detail of the first image (b), in which all the five DNA plasmids are in the supercoiled conformation. The graph (c) represents the distribution of the fraction of molecules as a function of the number of nodes. For the measurements, the plasmids were previously purified using spin-column.

A near-complete labelling conversion was expected for the Cu-catalysed reaction, because of its high efficiency. However, the fluorophore-coupling step provided a lower amount, 66% of plasmids fluorescently labelled, even in the presence of Cu(I)-stabilizing ligands and an enzymatic oxygen scavenger system, as previously discussed in the section 4.1. Therefore, AFM imaging was utilized to investigate the quality of the plasmids after the CuAAC reaction.

In total, 308 plasmid molecules were analysed after the CuAAC reaction. A typical AFM image can be seen in Figure 41 (a). Opposite to the control pUC19, the image demonstrated most part of the plasmids in a more relaxed conformation, which is the nicked open-circular. According to the analysis, 62% of the plasmids are open-circular, 28% supercoiled, and 10% linear. The graphic from Figure 41 (b) emphasizes that the highest fraction of molecules contains only two overlaps of the strands.

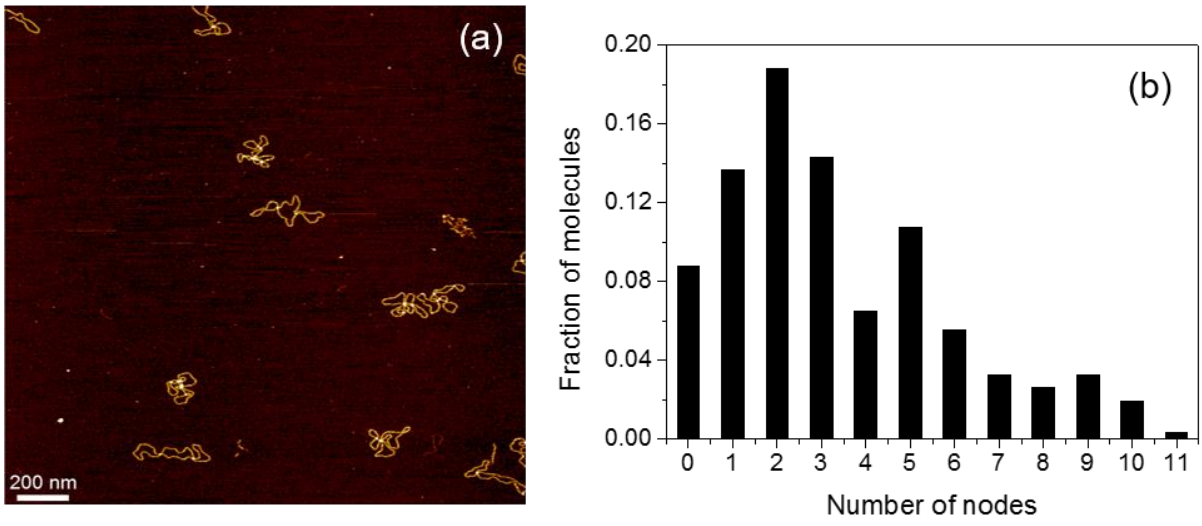

Figure 41. Typical AFM image of pUC19 after the fluorescent labelling using the standard CuAAC reaction (a). It is possible to note some plasmids carrying the open-circular conformation. The graph (b) represents the distribution of the fraction of molecules as a function of the number of nodes.

Even in the presence of the enzymatic oxygen scavenger system, ClickOx, a similar behaviour was found, as demonstrated in Figure 42 (a), with the majority of the plasmids in the open-circular conformation. The analysis of 150 molecules provided 58% of plasmids classified as open-circular, 17% as supercoiled and 25% as linear. A slight difference is related to the number of crossovers on the plasmid structure. Figure 42 (b) shows that the distribution of molecules containing from one to four nodes is quite similar.

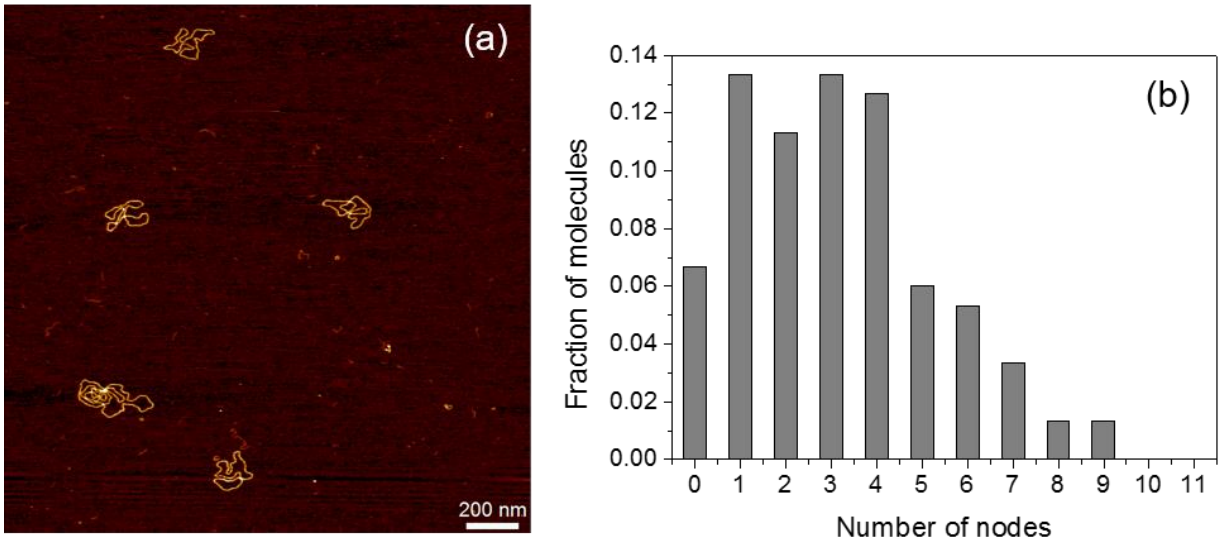

Figure 42. Typical AFM image of pUC19 after the fluorescent labelling using the CuAAC reaction, with the ClickOx approach (a). Most of the plasmids are in the open-circular conformation. The graph (b) represents the distribution of the fraction of molecules as a function of the number of nodes.

Therefore, one can infer that the Cu(I)-mediated reactions generate ROS[141] and may induce damage to the DNA structure, such as nicks and breaks, resulting in the lack of native structures, and hence favouring the predominant open-circular morphology. Such a difference in the DNA topology could not be detected by optics, so AFM images were crucial for understanding the system. These results are in agreement with recent reports in the literature, in which physical damage caused by ROS in plasmids was quantified also using the AFM technique, based on the heights of double and single strands.[149]

On the other hand, the click reaction in the absence of copper, SPAAC, performed under optimal conditions, did not induce damage to the DNA structure, as can be seen from Figure 43 (a) and (b). These images show that most of the DNA molecules retained their native, supercoiled structures. Moreover, the distribution of the fraction of molecules as a function of the number of nodes, Figure 43 (c), is in agreement with that found for the control. In this case, 200 plasmids were analysed and 82% of them were in the supercoiled conformation, 18% in the open-circular, and no linear plasmids were found. This result reinforces that the damage observed after the CuAAC reaction was introduced by the Cu(I)-catalyst.

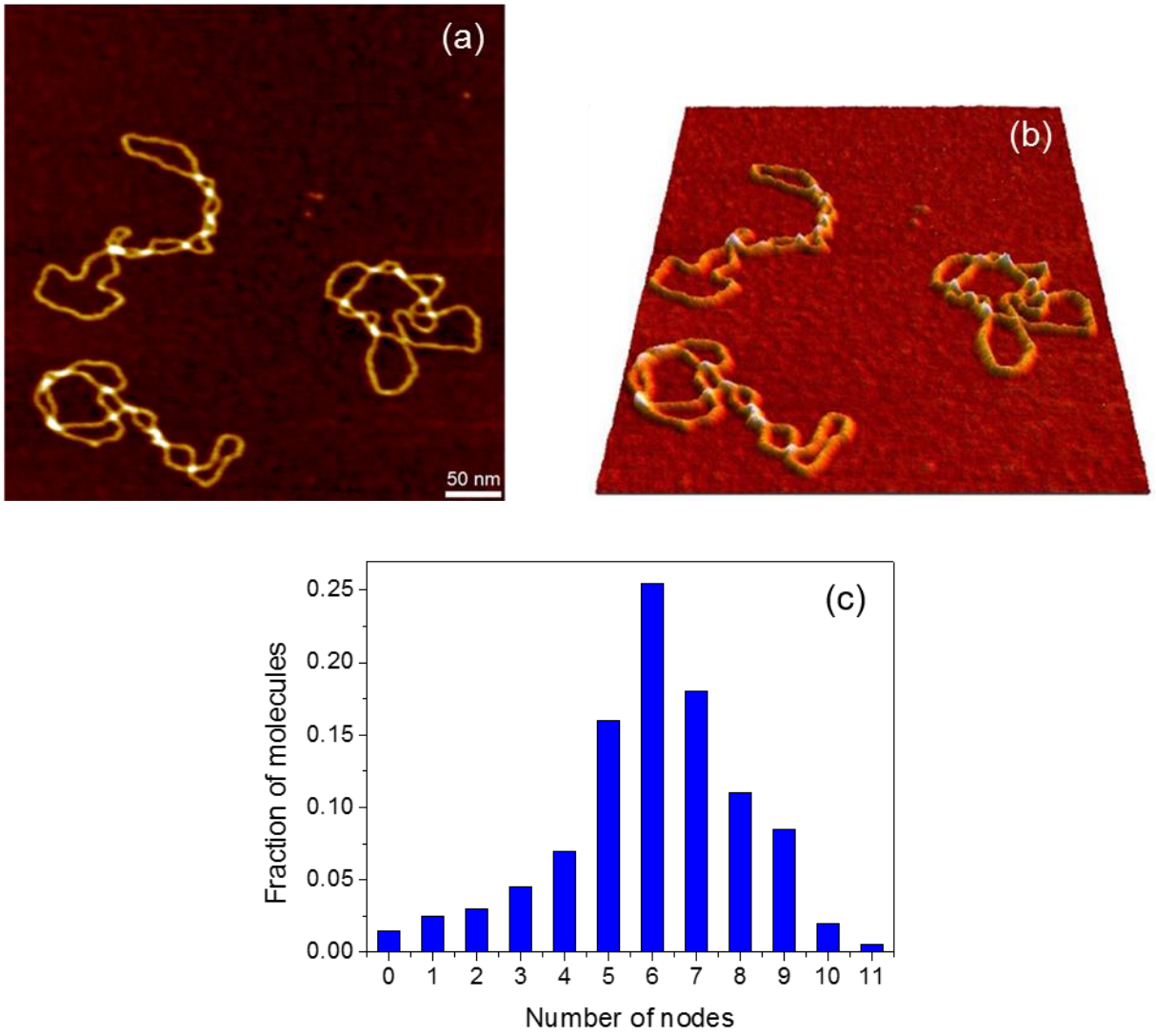

Figure 43. Zoomed AFM image of the pUC19 plasmids after the fluorescent labelling using the SPAAC reaction (a). All the plasmids are in their native, supercoiled morphology. Figure (b) shows the image (a) in 3D perspective. The graph (c) represents the distribution of the fraction of molecules as a function of the number of nodes.

Similarly, we verified that the plasmids labelled by the direct one-step approach also retained their native morphology, supercoiled, after the fluorescent labelling, as depicted in Figure 44 (a). Besides, the distribution of fraction of molecules according to the number of nodes, Figure 44 (b), was also very similar to that found for the pUC19 control. Most of the 165 molecules studied (90%) were in the native conformation, while 9% were in the open-circular and only 1% in the linear morphology.

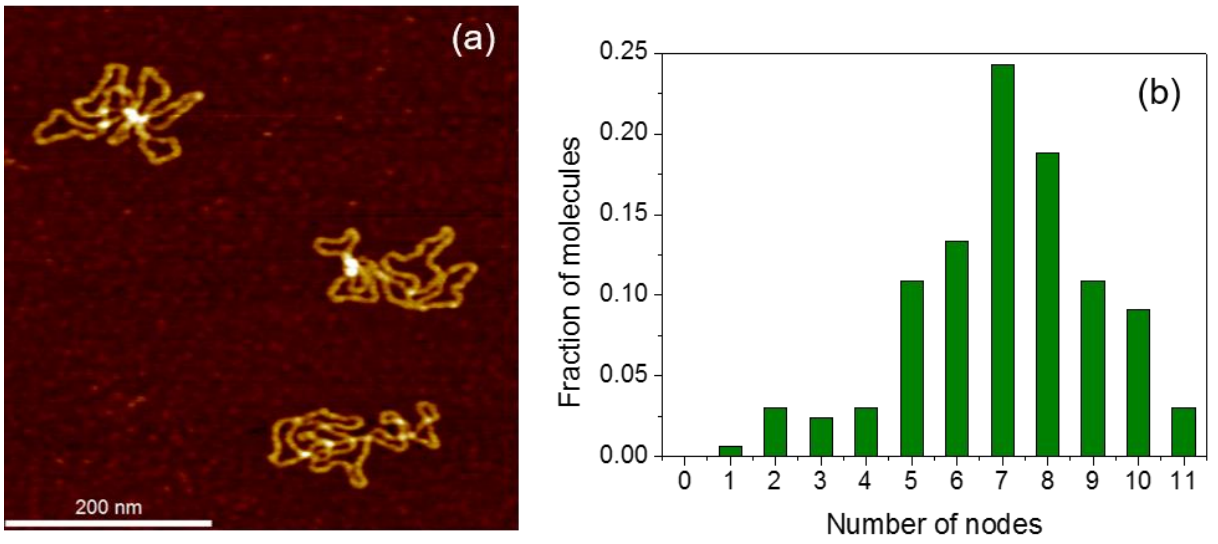

Figure 44. Zoomed AFM image of the pUC19 plasmids after the fluorescent labelling using the direct one-step reaction (a). All the plasmids are in their native conformation. The graph (b) represents the distribution of the fraction of molecules as a function of molecules as a function of the number of nodes.

Table 18. Number of plasmids classified according to the number of nodes, after each fluorescent labelling reaction.

Number of nodes per molecule	**pUC19 Control**	**CuAAC Standard**	**CuAAC ClickOx**	**SPAAC**	**Direct one-step**
0	0	27	10	3	0
1	4	42	20	5	1
2	7	58	17	6	5
3	4	44	20	9	4
4	13	20	19	14	5
5	37	33	9	32	18
6	40	17	8	51	22
7	53	10	5	36	40
8	31	8	2	22	31
9	20	10	2	17	18
10	11	6	0	4	15
11	4	1	0	1	5
Linear	0	32	38	0	1
Total	**224**	**308**	**150**	**200**	**165**

Therefore, based on the AFM images of the pUC19 plasmids, one can infer that both the strain-promoted azide-alkyne cycloaddition and direct one-step labelling reactions are reliable methodologies to fluorescently label DNA molecules without the introduction of structural damage to the DNA molecules. Thus, DNA labelled by these strategies may be potentially applied to biological processes, such as transfection, since most of the plasmids could retain their native topology.

4.7 Cell transfection and vector expression

For the fluorescent DNA labelling to be a successful method for use in applications such as transfection assays, it is crucial that the fluorophore is covalently associated with the plasmid to avoid dissociation of the labels at physiological conditions.[132] Furthermore, during the labelling process, the plasmids should retain their native form and the fluorophores should remain stably bound to the plasmid.[150] The presented SPAAC and direct one-step labelling approaches meet all the above mentioned conditions and further offers the advantage of labelling in a sequence-specific manner and therefore gives a way to control the number and the position of the labels in the plasmid.

The control of the labelling density is also very important, since it interferes with the transfection efficiency.[132; 151] Recent reports in the literature demonstrated that the transfection efficiency is unaffected for a labelling density lower than 10 labels per plasmid. A higher amount of labels results in a decreased transfection efficiency.[151] Our optimized methodologies provide, on average, approximately 3-4 labels per plasmid, which is an indication that the approaches presented here would not interfere with this efficiency.

As a proof-of-concept, we tested the use of DNA labelled by the mTAG technology in a cellular environment. In this study, we utilized a plasmid that encodes for the Venus protein targeted to the nucleus, fluorescently labelled by the direct single-step approach, for transfection into mammalian cells, HeLa, and protein expression. Venus is an improved version of the yellow fluorescent protein (YFP), which is a genetic mutant of the green fluorescent protein (GFP). This protein offers a faster maturation speed and tolerance of exposure to acidosis and chloride ions.[152] Venus has an excitation maximum wavelength at 515 nm and the emission maximum is at 528 nm. The molar extinction coefficient is 92,200 and the quantum yield is 0.57.[153]

Three hours after the transfection, many DNA-containing vesicles were observed, but no protein expression. Figure 45 shows the xy plane of the cell image and the small images are

the yz and xz sections. The cells can be visualized by contrast imaging and the pink spots are the lipid vesicles containing labelled DNA molecules, illuminated by a 635 nm laser.

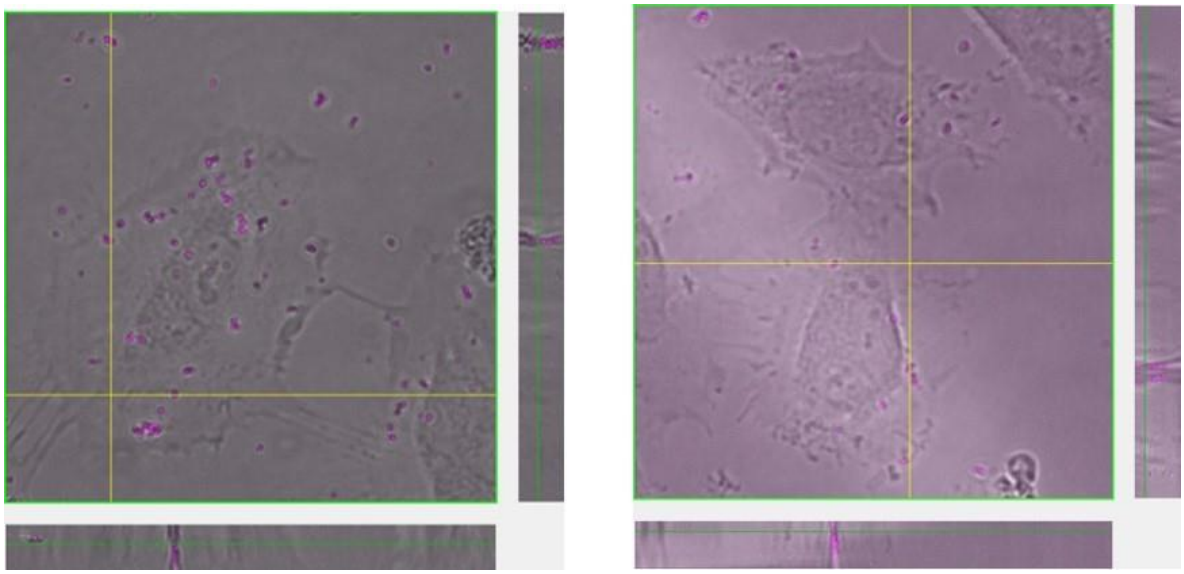

Figure 45. HeLa cells 3 h after the transfection procedure. The cells can be visualized by contrast and the magenta spots represent the lipid vesicles containing plasmids labelled by direct one-step labelling using Atto-657N dye.

After 24 h, protein expression was observed. Figure 46 shows the in green and the pink spots are the vesicles still containing some DNA molecules. These vesicles formed some agglomerates located close to the nucleus.

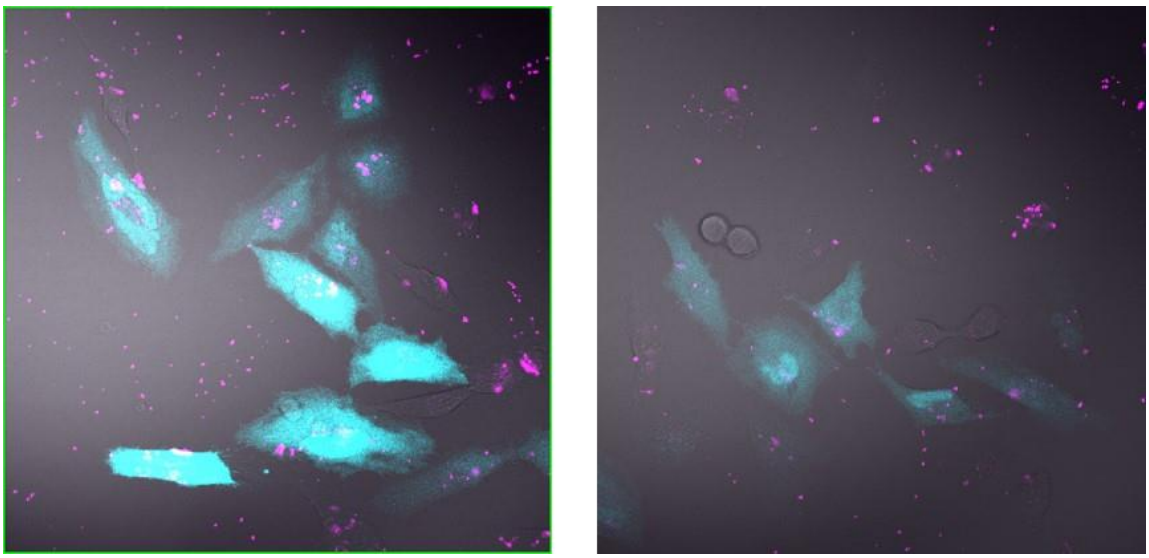

Figure 46. Confocal microscopy image of HeLa cells 24 h after transfection. The green fluorescence is due to the Venus protein already expressed in some cells at this time. The magenta spots represent the labelled DNA-containing vesicles, excited at 635 nm.

The DNA vesicles were detected in most of the cells, but some of them lack protein expression. To facilitate the identification of the cells and check the transfection efficiency, the cellular membranes were stained with DiI and imaged 48 h after the transfection procedure. DiI is a lipophilic cationic membrane stain that diffuses laterally to stain the entire cell.[154] It is an indocarbocyanine orange-red fluorescent dye, which has a maximum absorption wavelength at 549 nm and the emission is at 565 nm.[155] Figure 47 shows the cells with the membrane stained with DiI.

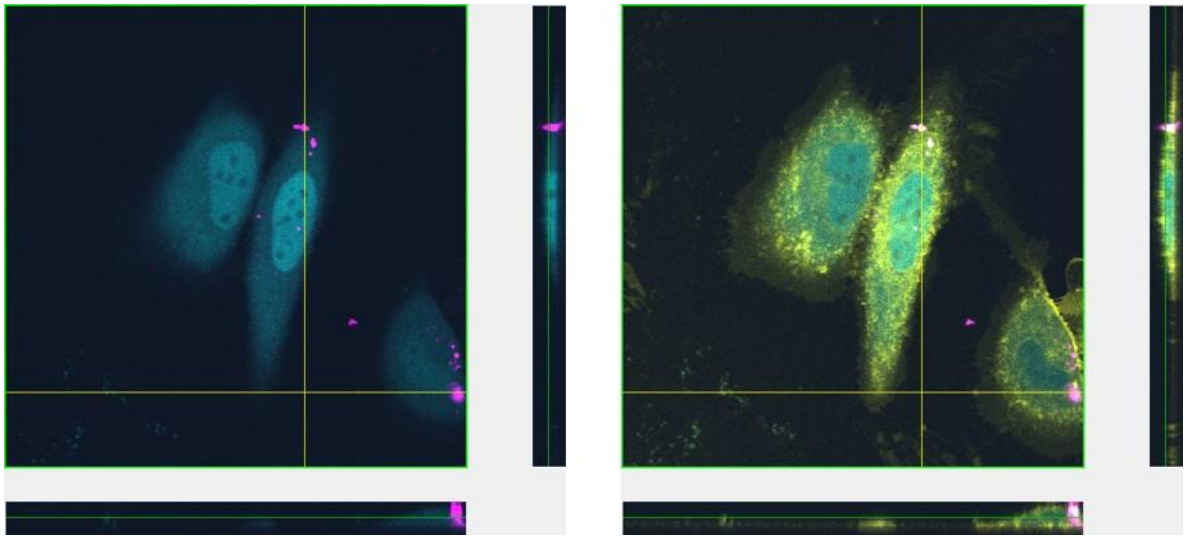

Figure 47. Confocal microscopy image of HeLa cells 48 h after transfection. The green fluorescence is provided by the Venus protein expressed. The same sample was stained with the dye DiI, which provides the visualization of the plasmatic membrane, as shown in yellow in the right image. Some magenta spots (vesicles containing plasmids) are still visible.

These results indicate that the DNA fluorescently labelled by the direct one-step reaction retains its ability to encode genetic information, despite the fact that they carry fluorophores in the DNA sequences encoding genes.

4.8 Fluorescence *in situ* hybridization

Fluorescence *in situ* hybridization (FISH) is a powerful cytogenetic technique that has attracted special attention over the last years, since it can detect chromosomal abnormalities. With the advent of the super-resolution approaches in fluorescence microscopy and the possibility to visualize multiple fluorophore colours, it is possible to detect even smaller genome regions.[136; 156] The basic principles of FISH are well-documented in the literature.[157] At this point, we proposed the use of our sequence-specific labelling technology as an effective way to control the number and position of the labels in the DNA-FISH-probe.

In this section, several platform experiments were established for the fluorescent labelling of the oligonucleotide probe and for the elaboration of a DNA hybridization protocol. As this project is in its initial stage, the pUC19 plasmid was chosen as a target DNA because they are much simpler to handle and purify than long genomic DNA molecules. The FISH probe was specifically designed to be hybridized along 60 bp of the pUC19 plasmid, as depicted in the Figure 48. The sequence of this FISH was developed to have seven labels in each strand.

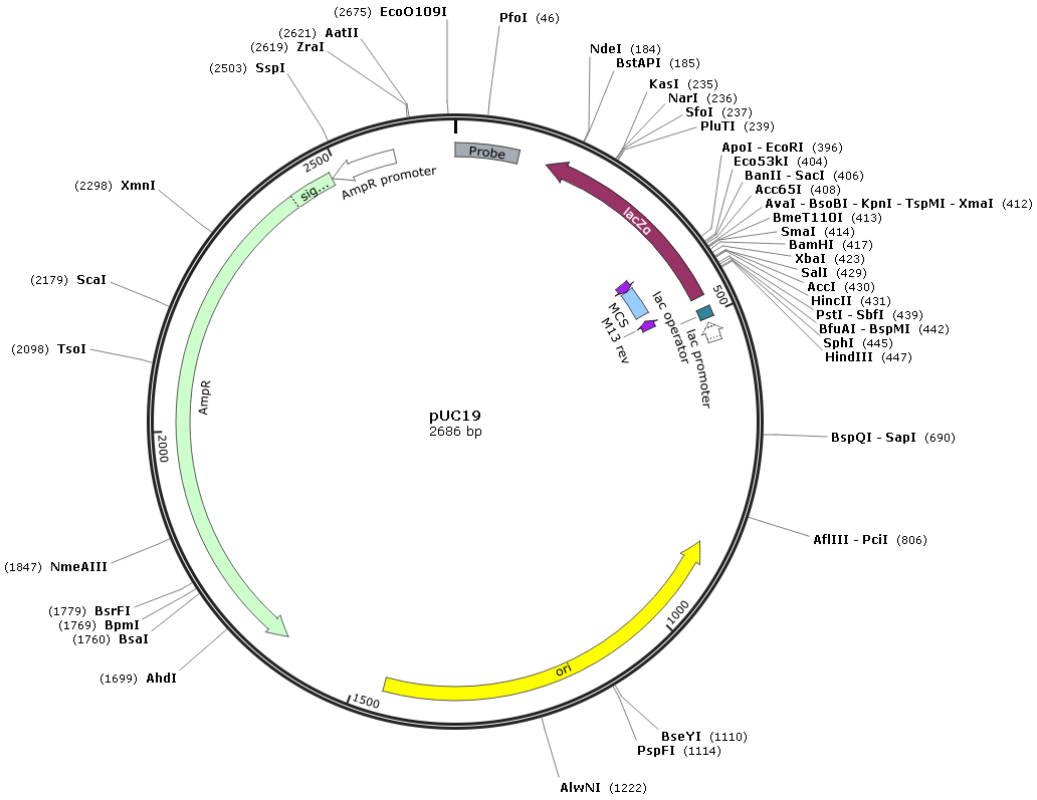

Figure 48. The pUC19 vector map, specifying in grey the hybridization position for the 60 bp oligo-probe.

All the methodologies for the fluorescent labelling of the probes and hybridization protocols are described in Appendices 3. The probe labelling *via* the direct one-step reaction using the cofactor with a rhodamine-B in the transferable moiety was carried out for all the three protocols developed. After BALM microscopy experiments and *Counter* analysis, it was possible to note that the hybridization occurred, but in low efficiency (around 1 – 2% of the plasmids hybridized). However, when the FISH-probe was labelled *via* direct one-step reaction using the Atto-647N-NHS-ester dye implementing *Protocol 3*, the performance was much more improved to approximately 20 – 40% of the plasmids hybridized. This considerable difference between 20 and 40% can be ascribed to the different observation regions of the sample, in which the movies were acquired. Besides, the process of hybridization is not completely homogeneous, due to the evaporation of a part of the "hybridization mix solution". As discussed previously in section 4.4, this direct single-step reaction also provided the best results for plasmid labelling. Therefore, we can infer this reaction has a great potential to be applied to FISH purposes, when performed under optimized conditions. This project continues with the implementation of the FISH approach to long DNA combing. The following figure (Figure 49) shows an example of a microscopy image after the hybridization procedure.

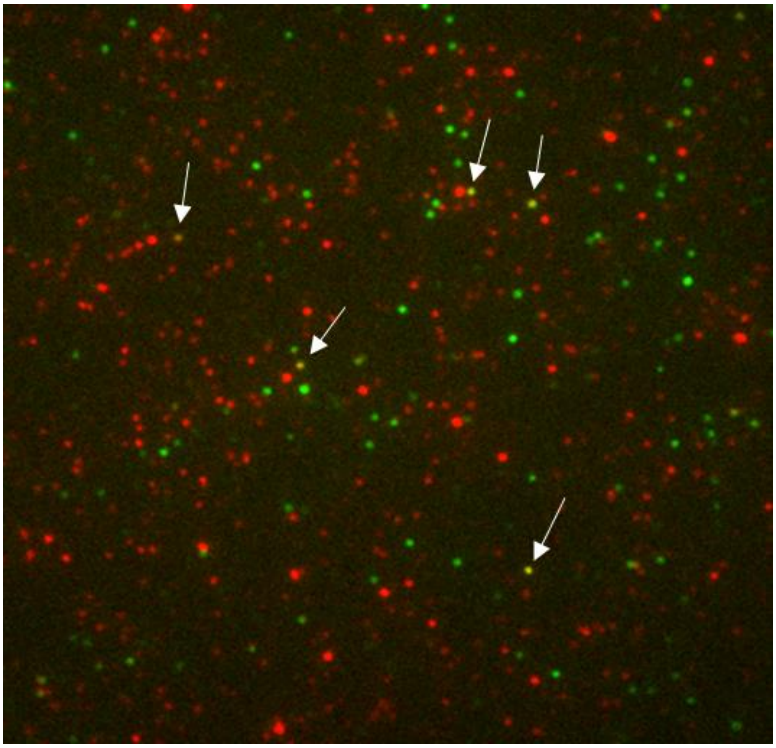

Figure 49. Wide field fluorescence microscopy image of the hybridization system composed by the FISH-probe labelled with rhodamine-6 (one-step reaction using the cofactor MTC-10 and the enzyme M.MpeI) and the plasmid DNA pUC19. The fluorescent red spots represent the probe molecules labelled with rhodamine (excitation laser at 561 nm) and the green spots the plasmids labelled with the intercalating dye YOYO-1 (excitation laser at 488 nm). The yellow fluorescent spots are an overlapping of both channels, indicating the plasmids where the hybridization process occurred. Arrows indicate some of these yellow spots. This experiment was performed using *Protocol 1* (Appendices 3.5.1).

The FISH technique was also studied using the Cu-free click reaction, SPAAC, to label the oligonucleotide with Cy3- or Cy5-di-benzylcyclooctyne dyes. However, after the hybridization performed using *Protocol 3*, it did not provide satisfactory results, since the dye molecules were immediately bleached. Moreover, hairpin probes were also fluorescently labelled for application in FISH purposes.

5 CONCLUSIONS

This study provided a significant contribution, since it was able to develop an optimal methodology for the sequence-specific fluorescent labelling of DNA. Among all the strategies, the great potential of the direct one-step reaction using a methyltransferase enzyme, as well as of the strain-promoted azide-alkyne cycloaddition were verified. These reactions provided more than 90% of the plasmids labelled with at least one fluorophore. Additionally, the investigation of the DNA morphology by AFM demonstrated that the plasmids retained their native structures after the fluorescent labelling using these approaches, which is pivotal for the normal functionality of DNA.

We also showed that even when carrying fluorophores, the plasmids labelled *via* our mTAG single-step approach retained their ability to encode genetic information, since they were successfully applied for transfection into mammalian cells and protein expression. Moreover, we could fluorescently label DNA probes for fluorescence *in situ* hybridization purposes.

Another important issue was the study of the Cu-catalysed azide-alkyne cycloaddition. We could observe based on AFM imaging that the most part of the plasmids were in the open-circular conformation, potentially caused by the nicks and breaks from ROS induced by the Cu(I)-catalyst.

REFERENCES

[1] MURPHY, D. B.; DAVIDSON, M. W. **Fundamentals of light microscopy and electronic imaging**. 2. ed. Hoboken: John Wiley, 2013. 538 p.

[2] TURRO, N. J. **Modern molecular photochemistry**. Sausalito: University Science Books, 1991. 628 p.

[3] SAUER, M.; HOFKENS, J.; ENDERLEIN, J. **Handbook of fluorescence spectroscopy and imaging**. Weinheim: Wiley-VCH, 2011. 281 p.

[4] LAKOWICZ, J. R. **Principles of fluorescence spectroscopy**. 3. ed. New York: Springer Science, 2006. 954 p.

[5] WOLTER, S.; LÖSCHBERGER, A.; HOLM, T.; AUFMKOLK, S.; DABAUVALLE, M. -C.; VAN DE LINDE, S.; SAUER, M. RapidSTORM: accurate, fast open-source software for localization microscopy. **Nature Methods,** v. 9, n. 11, p. 1040-1041, 2012.

[6] DEDECKER, P.; HOFKENS, J.; HOTTA, J.-I. Diffraction-unlimited optical microscopy. **Materials Today,** v. 11, p. 12-21, 2008.

[7] HUANG, B.; BATES, M.; ZHUANG, X. Super-resolution fluorescence microscopy. **Annual Review of Biochemistry**, v. 78, p. 993-1016, 2009.

[8] WOLL, D.; BRAEKEN, E.; DERES, A.; DE SCHRYVER, F. C.; UJI-I, H.; HOFKENS, J. Polymers and single molecule fluorescence spectroscopy, what can we learn? **Chemical Society Reviews,** v. 38, n. 2, p. 313-328, 2009.

[9] HUANG, B.; BABCOCK, H.; ZHUANG, X. Breaking the diffraction barrier: super-resolution imaging of cells. **Cell,** v. 143, n. 7, p. 1047-1058, 2010.

[10] MOERNER, W. E.; FROMM, D. P. Methods of single-molecule fluorescence spectroscopy and microscopy. **Review of Scientific Instruments,** v. 74, n. 8, p. 3597-3619, 2003.

[11] PADDOCK, S. W.; FELLERS, T. J.; DAVIDSON, M. D. **Confocal microscopy.** 2015. Available in: <http://www.microscopyu.com/articles/confocal/confocalintrobasics.html>. Access in: 26 jan. 2016.

[12] LENCIONE, D.; GEHLEN, M. H. **Grupo de fluorescência molecular.** 2016. Available in: <http://gfm.iqsc.usp.br/pesquisa/equipamentos/>. Access in: 16 jun. 2016.

[13] ROSS, S. T.; SCHWARTZ, S.; FELLERS, T. J.; DAVIDSON, M. W. **Total internal reflection fluorescence (TIRFM) microscopy.** 2015. Available in: <http://www.microscopyu.com/articles/fluorescence/tirf/tirfintro.html>. Access in: 10 oct. 2015.

[14] AXELROD, D.; DAVIDSON, M. **Total internal reflection fluorescence microscopy:** introduction and theoretical aspects. 2012. Available in: <http://olympus.magnet.fsu.edu/primer/techniques/fluorescence/tirf/tirfintro.html>. Access in: 10 oct. 2015.

[15] ABBE, E. Beiträge zur theorie des mikroskops und der mikroskopischen wahrnehmung. **Archive für Mikroskopische Anatomie,** v. 9, p. 413-420, 1873.

[16] HEILEMANN, M.; VAN DE LINDE, S.; SCHÜTTPELZ, M.; KASPER, R.; SEEFELDT, B.; MUKHERJEE, A.; TINNEFELD, P.; SAUER, M. Subdiffraction-resolution fluorescence imaging with conventional fluorescent probes. **Angewandte Chemie-International Edition,** v. 47, n. 33, p. 6172-6176, 2008.

[17] HELL, S. W.; WICHMANN, J. Breaking the diffraction resolution limit by stimulated-emission-depletion fluorescence microsccopy. **Optics Letters,** v. 19, n. 11, p. 780-782, 1994.

[18] BETZIG, E.; PATTERSON, G. H.; SOUGRAT, R.; LINDWASSER, O. W.; OLENYCH, S.; BONIFACINO, J. S.; DAVIDSON, M. W.; LIPPINCOTT-SCHWARTZ, J.; HESS, H. F. Imaging intracellular fluorescent proteins at nanometer resolution. **Science,** v. 313, n. 5793, p. 1642-1645, 2006.

[19] HESS, S. T.; GIRIRAJAN, T. P. K.; MASON, M. D. Ultra-high resolution imaging by fluorescence photoactivation localization microscopy. **Biophysical Journal,** v. 91, n. 11, p. 4258-4272, 2006.

[20] RUST, M. J.; BATES, M.; ZHUANG, X. Sub-diffraction-limit imaging by stochastic optical reconstruction microscopy (STORM). **Nature Methods,** v. 3, n. 10, p. 793-795, 2006.

[21] YAMANAKA, M.; SMITH, N. I.; FUJITA, K. Introduction to super-resolution microscopy. **Microscopy,** v. 63, n. 3, p. 177-192, 2014.

[22] ALLEN, J. R.; ROSS, S. T.; DAVIDSON, M. W. Single molecule localization microscopy for superresolution. **Journal of Optics,** v. 15, n. 9, p. 1-15, 2013.

[23] EGNER, A.; GEISLER, C.; VON MIDDENDORFF, C.; BOCK, H.; WENZEL, D.; MEDDA, R.; ANDRESEN, M.; STIEL, A. C.; JAKOBS, S.; EGGELING, C.; SCHÖNLE, A.; HELL, S. W. Fluorescence nanoscopy in whole cells by asynchronous localization of photoswitching emitters. **Biophysical Journal,** v. 93, n. 9, p. 3285-3290, 2007.

[24] VAN DE LINDE, S.; LÖSCHBERGER, A.; KLEIN, T.; HEIDBREDER, M.; WOLTER, S.; HEILEMANN, M.; SAUER, M. Direct stochastic optical reconstruction microscopy with standard fluorescent probes. **Nature Protocols,** v. 6, n. 7, p. 991-1009, 2011.

[25] NELSON, D. L.; COX, M. M. **Lehninger principles of biochemistry.** 5. ed. New York: W. H. Freeman, 2008. 1158 p.

[26] PRAY, L. A. **Discovery of DNA structure and function: Watson and Crick.** 2008. Available in: <http://www.nature.com/scitable/topicpage/discovery-of-dna-structure-and-function-watson-397>. Access in: 9 feb. 2016.

[27] WATSON, J. D.; CRICK, F. H. C. Molecular structure of nucleic acids: a structure for deoxyribose nucleic acid. **Nature,** v. 171, n. 4356, p. 737-738, 1953.

[28] FRANKLIN, R. E.; GOSLING, R. G. The analysis of x-ray fibre diagrams of DNA and the dependence of structure on water content. **Transactions of the Faraday Society,** v. 50, n. 3, p. 298-299, 1954.

[29] WILKINS, M. H. F. X-ray diffraction studies of DNA and nucleoproteins. **Transactions of the Faraday Society,** v. 50, n. 3, p. 299-299, 1954.

[30] PALCHAUDHURI, R.; HERGENROTHER, P. J. DNA as a target for anticancer compounds: methods to determine the mode of binding and the mechanism of action. **Current Opinion in Biotechnology,** v. 18, n. 6, p. 497-503, 2007.

[31] SISCHKA, A.; TOENSING, K.; ECKEL, R.; WILKING, S. D.; SEWALD, N.; ROS, R.; ANSELMETTI, D. Molecular mechanisms and kinetics between DNA and DNA binding ligands. **Biophysical Journal,** v. 88, n. 1, p. 404-411, 2005.

[32] JOHNSON, I.; SPENCE, M. T. Z. (Ed.) **The molecular probes handbook:** a guide to fluorescent probes and labeling technologies. 11. ed. Walthan: Life Technologies, 2010. 1060 p.

[33] PAIK, D. H.; PERKINS, T. T. Dynamics and multiple stable binding modes of DNA intercalators revealed by single-molecule force spectroscopy. **Angewandte Chemie-International Edition,** v. 51, n. 8, p. 1811-1815, 2012.

[34] CHAIRES, J. B. Energetics of drug-DNA interactions. **Biopolymers,** v. 44, n. 3, p. 201-215, 1997.

[35] SCHOEN, I.; RIES, J.; KLOTZSCH, E.; EWERS, H.; VOGEL, V. Binding-activated localization microscopy of DNA structures. **Nano Letters,** v. 11, n. 9, p. 4008-4011, 2011.

[36] FLORS, C. DNA and chromatin imaging with super-resolution fluorescence microscopy based on single-molecule localization. **Biopolymers,** v. 95, n. 5, p. 290-297, 2011.

[37] FLORS, C.; RAVARANI, C. N. J.; DRYDEN, D. T. F. Super-resolution imaging of DNA labelled with intercalating dyes. **Chemphyschem,** v. 10, n. 13, p. 2201-2204, 2009.

[38] FLORS, C. Photoswitching of monomeric and dimeric DNA-intercalating cyanine dyes for super-resolution microscopy applications. **Photochemical & Photobiological Sciences,** v. 9, n. 5, p. 643-648, 2010.

[39] DEEN, J.; SEMPELS, W.; DE DIER, R.; VERMANT, J.; DEDECKER, P.; HOFKENS, J.; NEELY , R. K. Combing of genomic DNA from droplets containing picograms of material. **ACS Nano,** v. 9, n. 1, p. 809-816, 2015.

[40] SHARONOV, A.; HOCHSTRASSER, R. M. Wide-field subdiffraction imaging by accumulated binding of diffusing probes. **Proceedings of the National Academy of Sciences of the United States of America,** v. 103, n. 50, p. 18911-18916, 2006.

[41] JELTSCH, A. Beyond Watson and Crick: DNA methylation and molecular enzymology of DNA methyltransferases. **Chembiochem,** v. 3, n. 5, p. 382-382, 2002.

[42] CHENG, X. D. Structure and function of DNA methyltransferases. **Annual Review of Biophysics and Biomolecular Structure,** v. 24, p. 293-318, 1995.

[43] LABAHN, J.; GRANZIN, J.; SCHLUCKEBIER, G.; ROBINSON, D. P.; JACK, W. E.; SCHILDKRAUT, I.; SAENGER, W. 3-Dimensional structure of the adenine-specific DNA methyltransferase M.TaqI in complex with the cofactor S-adenosilmethionine. **Proceedings of the National Academy of Sciences of the United States of America,** v. 91, n. 23, p. 10957-10961, 1994.

[44] GOEDECKE, K.; PIGNOT, M.; GOODY, R. S.; SCHEIDIG, A. J.; WEINHOLD, E. Structure of the N6-adenine DNA methyltransferase M.Taql in complex with DNA and a cofactor analog. **Nature Structural Biology,** v. 8, n. 2, p. 121-125, 2001.

[45] PLJEVALJCIC, G.; SCHMIDT, F.; WEINHOLD, E. Sequence-specific methyltransferase-induced labeling of DNA (SMILing DNA). **Chembiochem,** v. 5, n. 3, p. 265-269, 2004.

[46] PATTERSON, D. M.; NAZAROVA, L. A.; PRESCHER, J. A. Finding the right (bioorthogonal) chemistry. **ACS Chemical Biology,** v. 9, n. 3, p. 592-605, 2014.

[47] GRAMMEL, M.; HANG, H. C. Chemical reporters for biological discovery. **Nature Chemical Biology,** v. 9, n. 8, p. 475-484, 2013.

[48] SLETTEN, E. M.; BERTOZZI, C. R. Bioorthogonal chemistry: fishing for selectivity in a sea of functionality. **Angewandte Chemie-International Edition,** v. 48, n. 38, p. 6974-6998, 2009.

[49] GOTHELF, K. V.; JORGENSEN, K. A. Asymmetric 1,3-dipolar cycloaddition reactions. **Chemical Reviews,** v. 98, n. 2, p. 863-909, 1998.

[50] ROSTOVTSEV, V. V.; GREEN, L. G.; FOKIN, V. V.; SHARPLESS, K. B. A stepwise Huisgen cycloaddition process: Copper(I)-catalyzed regioselective "ligation" of azides and terminal alkynes. **Angewandte Chemie-International Edition,** v. 41, n. 14, p. 2596-2599, 2002.

[51] HUISGEN, R. 1.3-Dipolare cycloadditionen rückschau und ausblick. **Angewandte Chemie-International Edition,** v. 75, n. 13, p. 604-637, 1963.

[52] PRESCHER, J. A.; BERTOZZI, C. R. Chemistry in living systems. **Nature Chemical Biology,** v. 1, n. 1, p. 13-21, 2005.

[53] JEWETT, J. C.; BERTOZZI, C. R. Cu-free click cycloaddition reactions in chemical biology. **Chemical Society Reviews,** v. 39, n. 4, p. 1272-1279, 2010.

[54] TORNOE, C. W.; CHRISTENSEN, C.; MELDAL, M. Peptidotriazoles on solid phase: 1,2,3 -triazoles by regiospecific copper(I)-catalyzed 1,3-dipolar cycloadditions of terminal alkynes to azides. **Journal of Organic Chemistry,** v. 67, n. 9, p. 3057-3064, 2002.

[55] MELDAL, M.; TORNOE, C. W. Cu-catalyzed azide-alkyne cycloaddition. **Chemical Reviews,** v. 108, n. 8, p. 2952-3015, 2008.

[56] GIERLICH, J.; BURLEY, G. A.; GRAMLICH, P. M.; HAMMOND, D. M.; CARELL, T. Click chemistry as a reliable method for the high-density postsynthetic functionalization of alkyne-modified DNA. **Organic Letters,** v. 8, n. 17, p. 3639-3642, 2006.

[57] EL-SAGHEER, A. H.; BROWN, T. Click chemistry with DNA. **Chemical Society Reviews,** v. 39, n. 4, p. 1388-1405, 2010.

[58] GRAMLICH, P. M. E.; WARNCKE, S.; GIERLICH, J.; CARELL, T. Click-click-click: single to triple modification of DNA. **Angewandte Chemie-International Edition,** v. 47, n. 18, p. 3442-3444, 2008.

[59] GRAMLICH, P. M.; WIRGES, C. T.; MANETTO, A.; CARELL, T. Postsynthetic DNA modification through the copper-catalyzed azide-alkyne cycloaddition reaction. **Angewandte Chemie-International Edition,** v. 47, n. 44, p. 8350-8358, 2008.

[60] KOCALKA, P.; EL-SAGHEER, A. H.; BROWN, T. Rapid and efficient DNA strand cross-linking by click chemistry. **Chembiochem,** v. 9, n. 8, p. 1280-1285, 2008.

[61] GUTSMIEDL, K.; FAZIO, D.; CARELL, T. High-density DNA functionalization by a combination of Cu-catalyzed and Cu-free click chemistry. **Chemistry-A European Journal,** v. 16, n. 23, p. 6877-6883, 2010.

[62] EL-SAGHEER, A. H.; BROWN, T. Click nucleic acid ligation: applications in biology and nanotechnology. **Accounts of Chemical Research,** v. 45, n. 8, p. 1258-1267, 2012.

[63] VRANKEN, C.; DEEN, J.; DIRIX, L.; STAKENBORG, T.; DEHAEN, W.; LEEN, V.; HOFKENS, J.; NEELY, R. K. Super-resolution optical DNA Mapping via DNA methyltransferase-directed click chemistry. **Nucleic Acids Research,** v. 42, n. 7, p. 1-10, 2014.

[64] SALIC, A.; MITCHISON, T. J. A chemical method for fast and sensitive detection of DNA synthesis in vivo. **Proceedings of the National Academy of Sciences of the United States of America,** v. 105, n. 7, p. 2415-2420, 2008.

[65] NING, X.; GUO, J.; WOLFERT, M. A.; BOONS, G. J. Visualizing metabolically labeled glycoconjugates of living cells by copper-free and fast huisgen cycloadditions. **Angewandte Chemie-International Edition,** v. 47, n. 12, p. 2253-2255, 2008.

[66] AGARD, N. J.; PRESCHER, J. A.; BERTOZZI, C. R. A strain-promoted 3+2 azide-alkyne cycloaddition for covalent modification of blomolecules in living systems. **Journal of the American Chemical Society,** v. 126, n. 46, p. 15046-15047, 2004.

[67] WITTIG, G.; KREBS, A. Zur existenz niedergliedriger cycloalkine, I. **Chemische Berichte,** v. 94, p. 3260-3275, 1961.

[68] BECER, C. R.; HOOGENBOOM, R.; SCHUBERT, U. S. Click chemistry beyond metal-catalyzed cycloaddition. **Angewandte Chemie-International Edition,** v. 48, n. 27, p. 4900-4908, 2009.

[69] ESS, D. H.; JONES, G. O.; HOUK, K. N. Transition states of strain-promoted metal-free click chemistry: 1,3-dipolar cycloadditions of phenyl azide and cyclooctynes. **Organic Letters,** v. 10, n. 8, p. 1633-1636, 2008.

[70] AGARD, N. J.; BASKIN, J. M.; PRESCHER, J. A.; LO, A.; BERTOZZI, C. R. A comparative study of bioorthogonal reactions with azides. **ACS Chemical Biology,** v. 1, n. 10, p. 644-648, 2006.

[71] BASKIN, J. M.; PRESCHER, J. A.; LAUGHLIN, S. T.; AGARD, N. J.; CHANG, P. V.; MILLER, I. A.; LO, A.; CODELLI, J. A.; BERTOZZI, C. R. Copper-free click chemistry for dynamic in vivo imaging. **Proceedings of the National Academy of Sciences of the United States of America,** v. 104, n. 43, p. 16793-16797, 2007.

[72] CODELLI, J. A.; BASKIN, J. M.; AGARD, N. J.; BERTOZZI, C.R. Second-generation difluorinated cyclooctynes for copper-free click chemistry. **Journal of the American Chemical Society,** v. 130, n. 34, p. 11486-11493, 2008.

[73] SLETTEN, E. M.; BERTOZZI, C. R. A hydrophilic azacyclooctyne for Cu-free click chemistry. **Organic Letters,** v. 10, n. 14, p. 3097-3099, 2008.

[74] JEWETT, J. C.; SLETTEN, E. M.; BERTOZZI, C. R. Rapid Cu-free click chemistry with readily synthesized biarylazacyclooctynones. **Journal of the American Chemical Society,** v. 132, n. 11, p. 3688-3690, 2010.

[75] LAUGHLIN, S. T.; BERTOZZI, C. R. In vivo imaging of Caenorhabditis elegans glycans. **ACS Chemical Biology,** v. 4, n. 12, p. 1068-1072, 2009.

[76] LAUGHLIN, S. T.; BASKIN, J. M.; AMACHER, S. L.; BERTOZZI, C.R. In vivo imaging of membrane-associated glycans in developing zebrafish. **Science,** v. 320, n. 5876, p. 664-667, 2008.

[77] MERKEL, M.; PEEWASAN, K.; ARNDT, S.; PLOSCHIK, D.; WAGENKNECHT, H.A. Copper-free postsynthetic labeling of nucleic acids by means of bioorthogonal reactions. **Chembiochem,** v. 16, n. 11, p. 1541-1553, 2015.

[78] HEUER-JUNGEMANN, A.; KIRKWOOD, R.; EL-SAGHEER, A. H.; BROWN, T.; KANARAS, A.G. Copper-free click chemistry as an emerging tool for the programmed ligation of DNA-functionalised gold nanoparticles. **Nanoscale,** v. 5, n. 16, p. 7209-7212, 2013.

[79] SHELBOURNE, M.; CHEN, X.; BROWN, T.; EL-SAGHEER, A.H. Fast copper-free click DNA ligation by the ring-strain promoted alkyne-azide cycloaddition reaction. **Chemical Communications,** v. 47, n. 22, p. 6257-6259, 2011.

[80] MARKS, I. S.; KANG, J. S.; JONES, B. T.; LANDMARK, K. J.; CLELAND, A. J.; TATON, T. A. Strain-promoted "click" chemistry for terminal labeling of DNA. **Bioconjugate Chemistry,** v. 22, n. 7, p. 1259-1263, 2011.

[81] SHELBOURNE, M.; BROWN JR, T.; EL-SAGHEER, A. H.; BROWN, T. Fast and efficient DNA crosslinking and multiple orthogonal labelling by copper-free click chemistry. **Chemical Communications,** v. 48, n. 91, p. 11184-11186, 2012.

[82] ALEXANDER, M. D.; BURKART, M. D.; LEONARD, M. S.; PORTONOVO, P.; LIANG, B.; DING, X.; JOULLIÉ, M. M.; GULLEDGE, B. M.; AGGEN, J. B.; CHAMBERLIN, A. R.; SANDLER, J.; FENICAL, W.; CUI, J.; GHARPURE, S. J.; POLOSUKHIN, A.; ZHANG, H. R.; EVANS, P. A.; RICHARDSON, A. D.; HARPER, M. K.; IRELAND, C. M.; VONG, B. G.; BRADY, T. P.; THEODORAKIS, E. A.; LA CLAIR, J. J. A central strategy for converting natural products into fluorescent probes. **Chembiochem,** v. 7, n. 3, p. 409-416, 2006.

[83] SANDLER, J. S.; FENICAL, W.; GULLEDGE, B. M.; CHAMBERLIN, A. R.; LA CLAIR, J. J. Fluorescent profiling of natural product producers. **Journal of the American Chemical Society,** v. 127, n. 26, p. 9320-9321, 2005.

[84] HENTSCHEL, F.; SASSE, F.; LINDEL, T. Fluorescent analogs of the marine natural product psammaplin A: synthesis and biological activity. **Organic & Biomolecular Chemistry,** v. 10, n. 35, p. 7120-7133, 2012.

[85] BURES, F. Fundamental aspects of property tuning in push-pull molecules. **RSC Advances,** v. 4, n. 102, p. 58826-58851, 2014.

[86] ZOON, P. D.; BROUWER, A. M. A push-pull aromatic chromophore with a touch of merocyanine. **Photochemical & Photobiological Sciences,** v. 8, n. 3, p. 345-353, 2009.

[87] PETSALAKIS, I. D.; GEORGIADOU, D. G.; VASILOPOULOU, M.; PISTOLIS, G.; DIMOTIKALI, D.; ARGITIS, P.; THEODORAKOPOULOS, G. Theoretical investigation on the effect of protonation on the absorption and emission spectra of two amine-group-bearing, red "push-pull" emitters, 4-dimethylamino-4'-nitrostilbene and 4-(dicyanomethylene)-2-methyl-6-p-(dimethylamino) styryl-4H-pyran, by DFT and TDDFT calculations. **Journal of Physical Chemistry A,** v. 114, n. 17, p. 5580-5587, 2010.

[88] BERGEN, A.; BOHNE, C.; FUENTEALBA, D.; IHMELS, H.; BATS, J. W.; DEISEROTH, H. J.; NEUMANN, E. Studies of the solvatochromic emission properties of N-aroylurea derivatives I: Influence of the substitution pattern. **Photochemical & Photobiological Sciences,** v. 11, n. 4, 2012.

[89] PEREIRA, R. V.; GEHLEN, M. H. Polymerization and conformational transition of poly(methacrylic acid) probed by electronic spectroscopy of aminoacridines. **Macromolecules,** v. 40, n. 6, p. 2219-2223, 2007.

[90] SHEIKH-ALI, B. M.; WEISS, R. G. Effects of aggregation and mesomorphic order on the photophysical properties of 4-alkyl-N-(p-cyanophenyl)piperidines: molecules capable of forming intramolecular charge transfer states. **Journal of the American Chemical Society,** v. 116, n. 14, p. 6111-6120, 1994.

[91] FERREIRA, A. P. G.; FREDERICE, R.; JANSSEN, K. P. F.; GEHLEN, M. H. Dually fluorescent silica nanoparticles. **Journal of Luminescence,** v. 131, n. 5, p. 888-893, 2011.

[92] SUZUKI, Y.; YOKOYAMA, K. Design and synthesis of intramolecular charge transfer-based fluorescent reagents for the highly-sensitive detection of proteins. **Journal of the American Chemical Society,** v. 127, n. 50, p. 17799-17802, 2005.

[93] GRABOWSKI, Z. R.; ROTKIEWICZ, K.; RETTIG, W. Structural changes accompanying intramolecular electron transfer: Focus on twisted intramolecular charge-transfer states and structures. **Chemical Reviews,** v. 103, n. 10, p. 3899-4032, 2003.

[94] FORREST, S. R.; THOMPSON, M. E. Introduction: organic electronics and optoelectronics. **Chemical Reviews,** v. 107, n. 4, p. 923-925, 2007.

[95] MILLER, R. D.; CHANDROSS, E. A. Introduction: materials for electronics. **Chemical Reviews,** v. 110, n. 1, p. 1-2, 2010.

[96] MALYTSKYI, V.; SIMON, J. J; PATRONE, L.; RAIMUNDO, J. M. Thiophene-based push-pull chromophores for small molecule organic solar cells (SMOSCs). **RSC Advances,** v. 5, n. 1, p. 354-397, 2015.

[97] KALETAS, B. K.; WILLIAMS, R. M.; KÖNIG, B.; DE COLA, L. Strong fluorescence enhancement of 2-bromo-3-(1H-indol-3-yl)maleimide upon coordination to a Lewis-acidic metal complex. **Chemical Communications**, n. 7, p. 776-777, 2002.

[98] KALETAS, B. K.; JOSHI, H. C.; VAN DER ZWAN, G.; FANTI, M.; ZERBETTO, F.; GOUBITZ, K.; DE COLA, L.; KÖNIG, B.; WILLIAMS, R. M. Asymmetric indolylmaleimide derivatives and their complexation with zinc(II)-cyclen. **Journal of Physical Chemistry A,** v. 109, n. 42, p. 9443-9455, 2005.

[99] KALETAS, B. K.; MANDL, C.; VAN DER ZWAN, G.; FANTI, M.; ZERBETTO, F.; DE COLA, L.; KÖNIG, B.; WILLIAMS, R.M. Unexpected photophysical properties of symmetric indolylmaleimide derivatives. **Journal of Physical Chemistry A,** v. 109, n. 29, p. 6440-6449, 2005.

[100] KOSOWER, E. M.; DE SOUZA, J. R. n(pi)-ct-pi* transitions: n pi* transitions of the second kind. **Chemical Physics,** v. 324, n. 1, p. 3-7, 2006.

[101] NAKAZONO, M.; JINGUJI, A.; NANBU, S.; KUWANO, R.; ZHENG, Z.; SAITA, K.; OSHIKAWA, Y.; MIKUNI, Y.; MURAKAMI, T.; ZHAO, Y.; SASAKI, S.; ZAITSU, K. Fluorescence and chemiluminescence properties of indolylmaleimides: experimental and theoretical studies. **Physical Chemistry Chemical Physics,** v. 12, n. 33, p. 9783-9793, 2010.

[102] ZHENG, Z.; ZHAO, Y.; NAKAZONO, M.; NANBU, S. Theoretical study of photo-physical properties of indolylmaleimide derivatives. **Physical Chemistry Chemical Physics,** v. 14, n. 9, p. 3017-3024, 2012.

[103] MANNING, S.; BOGEN, W.; KELLY, L. Synthesis, characterization, and photophysical study of fluorescent N-substituted benzo[ghi]perylene "swallow tail" monoimides. **The Journal of Organic Chemistry,** v. 76, p. 6007-6013, 2011.

[104] DALTON, M. J.; KANNAN, R.; HALEY, J. E.; HELL, G. S.; MCLEAN, D. G.; COOPER, T. M.; PRASAD, P. N.; TAN, L. -S. Aromatic polyimides containing main-chain diphenylaminofluorene-benzothiazole motif: fluorescence quenching, two-photon properties, and exciplex formation in a solid state. **Macromolecules,** v. 44, n. 18, p. 7194-7206, 2011.

[105] YEH, H. C.; WU, W. C.; CHEN, C. T. The colourful fluorescence from readily-synthesised 3,4-diaryl-substituted maleimide fluorophores. **Chemical Communications**, n. 3, p. 404-405, 2003.

[106] FIELDS, E. K.; BEHREND, S. J.; MEYERSON, S.; WINZENBURG, M. L.; ORTEGA, B. R.; HALL JUNIOR, H. K. Diaryl-substituted maleic anhydrides. **Journal of Organic Chemistry,** v. 55, n. 17, p. 5165-5170, 1990.

[107] DEAN, W. D.; BLUM, D. M. Condensation of arylacetonitriles with glyoxylic acid: facile synthesis of arylmaleic acid derivatives. **Journal of Organic Chemistry,** v. 58, n. 27, p. 7916-7917, 1993.

[108] NEWMAN, M. S.; STALICK, W. M. Novel synthesis of disubstituted maleic anhydrides by the pyrolysis of 1-ethoxy-1-alkenyl esters of alpha-keto acids. **Journal of Organic Chemistry,** v. 38, n. 19, p. 3386-3389, 1973.

[109] RUDI, A.; GOLDBERG, I.; STEIN, Z.; FROLOW, F.; BENAYAHU, Y.; SCHLEYER, M.; KASHMAN, Y. Polycitone A and polycitrins A and B: new alkaloids from the marine ascidian Polycitor sp. **Journal of Organic Chemistry,** v. 59, n. 5, p. 999-1003, 1994.

[110] BURTOLOSO, A. C. B.; GARCIA, A. L. L.; MIRANDA, K. C.; CORREIA, C. R. D. Heck arylation of maleic anhydrides using arenediazonium tetrafluoroborates: synthesis of mono- and diarylated maleic anhydrides and of the marine alkaloids prepolycitrin A and polycitrin A. **Synlett**, n. 18, p. 3145-3149, 2006.

[111] CANTO, K.; RIBEIRO, R. S.; BIAJOLI, A. F. P.; CORREIA, C. R. D. Expeditious synthesis of the marine natural products prepolycitrin A and polycitrins A and B through Heck arylations. **European Journal of Organic Chemistry,** v. 2013, n. 35, p. 8004-8013, 2013.

[112] LAUER, M. H.; DREKENER, R. L.; CORREIA, C. R.; GEHLEN, M. H. Fluorescence from bisaryl-substituted maleimide derivatives. **Photochemical & Photobiological Sciences,** v. 13, n. 6, p. 859-866, 2014.

[113] LAUER, M. H.; GEHLEN, M. H.; DE JESUS, K.; BERLINCK, R. G. Fluorescence spectroscopy and confocal microscopy of the mycotoxin citrinin in condensed phase and hydrogel films. **Journal of Fluorescence,** v. 24, n. 3, p. 745-750, 2014.

[114] SIMAS, E. R.; GEHLEN, M. H.; PINTO, M. F. S.; SIQUEIRA, J.; MISOGUTTI, L. Intrachain energy migration to weak charge-transfer state in polyfluorene end-capped with naphthalimide derivative. **Journal of Physical Chemistry A,** v. 114, n. 47, p. 12384-12390, 2010.

[115] LIPPERT, E. V. Spektroscopische bistimmung des dipolmomentes aromatischer verbindungen im ersten angeregten singulettzustand. **Zeitschrift für Elektrochemie.** v. 61, p. 962-975, 1957.

[116] MATAGA, N.; KAIFU, Y.; KOIZUMI, M. Solvent effects upon fluorescence spectra and the dipolemoments of ecited molecules. **Bulletin of the Chemical Society of Japan,** v. 29, n. 4, p. 465-470, 1956.

[117] FRISCH, M. J.; TRUCKS, G. W.; SCHLEGEL, H. B.; SCUSERIA, G. E.; ROBB, M. A.; CHEESEMAN, J. R.; MONTGOMERY, JR., J. A.; VREVEN, T.; KUDIN, K. N.; BURANT, J. C.; MILLAM, J. M.; IYENGAR, S. S.; TOMASI, J.; BARONE, V.; MENNUCCI, B.; COSSI, M.; SCALMANI, G.; REGA, N.; PETERSSON, G. A.; NAKATSUJI, H.; HADA, M.; EHARA, M.; TOYOTA, K.; FUKUDA, R.; HASEGAWA, J.; ISHIDA, M.; NAKAJIMA, T.; HONDA, Y.; KITAO, O.; NAKAI, H.; KLENE, M.; LI, X.; KNOX, J. E.; HRATCHIAN, H. P.; CROSS, J. B.; BAKKEN, V.; ADAMO, C.; JARAMILLO, J.; GOMPERTS, R.; STRATMANN, R. E.; YAZYEV, O.; AUSTIN, A. J.; CAMMI, R.; POMELLI, C.; OCHTERSKI, J. W.; AYALA, P. Y.; MOROKUMA, K.; VOTH, G. A.; SALVADOR, P.; DANNENBERG, J. J.; ZAKRZEWSKI, V. G.; DAPPRICH, S.; DANIELS, A. D.; STRAIN, M. C.; FARKAS, O.; MALICK, D. K.; RABUCK, A. D.; RAGHAVACHARI, K.; FORESMAN, J. B.; ORTIZ, J. V.; CUI, Q.; BABOUL, A. G.; CLIFFORD, S.; CIOSLOWSKI, J.; STEFANOV, B. B.; LIU, G.; LIASHENKO, A.; PISKORZ, P.; KOMAROMI, I.; MARTIN, R. L.; FOX, D. J.; KEITH, T.; AL-LAHAM, M. A.; PENG, C. Y.; NANAYAKKARA, A.; CHALLACOMBE, M.; GILL, P. M. W.; JOHNSON, B.; CHEN, W.; WONG, M. W.; GONZALEZ, C.; POPLE, J. A. **Gaussian 03**. Wallingford CT: Gaussian. 2004. Computer programme.

[118] CHANDROSS, E. A.; THOMAS, H. T. The interaction of amine-hydrocarbon exciplexes with small dipolar molecules - stoichiometric complex formation. **Chemical Physics Letters,** v. 9, n. 5, p. 397-400, 1971.

[119] DAS, R.; MITRA, S.; MUKHERJEE, S. Proton transfer and anion formation in the ground and excited states of 4-methyl-2,6-diformyl phenol in highly polar aprotic solvents. **Journal of Photochemistry and Photobiology a-Chemistry,** v. 76, n. 1-2, p. 33-38, 1993.

[120] KASHA, M. Proton-transfer spectroscopy: perturbation of the tautomerization potential. **Journal of the Chemical Society-Faraday Transactions II,** v. 82, p. 2379-2392, 1986.

[121] CARMICHAEL, A. J.; SEDDON, K. R. Polarity study of some 1-alkyl-3-methylimidazolium ambient-temperature ionic liquids with the solvatochromic dye, Nile Red. **Journal of Physical Organic Chemistry,** v. 13, n. 10, p. 591-595, 2000.

[122] FERYFORGUES, S.; FAYET, J. P.; LOPEZ, A. Drastic changes in the fluorescence properties of NBD probes with the polarity of the medium: involvement of a TICT state? **Journal of Photochemistry and Photobiology A-Chemistry,** v. 70, n. 3, p. 229-243, 1993.

[123] PEREIRA, R. V.; GEHLEN, M. H. Picosecond fluorescence dynamics of auramine with a long aliphatic chain. **Chemical Physics Letters,** v. 417, n. 4-6, p. 425-429, 2006.

[124] OLIVEIRA, E.; BAPTISTA, R. M.; COSTA, S. P.; RAPOSO, M. M.; LODEIRO, C. Synthesis and solvatochromism studies of novel bis(indolyl)methanes bearing functionalized arylthiophene groups as new colored materials. **Photochemical & Photobiological Sciences,** v. 13, p. 492-498, 2014.

[125] KLIMASAUSKAS, S.; WEINHOLD, E. A new tool for biotechnology: AdoMet-dependent methyltransferases. **Trends in Biotechnology,** v. 25, n. 3, p. 99-104, 2007.

[126] DALHOFF, C.; LUKINAVICIUS, G.; KLIMASĂUSKAS, S.; WEINHOLD, E. Direct transfer of extended groups from synthetic cofactors by DNA methyltransferases. **Nature Chemical Biology,** v. 2, n. 1, p. 31-32, 2006.

[127] PETERS, W.; WILLNOW, S.; DUISKEN, M.; KLEINE, H.; MACHEREY, T.; DUNCAN, K. E.; LITCHFIELD, D. W.; LÜSCHER, B.; WEINHOLD, E. Enzymatic site-specific functionalization of protein methyltransferase substrates with alkynes for click labeling. **Angewandte Chemie-International Edition,** v. 49, n. 30, p. 5170-5173, 2010.

[128] LUKINAVICIUS, G.; TOMKUVIENĖ, M.; MASEVIČIUS, V.; KLIMAŠAUSKAS, S. Enhanced chemical stability of AdoMet analogues for improved methyltransferase-directed labeling of DNA. **ACS Chemical Biology,** v. 8, n. 6, p. 1134-1139, 2013.

[129] DALHOFF, C.; LUKINAVICIUS, G.; KLIMASAUSKAS, S.; WEINHOLD, E. Synthesis of S-adenosyl-L-methionine analogs and their use for sequence-specific transalkylation of DNA by methyltransferases. **Nature Protocols,** v. 1, n. 4, p. 1879-1886, 2006.

[130] LUKINAVICIUS, G.; LAPIENE, V.; STASEVSKIJ, Z.; DALHOFF, C.; WEINHOLD, E.; KLIMASAUSKAS, S. Targeted labeling of DNA by methyltransferase-directed transfer of activated groups (mTAG). **Journal of the American Chemical Society,** v. 129, n. 10, p. 2758-27589, 2007.

[131] PLJEVALJCIC, G.; PIGNOT, M.; WEINHOLD, E. Design of a new fluorescent cofactor for DNA methyltransferases and sequence-specific labeling of DNA. **Journal of the American Chemical Society,** v. 125, n. 12, p. 3486-3492, 2003.

[132] SCHMIDT, F. H. G.; HÜBEN, M.; GIDER, B.; RENAULT, F.; TEULADE-FICHOU, M. P.; WEINHOLD, E. Sequence-specific methyltransferase-induced labelling (SMILing) of plasmid DNA for studying cell transfection. **Bioorganic & Medicinal Chemistry,** v. 16, n. 1, p. 40-48, 2008.

[133] PLOTNIKOVA, A.; OSIPENKO, A.; MASEVIČIUS, V.; VILKAITIS, G.; KLIMAŠAUSKAS, S. Selective covalent labeling of miRNA and siRNA duplexes using HEN1 methyltransferase. **Journal of the American Chemical Society,** v. 136, n. 39, p. 13550-13553, 2014.

[134] KUNKEL, F.; LURZ, R.; WEINHOLD, E. A 7-Deazaadenosylaziridine cofactor for sequence-specific labeling of DNA by the DNA cytosine-C5 methyltransferase M. HhaI. **Molecules,** v. 20, n. 11, p. 20805-20822, 2015.

[135] NEELY, R. K.; DEDECKER, P.; HOTTA, J. -I.; URBANAVIČIŪTĖ, G.; KLIMAŠAUSKAS, S. HOFKENS, J. DNA fluorocode: A single molecule, optical map of DNA with nanometre resolution. **Chemical Science,** v. 1, n. 4, p. 453-460, 2010.

[136] BELIVEAU, B. J.; BOETTIGER, A. N.; AVENDAÑO, M. S.; JUNGMANN, R.; MCCOLE, R. B.; JOYCE, E. F.; KIM-KISELAK, C.; BANTIGNIES, F.; FONSEKA, C.; ERCEG, J.; HANNAN, M. A.; HOANG, H. G.; COLOGNORI, D.; LEE, J. T.; SHIH, W. M.; YIN, P.; ZHUANG, X.; WU, C. T. Single-molecule super-resolution imaging of chromosomes and in situ haplotype visualization using Oligopaint FISH probes. **Nature Communications,** v. 6, n. 7147, p. 1-13, 2015.

[137] LOESCHBERGER, A.; NIEHOERSTER, T.; SAUER, M. Click chemistry for the conservation of cellular structures and fluorescent proteins: ClickOx. **Biotechnology Journal,** v. 9, n. 5, p. 693-697, 2014.

[138] DEDECKER, P.; DUWÉ, S.; NEELY, R. K.; ZHANG, J. Localizer: fast, accurate, open-source, and modular software package for superresolution microscopy. **Journal of Biomedical Optics,** v. 17, n. 12, p. 1-5, 2012.

[139] VANDERLINDEN, W.; BLUNT, M.; DAVID, C. C.; MOUCHERON, C.; KIRSCH-DE MESMAEKER, A.; DE FEYTER, S. Mesoscale DNA structural changes on binding and photoreaction with Ru (TAP)(2)PHEHAT (2+). **Journal of the American Chemical Society,** v. 134, n. 24, p. 10214-10221, 2012.

[140] SCHERER, W. F.; SYVERTON, J. T.; GEY, G. O. Studies on the propagation in vitro of poliomyelitis viruses. IV. Viral multiplication in a stable strain of human malignant epithelial cells (strain HeLa) derived from an epidermoid carcinoma of the cervix. **Journal of Experimental Medicine,** v. 97, n. 5, p. 695-710, 1953.

[141] BURROWS, C. J.; MULLER, J. G. Oxidative nucleobase modifications leading to strand scission. **Chemical Reviews,** v. 98, n. 3, p. 1109-1151, 1998.

[142] LIU, P.-Y.; JIANG, N.; ZHANG, J.; WEI, X.; LIN, H. H.; YU, X. Q. The oxidative damage of plasmid DNA by ascorbic acid derivatives in vitro: the first research on the relationship between the structure of ascorbic acid and the oxidative damage of plasmid DNA. **Chemistry & Biodiversity,** v. 3, n. 9, p. 958-966, 2006.

[143] HONG, V.; STEINMETZ, N. F.; MANCHESTER, M.; FINN, M. G. Labeling live cells by copper-catalyzed alkyne-azide click chemistry. **Bioconjugate Chemistry,** v. 21, n. 10, p. 1912-1916, 2010.

[144] ENGLANDER, S. W.; CALHOUN, D. B.; ENGLANDER, J. J. Biochemistry without oxygen. **Analytical Biochemistry,** v. 161, n. 2, p. 300-306, 1987.

[145] VOGELSANG, J.; KASPER, R.; STEINHAUER, C.; PERSON, B.; HEILEMANN, M.; SAUER, M.; TINNEFELD, P. A reducing and oxidizing system minimizes photobleaching and blinking of fluorescent dyes. **Angewandte Chemie-International Edition,** v. 47, n. 29, p. 5465-5469, 2008.

[146] KIM, S.; GOTTFRIED, A.; LIN, R. R.; DERTINGER, T.; KIM, A. S.; CHUNG, S.; COLYER, R. A.; WEINHOLD, E.; WEISS, S.; EBENSTEIN, Y. Enzymatically incorporated genomic tags for optical mapping of DNA-binding proteins. **Angewandte Chemie-International Edition,** v. 51, n. 15, p. 3578-3581, 2012.

[147] BARANY, F. The TaqI 'star' reaction: strand preferences reveal hydrogen-bond donor and acceptor sites in canonical sequence recognition. **Gene,** v. 65, n. 2, p. 149-165, 1988.

[148] BITINAITE, J.; SCHILDKRAUT, I. Self-generated DNA termini relax the specificity of SgrAI restriction endonuclease. **Proceedings of the National Academy of Sciences of the United States of America,** v. 99, n. 3, p. 1164-1169, 2002.

[149] BERG, F.; WILKEN, J.; HELM, C. A.; BLOCK, S. AFM-based quantification of conformational changes in DNA caused by reactive oxygen species. **Journal of Physical Chemistry B,** v. 119, n. 1, p. 25-32, 2015.

[150] SLATTUM, P. S.; LOOMIS, A. G.; MACHNIK, K. J.; WATT, M. A.; DUZESKI, J. L.; BUDKER, V. G.; WOLFF, J. A.; HAGSTROM, J. E. Efficient in vitro and in vivo expression of covalently modified plasmid DNA. **Molecular Therapy,** v. 8, n. 2, p. 255-263, 2003.

[151] ROMBOUTS, K.; MARTENS, T. F.; ZAGATO, E.; DEMEESTER, J.; DE SMEDT, S. C.; BRAECKMANS, K.; REMAUT, K. Effect of covalent fluorescence labeling of plasmid DNA on its intracellular processing and transfection with lipid-based carriers. **Molecular Pharmaceutics,** v. 11, n. 5, p. 1359-1368, 2014.

[152] NAGAI, T.; IBATA, K.; PARK, E. S.; KUBOTA, M.; MIKOSHIBA, K.; MIYAWAKI, A. A variant of yellow fluorescent protein with fast and efficient maturation for cell-biological applications. **Nature Biotechnology,** v. 20, n. 1, p. 87-90, 2002.

[153] PISTON, W. D.; PATTERSON, G. H.; LIPPINCOTT-SCHWARTZ, J.; CLAXTON, N. S.; DAVIDSON, M. W. **Introduction to fluorescent proteins.** 2016. Available in: <http://www.microscopyu.com/articles/livecellimaging/fpintro.html>. Access in: 21 jan. 2016.

[154] THERMO FISHER SCIENTIFIC. **Dil Stain.** 2016. Available in: <https://www.thermofisher.com/order/catalog/product/D282>. Access in: 21 jan. 2016.

[155] SABNIS, R. W. **Handbook of biological dyes and stains:** synthesis and industrial applications. New York: John Wiley, 2010. 521 p.

[156] ZHANG, W. I.; RÖHSE, H.; RIZZOLI, S. O.; OPAZO, F. Fluorescent in situ hybridization of synaptic proteins imaged with super-resolution STED microscopy. **Microscopy Research and Technique,** v. 77, n. 7, p. 517-527, 2014.

[157] O'CONNOR, C. **Fluorescence in situ hybridization (FISH)**. 2008. Available in: <http://www.nature.com/scitable/topicpage/fluorescence-in-situ-hybridization-fish-327:> Access in: 21 sep. 2015.

[158] SIGMA ALDRICH. **Protocol for annealing oligonucleotides.** 2015. Available in: <http://www.sigmaaldrich.com/technical-documents/protocols/biology/annealing-oligos.html>. Access in: 21 sep. 2015.

[159] SIGMA ALDRICH. **Fluorescent in situ hybridization (FISH).** 2015. Available in: <http://www.sigmaaldrich.com/life-science/cell-biology/antibodies/antibodies-application/protocols/fish.html>. Access in: 21 sep. 2015.

[160] MICHALET, X.; EKONG, R.; FOUGEROUSSE, F.; ROUSSEAUX, S.; SCHURRA, C.; HORNIGOLD, N.; VAN SLEGTENHORST, M.; WOLFE, J.; POVEY, S.; BECKMANN, J. S.; BENSIMON, A. Dynamic molecular combing: stretching the whole human genome for high-resolution studies. **Science,** v. 277, n. 5331, p. 1518-1523, 1997.

APPENDICES

Supplementary information of chapters 2 and 3

CHAPTER 2

Photophysical and confocal microscopy studies of maleic anhydride and maleimide derivatives

1 SUPPLEMENTARY STATIONARY DATA

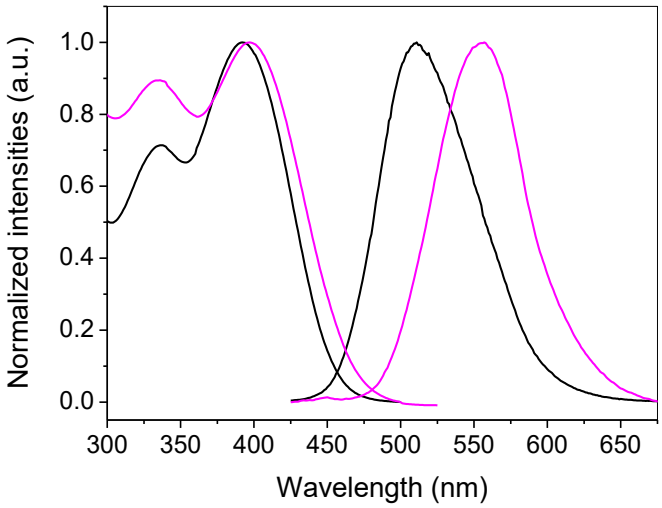

Figure 50. Normalized absorption and emission spectra of compound **4a** in 1,4-dioxane (black) and in DMSO (magenta).

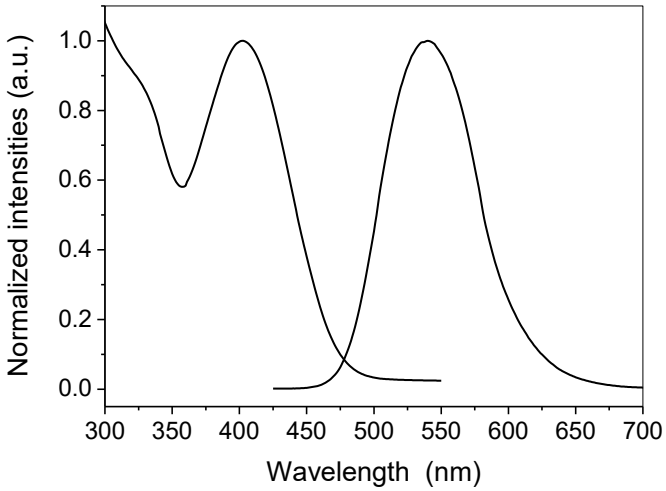

Figure 51. Normalized absorption and emission spectra of compound **5a** in 1,4-dioxane.

2 GEOMETRY OPTIMIZATIONS

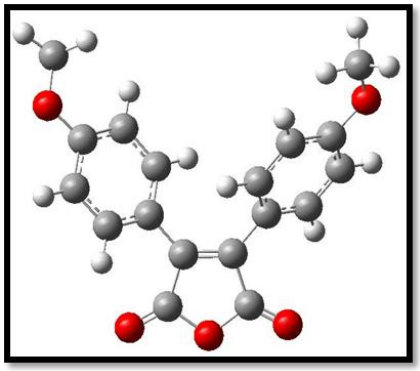

Figure 52. Optimized geometry of the maleic anhydride derivative **4a**.

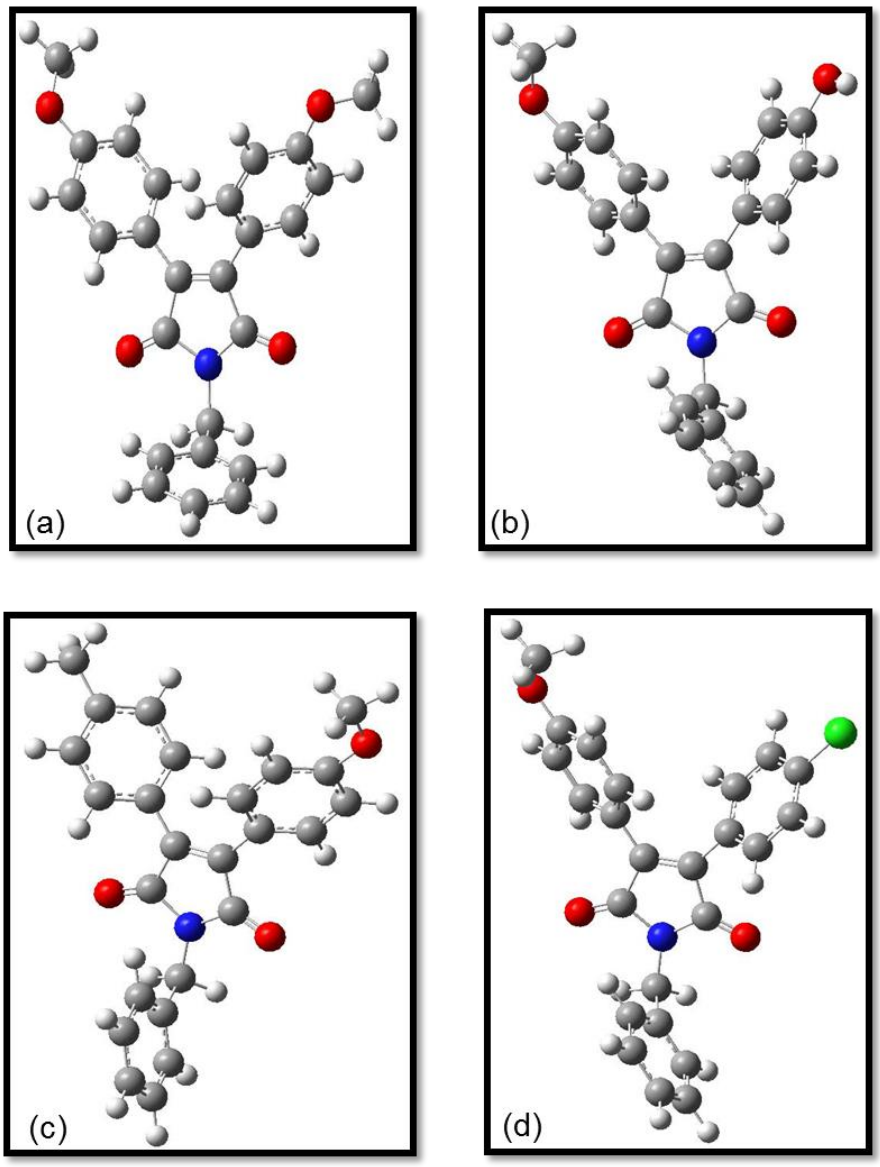

Figure 53. Optimized geometry of the maleimide derivatives. The pictures represent compound **5a** (a), **5b** (b), **5c** (c), and **5d** (d).

Table 19. Contribution of the dipole moments in each direction.

Compound	Axis x (D)	Axis y (D)	Axis z (D)	Total dipole moment (D)
4	-0.0007	-8.6844	0.0005	8.6844
5a	-3.9814	1.5388	-0.2952	4.2786
5c	3.6023	0.6310	1.9853	4.1613
5d	1.8742	1.7808	1.6228	3.0524

CHAPTER 3

Investigation of DNA fluorescent labelling strategies by super-resolution optical microscopy and atomic force microscopy

FISH PROBES PREPARATION AND DNA HYBRIDIZATION

3 METHODOLOGY

3.1 Preparation of the double-stranded oligonucleotide

To prepare the double-stranded DNA, two single-stranded complementary primers were used, with a 60 base pairs length. The primer sequence is 5'- GCA GCT CCC GGA GAC GGT CAC AGC TTG TCT GTA AGC GGA TGC CGG GAG CAG ACA AGC CCG -3' and its complement.

Firstly, the oligonucleotides were suspended in a specific buffer for the annealing procedure at a final concentration of 100 µM. The annealing buffer is composed by 10 mM Tris-Cl, 50 mM NaCl, and 1 mM EDTA, at pH = 7.75. Secondly, 100 µL of both complementary primers were mixed. This system was kept at 94 °C for 3 minutes. Then, it was slowly cooled down until room temperature by turning off the heating block.[158] After this process, the double-stranded oligonucleotide was stored at 2 °C. The final DNA concentration was 1845 ng/µL.

3.2 Fluorescent labelling of the oligo-probes

3.2.1 Direct one-step fluorescent labelling using a rhodamine-B dye

For a 50 µL-reaction, 10 vol% CutSmart® buffer (10x), 70 ng/µL double-stranded oligonucleotide (prepared in paragraph 3.1), 300 µM of cofactor MTC-10, 0.12 mg/mL of M.MpeI enzyme (at an initial concentration of 18.835 mg/mL) and Milli-Q water were gently

mixed. The enzyme M.MpeI targets the sequence GC for DNA modification. Each strand of the primer has 7 GC sites. The cofactor MTC-10 has a transferable moiety containing a rhodamine-B dye. The system was incubated at 37 °C for 1 h. Then, 1 µL of proteinase K was added. The system was subsequently incubated for 1 h at 55 °C and purified using spin-columns. The final concentration of DNA was approximately 29 ng/µL. The scheme of this one-step reaction is depicted in Figure 54.

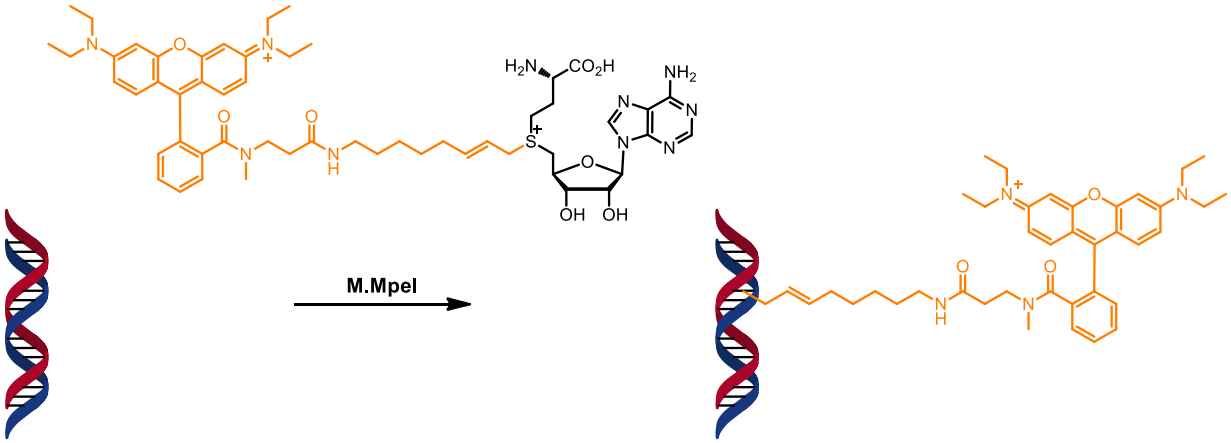

Figure 54. Scheme of the direct one-step fluorescent labelling, using the cofactor MTC-10, which contains in its transferable moiety a rhodamine B dye.

3.2.2 Direct one-step fluorescent labelling using the amine-to-NHS-ester coupling

This reaction is very similar to the one that described in the paragraph 3.5 (Chapter 3). Firstly, it is necessary to couple the dye to the cofactor *via* the primary amine-to-NHS-ester coupling reaction. For a 5 µL-reaction, 10 vol% of the buffer PBS (10x, pH = 7.4), 800 µM of cofactor MTC-6, 2.4 mM of Atto-647N-NHS-ester dye and Milli-Q water were mixed in a tube. It was placed on ice for 25 minutes. After that, 2 µL of CutSmart® buffer was added to quench the reaction and the system was kept on ice for one more minute.

Subsequently, the enzymatic transfer of the moiety containing the fluorophore to the specific sequence of the oligo, in this case GC, was performed. Therefore, to the previous reaction mixture 30 ng/µL of the double-stranded oligo (prepared according to item 3.1), 0.94 mg/mL of the M.MpeI enzyme, and Milli-Q water were added, so that the final volume was 20 µL. The system was incubated for 1 h at 37 °C. Following, 1 µL of proteinase K was included to the system, which was incubated for 1 h at 55 °C. The purification was performed using spin-columns. The final concentration of the labelled oligo-probe was approximately 12 ng/µL.

3.2.3 Fluorescent labelling using the Cu-free click reaction

This reaction is based on a two-step methodology, very similar to the reaction previously described in paragraph 3.3 (Chapter 3). The first step is related to the enzymatic transfer of the azide moiety, from the cofactor MTC-8, to the DNA with the specific sequence GC. For a 150 µL-reaction, 10 vol% of the buffer NEBuffer 4 (10x, pH = 7.9), 50 ng/µL of the double-stranded oligo (prepared according to paragraph 3.1), 300 µM of the MTC-8 cofactor, 0.75 mg/mL of the M.MpeI enzyme and Milli-Q water were gently mixed and incubated at 37 °C for 1 h. Then, 2 µL of proteinase K were added and the reaction tube was incubated at 55 °C for 1 h. The system was eluted using 20 µL of Milli-Q water. The final concentration of DNA functionalized with azide groups was 25 ng/µL.

The second step is the fluorophore coupling to the modified DNA by the copper-free click reaction. For a 50 µL-reaction, 25 vol% of DMSO, 0.5 mM of the Cy3 functionalized with a cyclooctyne group, 10 µL of the oligo functionalized with azide groups (from the first step), and Milli-Q water were mixed and incubated at room temperature for 12 h. The purification was performed using spin-columns and eluted using the elution buffer (provided by the manufacturer). The same procedure was carried out using the dye Cy5 functionalized with a cyclooctyne group. In general, the methodology for the fluorescent labelling of the oligo-probes can be represented by the Figure 55.

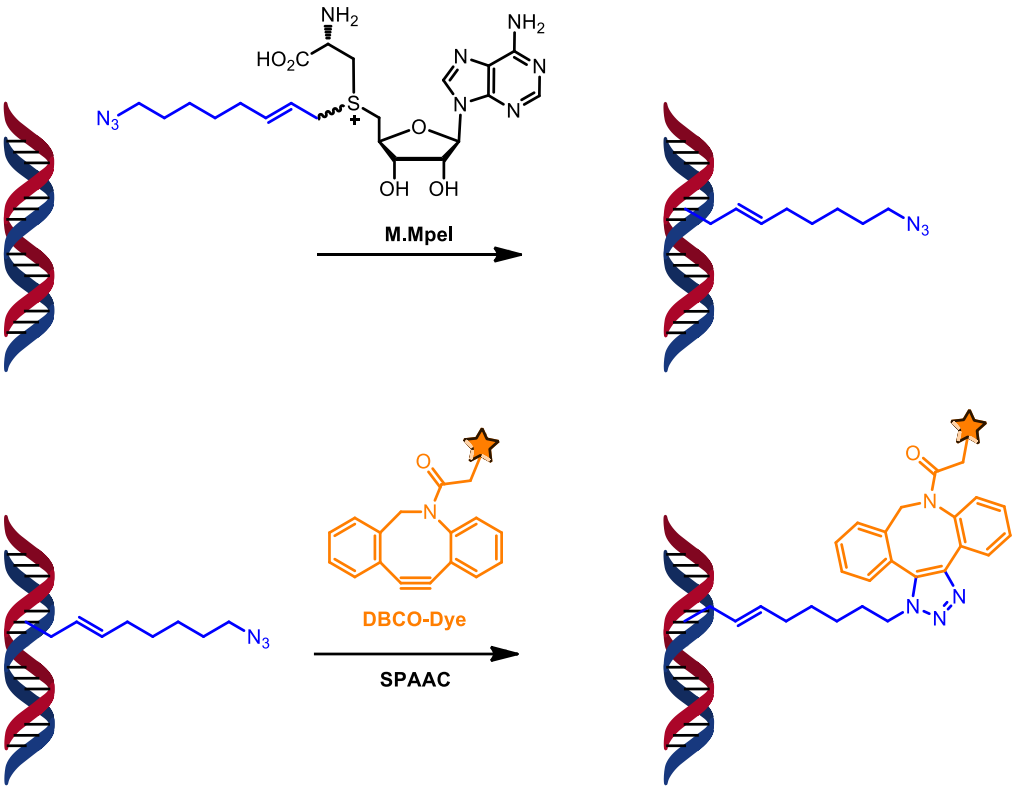

Figure 55. Scheme of the two-step fluorescent labelling of the probes used for the FISH approach, using the SPAAC reaction.

3.3 Preparation of hairpin oligonucleotides

To design a hairpin oligo-probe, a single-stranded oligonucleotide to target the sequence TCGA was developed. The TCGA sites of the double-stranded part of the oligo hairpin structure will be fluorescently labelled by the action of the methyltransferase M.TaqI. Its sequence is the following: 5'- CCG GTC GAT CGA CTT TTG TCG ATC GAC CGG TTC CAG TGC TGC AAT GAT ACC GCG AGA CCC ACG C -3'.

To generate the hairpin structure, the macromolecule was firstly suspended in a Tris-EDTA buffer (pH = 7.78) so that the final concentration was 100 µM. Then, the suspension was diluted again to a concentration of 10 µM. The annealing was performed using the most diluted suspension. For that, 50 µL of the primer suspension was incubated at 95 °C for 5 minutes. After that, the sample was immediately placed on ice for 15 minutes. After this procedure, the sample was stored at 2 °C.

3.4 Fluorescent labelling of the hairpin FISH probes

3.4.1 Direct one-step reaction using the amine-to-NHS-ester coupling

This labelling methodology is very similar to the one described in paragraph 3.2.2, and is also performed in two steps. Firstly, the fluorophore is coupled to the cofactor by an amino-to-NHS ester coupling reaction. To this end, 10 vol% of PBS buffer (pH = 7.4), 800 µM of the Ado-6-amine cofactor, 2.4 mM of the Atto-647N-NHS ester dye, and Milli-Q water were gently mixed. This reaction mixture had a final volume of 5 µL. This system was then kept on ice for 25 minutes. Subsequently, 2 µL of the CutSmart® buffer was added and the system was incubated for one more minute.

The second step is related to the enzymatic transfer of the moiety containing the fluorophore from the cofactor to the target site of the oligonucleotide, in this case the sequence 5'- TCGA -3'. Therefore, 30 ng/µL of the hairpin oligonucleotide (prepared in paragraph 3.3), 2 µL of the M.TaqI enzyme, and Milli-Q water were added to the previous reaction mixture. The final volume was 20 µL. The system was incubated for 1 h at 40 °C. The temperature was lower than the optimal enzymatic work temperature of the M.TaqI to avoid the structural modification of the hairpin probe. The system was purified using a spin-column. The final concentration was approximately 2.3 ng/µL.

The hairpin probes were also designed, prepared, and fluorescently labelled to perform hybridizations using T7 DNA as a target. However, this discussion is not part of the scope of this thesis.

3.5 DNA hybridization protocols

3.5.1 Protocol 1

3.5.1.1 Hybridization

This protocol was developed so that the DNA is firstly hybridized with the probe, then the hybridized DNA is coated onto a microscope coverslip. This protocol was adapted from the literature,[159] since we were not working with hybridizations in cell lines. For the hybridization procedure, the "hybridization mix solution" (containing the fluorescently labelled probe) was incubated at 76 °C for 10 minutes. This "hybridization mix solution" is composed by: 50% formamide (v/v), 10% dextran sulphate (w/v), 0.1% sodium dodecyl sulphate (SDS, w/v) and

2 ng/µL of the labelled oligo-probe. The solution is made in 2x SSC (Saline-Sodium Citrate buffer. The stock solution of the buffer is 20x SSC, which is composed of: 3 M sodium chloride and 0.3 M sodium citrate; pH = 7.09, filtered through a 0.2 µM filter). Four hybridization systems were prepared, then they were kept on ice.

Each sample received 6, 10, 20 and 30 ng/µL plasmid DNA pUC19, respectively. Afterwards, they were denatured at 76 °C for 5 minutes and the temperature was lowered to 37 °C. The hybridization was performed at 37 °C for 16 h.

3.5.1.2 DNA Stretching

In this procedure, the hybridized DNA with the oligo-probe was deposited onto the microscope coverslip. Initially, 50 µL of a 0.01% (w/v) PLL in water solution is coated onto the coverslip (Menzel-Gläser, 22 x 22, #1.5) for 15 minutes. After that, the coverslip was carefully rinsed with Milli-Q water and dried under a gentle flow of nitrogen gas.

50 µL of the hybridized solution, containing approximately 1 ng/µL pUC19 (dilutions done in “imaging buffer” as a solvent), was spin-coated onto the PLL-coated coverslip, at 2500 rpm for 60 s.

3.5.1.3 Washing step

The coverslips passed through several washing steps, which are important to remove unbound materials and to detect the hybridized DNA with the oligo-probe. The first wash was performed in a “washing buffer” at 40 °C for 5 minutes. This process was repeated twice. The “washing buffer” is composed by 20 vol% of formamide in 0.1x SSC.

The second wash was carried out in 0.1x SSC at 40 °C for 5 – 15 minutes. The third one was performed in 2x SSC at 40 °C for 5 – 15 minutes. The coverslips were cooled to room temperature. Subsequently, they were equilibrated in a “detection buffer” for 5 minutes. The “detection buffer” is constituted of 0.2% Tween-20 in 4x SSC.

The coverslips were finally washed in 2x SSC for 5 minutes and this procedure was repeated two times. Subsequently, the coverslips were air dried and stored in a desiccator. At this point, the samples were ready to be analysed by fluorescence microscopy. To this end, the BALM methodology was employed, as described in paragraph 3.8.

3.5.2 Protocol 2

Protocol 2 is similar to *Protocol 1*. However, in this case, the plasmid pUC19 was firstly coated onto the microscope coverslip and, afterwards, the hybridization procedure was carried out.

3.5.2.1 DNA Stretching

Similar to the procedure 3.5.1.2, 50 µL of a 0.01% PLL solution was coated onto a microscope coverslip for 15 minutes, which was rinsed with Milli-Q water and dried with nitrogen gas. With the coverslip prepared, approximately 0.5 – 1 ng/µL of the pUC19 plasmid was spin-coated onto it, at 2500 rpm for 180 s. After the plasmid deposition, 4 mL of Milli-Q water was added drop wise, while spinning, to remove unbound DNA molecules. Then, the coverslips were dried under a gentle flow of nitrogen gas.

3.5.2.2 Hybridization

The “hybridization mix solution” was incubated at 76 °C for 10 minutes, then, stored on ice. A perfusion chamber was sealed to the coverslip (with the plasmid already coated) to insert the “hybridization mix solution” as well as to avoid its evaporation.

After the addition of 50 µL of the “hybridization mix solution”, the coverslip was submitted to the denaturation process of the DNA. For that, the coverslip was incubated at 76 °C for 10 minutes. Then, the temperature was lowered to 37 °C and the hybridization was carried out at this temperature for at least 16 h. The perfusion chamber was carefully removed and the washing steps were performed as explained in item 3.5.1.3. After all washing steps, the coverslip could be stored in a desiccator and utilized for microscopy experiments.

3.5.3 Protocol 3

This protocol was also adapted from a previously reported protocol.[160] This one is also based on the coating of the target DNA onto a surface, and the hybridization procedure with the oligo-probe is performed *a posteriori*. However, *Protocol 3* offers additional steps for the

coverslip preparation as well as more drastic conditions for the denaturation of the DNA already attached to the cover slide, involving both high temperature and denaturing agents.

3.5.3.1 Denaturation of the oligo-probe

Approximately 0.5 ng/µL of the fluorescently labelled oligo-probe was added to the "hybridization mix solution". Subsequently, it was denatured at 80 °C for 5 minutes and immediately stored on ice. This "hybridization mix solution" is composed by 50% (v/v) formamide, 10% (w/v) dextran sulphate and 1% (v/v) Tween-20 in 2x SSC.

3.5.3.2 Coverslip preparation

As previously described in paragraph 3.6, around 0.5 ng/µL of the pUC19 plasmid was spin-coated onto a PLL-coated coverslip. Then, the coverslips containing the deposited DNA were dehydrated by immersion in a series of ethanol solutions (70, 90 and 100%), for 5 minutes each and at room temperature. This process was repeated three times. After that, the coverslips were air dried or dried under a gentle flow of nitrogen gas.

The next step was the denaturation of the target DNA deposited onto the cover slide. For that, it was immersed in a "denaturation solution" composed of 50% formamide in 2x SSC at 75 °C for 2 minutes. To quench the denaturing process, the coverslips were passed through a series of ice-cold ethanol solutions (70, 90 and 100%) for 3 minutes in each one. Finally, they were dried under a gentle flow of nitrogen gas.

3.5.3.3 Hybridization

In this protocol, the hybridization is performed by the incubation of the denatured oligo-probe with the coverslip containing the target plasmid DNA, also previously denatured. Thus, a perfusion chamber was sealed onto the coverslip (prepared in item 3.5.4.2) and the solution prepared in paragraph 3.5.4.1 was introduced in the chamber. This system was incubated at 37 °C for at least 16 h.

3.5.3.4 Washing step

After the hybridization, the coverslip was submitted through several washing steps. The first washing step used 50% formamide in 2x SSC for 5 minutes at room temperature. This step was repeated three times. Subsequently, the coverslips were washed in 2x SSC for 5 minutes at room temperature, and it was also repeated three times. The final wash was performed using the buffer PBS. While rotating at 2500 rpm on the spin-coating, 4 mL of the PBS buffer was added drop wise to the surface. This procedure was utilized in order to provide a more homogeneous dry. Subsequently, the slide was carefully dried with nitrogen gas and stored in a desiccator. At this stage, the sample is ready to use.

4 DATA CONCERNING THE BALM EXPERIMENTS

- CuAAC

Table 20. Experimental data of CuAAC: standard.

Movie	**1**	**2**	**3**	**4**	**5**	**6**	**7**	**Total**
Total Plasmids	1056	970	963	1033	888	808	940	6658
No labels	401	366	272	382	217	330	299	2267
1	226	182	190	225	180	191	182	1376
2	208	198	209	215	208	142	214	1394
3	130	133	153	116	155	97	141	925
4	54	55	94	58	80	37	51	429
5	27	30	27	28	41	9	34	196
6	8	4	8	8	5	1	9	43
7	2	2	6	1	2	0	6	19
8	0	0	3	0	0	1	1	5
9	0	0	0	0	0	0	2	2
10	0	0	1	0	0	0	1	2
Free dye	987	1468	1509	926	1207	1068	1060	8225

Total plasmids	6658
No labels	2267
Labelled	4391
Efficiency	**66%**

Table 21. Experimental data of CuAAC with the ClickOx approach.

Movie	**1**	**2**	**3**	**4**	**5**	**6**	**7**	**8**	**Total**
Total Plasmids	536	526	626	636	570	619	583	553	4649
No labels	161	269	205	197	275	187	206	162	1662
1	113	122	140	139	163	125	126	122	1050
2	119	85	142	153	92	166	123	124	1004
3	65	37	78	88	25	81	65	81	520
4	52	10	37	35	14	47	47	43	285
5	18	2	19	16	1	8	13	12	89
6	6	1	6	5	0	5	2	7	32
7	1	0	0	2	0	0	1	1	5
8	1	0	0	0	0	0	0	1	2
9	0	0	0	1	0	0	0	0	1
Free dye	446	521	617	497	804	582	527	566	4560

Total plasmids	4649
No labels	1662
Labelled	2987
Efficiency	**64%**

- SPAAC

SPAAC: different solvents

Table 22. Experimental data of SPAAC in H_2O.

	1449	**1453**	**1457**	**1465**	**1469**	**1476**	**Total**
Total plasmids	247	217	220	290	298	272	1544
No labels	76	39	24	58	49	30	276
1	49	31	21	30	31	35	197
2	37	50	50	46	39	54	276
3	42	48	50	63	71	39	313
4	24	20	34	31	47	48	204
5	6	17	24	31	29	29	136
6	8	10	11	15	16	25	85
7	3	2	5	12	10	8	40
8	2	0	1	1	4	2	10
9	0	0	0	2	2	0	4
10	0	0	0	1	0	1	2
11	0	0	0	0	0	1	1
free dye	268	354	371	376	360	412	2141

Total plasmids	1544
No labels	276
Labelled	1268
Efficiency	**82%**

Table 23. Experimental data of SPAAC in 60% etanol.

Movie	**1**	**2**	**3**	**4**	**5**	**6**	**7**	**Total**
Total plasmids	447	426	358	391	398	387	438	2845
no labels	302	271	83	77	166	160	103	1162
1	77	73	88	93	106	98	118	653
2	42	39	81	86	66	62	101	477
3	21	29	64	66	30	38	59	307
4	3	9	24	44	21	19	32	152
5	2	4	11	14	8	7	16	62
6	0	1	6	9	0	2	8	26
7	0	0	0	2	0	0	1	3
8	0	0	0	0	0	1	0	1
9	0	0	1	0	0	0	0	1
10	0	0	0	0	1	0	0	1
Free dye	370	337	705	669	465	422	489	3457

Total plasmids	2845
No labels	1162
Labelled	1683
Efficiency	**59%**

Table 24. Experimental data of SPAAC in 50% DMSO.

Movie	**1**	**2**	**3**	**4**	**5**	**6**	**7**	**8**	**9**	**Total**
Total plasmids	229	235	178	191	178	185	174	144	138	1652
No labels	19	32	15	16	14	15	17	18	16	162
1	17	36	22	18	18	12	28	12	15	178
2	30	42	33	27	43	23	22	26	19	265
3	52	50	30	34	38	40	35	32	28	339
4	49	31	38	33	27	39	33	31	17	298
5	36	17	21	34	22	28	18	13	18	207
6	13	16	11	18	8	15	11	7	10	109
7	7	5	5	7	7	7	9	4	5	56
8	4	1	2	1	0	3	1	0	6	18
9	1	2	1	1	1	0	0	1	3	10
10	1	1	0	1	0	2	0	0	1	6
11	0	0	0	0	0	1	0	0	0	1
12	0	0	0	0	0	0	0	0	0	0
13	0	0	0	0	0	0	0	0	0	0
14	0	0	0	1	0	0	0	0	0	1
Free dye	821	662	792	835	937	988	564	747	1043	7389

Total plasmids	1652
No labels	162
Labelled	1490
Efficiency	**90%**

Table 25. Experimental data of SPAAC in 30% DMF.

Movie	**1**	**2**	**3**	**4**	**5**	**6**	**7**	**8**	**Total**
Total plasmids	359	300	314	336	318	346	288	362	2623
No labels	67	98	86	75	72	51	95	80	624
1	68	61	58	59	54	48	68	84	500
2	88	40	64	67	72	69	52	70	522
3	64	47	62	58	52	70	40	75	468
4	48	33	23	38	34	50	20	41	287
5	13	15	13	17	18	37	7	9	129
6	8	4	6	14	9	14	5	3	63
7	3	1	2	5	6	3	1	0	21
8	0	1	0	3	0	2	0	0	6
9	0	0	0	0	1	1	0	0	2
10	0	0	0	0	0	1	0	0	1
Free dye	419	376	409	443	344	478	398	393	3260

Total plasmids	2623
No labels	624
Labelled	1999
Efficiency	**76%**

SPAAC: different concentrations of DMSO

Table 26. Experimental data of SPAAC in 0% DMSO.

Movie	**1**	**2**	**3**	**4**	**5**	**Total**
Total plasmids	422	366	376	453	374	1991
No labels	133	130	49	86	87	485
1	57	59	61	52	62	291
2	82	79	87	83	86	417
3	58	46	88	97	69	358
4	55	27	49	72	39	242
5	21	11	28	38	24	122
6	6	9	10	16	5	46
7	7	2	2	5	2	18
8	1	2	0	2	0	5
9	0	1	1	1	0	3
10	1	0	0	0	0	1
11	0	0	1	0	0	1
12	0	0	0	0	0	0
13	0	0	0	1	0	1
14	1	0	0	0	0	1
Free dye	704	719	670	691	686	3470

Total plasmids	1991
No labels	485
Labelled	1506
Efficiency	**76%**

Table 27. Experimental data of SPAAC in 10% DMSO.

Movie	**1**	**2**	**3**	**4**	**Total**
Total plasmids	447	467	475	559	1948
No labels	91	52	77	89	309
1	84	45	49	82	260
2	100	77	90	101	368
3	78	77	99	118	372
4	43	89	71	85	288
5	32	68	38	41	179
6	11	40	25	24	100
7	5	11	18	12	46
8	3	3	5	5	16
9	0	3	2	1	6
10	0	1	0	1	2
11	0	1	0	0	1
12	0	0	1	0	1
Free dye	445	562	473	639	2119

Total plasmids	1948
No labels	309
Labelled	1639
Efficiency	**84%**

Table 28. Experimental data of SPAAC in 25% DMSO.

Movie	**1**	**2**	**3**	**4**	**Total**
Total plasmids	209	211	187	213	820
No labels	24	16	14	25	79
1	28	27	34	27	116
2	44	44	42	48	178
3	33	41	39	45	158
4	38	37	34	33	142
5	24	20	13	23	80
6	10	18	8	6	42
7	6	5	2	3	16
8	1	1	1	3	6
9	1	1	0	0	2
Free dye	614	643	482	581	2320

Total plasmids	820
No labels	79
Labelled	741
Efficiency	**90%**

Table 29. Experimental data of SPAAC in 50% DMSO.

Movie	**1**	**2**	**3**	**4**	**5**	**6**	**Total**
Total plasmids	414	472	371	370	369	350	2346
No labels	174	119	111	102	118	66	690
1	74	88	70	83	80	64	459
2	72	99	72	76	68	59	446
3	44	84	53	50	52	70	353
4	25	36	37	36	37	48	219
5	16	20	20	10	15	22	103
6	3	16	5	6	1	10	41
7	4	5	2	2	4	6	23
8	1	2	1	3	1	4	12
9	0	2	0	1	0	0	3
10	1	1	0	0	2	1	5
11	0	0	0	0	0	0	0
12	0	0	0	1	0	0	1
Free dye	1080	1162	1084	974	1075	1110	6485

Total plasmids	2346
No labels	690
Labelled	1656
Efficiency	**71%**

Table 30. Experimental data of SPAAC in 75% DMSO.

Movie	**1**	**2**	**3**	**4**	**5**	**Total**
Total plasmids	350	73	455	449	411	1738
No labels	52	23	114	88	76	353
1	93	12	58	79	107	349
2	116	16	91	79	99	401
3	62	14	73	71	85	305
4	14	2	56	68	37	177
5	9	3	36	31	7	86
6	3	1	15	19	0	38
7	1	2	7	10	0	20
8	0	0	5	1	0	6
9	0	0	0	2	0	2
10	0	0	0	1	0	1
Free dye	1374	1315	1032	1068	1443	6232

Total plasmids	1738
No labelled	353
Labelled	1385
Efficiency	**80%**

- Amine-to-NHS-ester coupling

Table 31. Experimental data of the amine-to-NHS-ester coupling in 5% DMSO.

Movie	**1**	**2**	**3**	**4**	**5**	**Total**
Total plasmids	835	924	866	905	898	4428
No labels	564	643	614	613	613	3047
1	155	143	128	131	121	678
2	75	79	71	85	94	404
3	23	34	38	53	42	190
4	14	17	11	15	19	76
5	3	4	3	4	6	20
6	1	3	0	2	1	7
7	0	0	0	2	1	3
8	0	0	1	0	0	1
9	0	1	0	0	1	2
Free dye	331	450	344	352	389	1866

Total plasmids	4428
No labelled	3047
Labelled	1381
Efficiency	**31%**

Table 32. Experimental data of the amine-to-NHS-ester coupling in 10% DMSO.

Movie	**1**	**2**	**3**	**4**	**5**	**Total**
Total plasmids	605	611	610	698	742	3266
No labels	445	476	499	570	619	2609
1	94	76	64	70	77	381
2	43	36	34	39	31	183
3	18	17	9	11	10	65
4	3	4	4	5	3	19
5	1	1	0	2	2	6
6	1	1	0	1	0	3
Free dye	204	214	163	163	175	919

Total plasmids	3266
No labelled	2609
Labelled	657
Efficiency	**20%**

Table 33. Experimental data of the amine-to-NHS-ester coupling in 25% DMSO.

Movie	**1**	**2**	**3**	**4**	**5**	**Total**
Total plasmids	317	604	585	613	492	2611
No labels	173	305	364	331	362	1535
1	61	123	122	130	75	511
2	41	104	57	89	38	329
3	24	43	32	37	13	149
4	12	18	7	16	1	54
5	1	8	0	8	3	20
6	3	0	1	2	0	6
7	1	1	2	0	0	4
8	0	0	0	0	0	0
9	0	0	0	0	0	0
10	0	0	0	0	0	0
11	1	1	0	0	0	2
12	0	0	0	0	0	0
13	0	1	0	0	0	1
Free dye	278	614	451	425	218	1986

Total plasmids	2611
No labelled	1535
Labelled	1076
Efficiency	**41%**

Table 34. Experimental data of the amine-to-NHS-ester coupling in 30% DMSO.

Movie	**1**	**2**	**3**	**4**	**5**	**6**	**Total**
Total plasmids	749	626	781	810	719	794	4479
No labels	341	323	262	338	305	281	1850
1	171	122	173	210	163	194	1033
2	141	92	150	131	119	153	786
3	60	55	104	82	73	96	470
4	23	26	45	30	31	45	200
5	8	3	25	13	18	14	81
6	1	4	10	3	5	8	31
7	2	0	5	1	3	2	13
8	1	1	5	0	1	1	9
9	0	0	1	1	1	0	3
10	0	0	0	1	0	0	1
11	1	0	1	0	0	0	2
Free dye	392	303	572	385	486	421	2559

Total plasmids	4479
No labelled	1850
Labelled	2629
Efficiency	**59%**

- Direct reaction

Table 35. Experimental data of the direct reaction using the dye Atto-647N-NHS ester.

Movie	**1**	**2**	**3**	**4**	**5**	**6**	**7**	**8**	**9**	**Total**
Total plasmids	687	728	659	737	793	780	673	603	646	6306
No labels	18	39	34	28	20	32	26	39	38	274
1	62	74	183	106	74	62	49	42	44	696
2	15	126	205	173	108	116	102	78	101	1024
3	157	120	144	179	154	148	130	100	122	1254
4	140	130	46	122	152	156	142	120	125	1133
5	89	93	37	77	119	125	104	80	105	829
6	42	61	6	33	90	78	54	70	59	493
7	16	37	4	13	41	41	35	34	27	248
8	9	20	0	3	14	12	19	19	15	111
9	1	18	0	1	13	6	8	11	8	66
10	1	5	0	1	4	0	0	3	1	15
11	1	3	0	0	2	3	0	5	0	14
12	0	1	0	1	0	1	0	0	0	3
13	0	0	0	0	1	0	2	0	0	3
14	0	0	0	0	0	0	1	0	0	1
15	1	0	0	0	1	0	1	1	0	4
16	0	0	0	0	0	0	0	0	0	0
17	0	0	0	0	0	0	0	0	1	1
18	0	0	0	0	0	0	0	1	0	1
19	0	0	0	0	0	0	0	0	0	0
20	0	1	0	0	0	0	0	0	0	1
Free dye	1392	1673	957	1169	1661	1554	1563	1461	1356	12786

Total plasmids	6306
No labelled	274
Labelled	6032
Efficiency	**96%**

Table 36. Experimental data of the direct reaction using the dye Atto-565-NHS ester.

Movie	**1**	**2**	**3**	**4**	**5**	**6**	**7**	**8**	**Total**
Total plasmids	1073	820	898	946	758	973	971	982	7421
No labels	205	136	150	199	149	78	129	78	1124
1	186	150	186	189	144	127	164	173	1319
2	201	143	177	190	189	174	193	187	1454
3	208	146	145	172	128	195	194	216	1404
4	127	129	135	99	86	174	139	147	1036
5	85	59	55	52	41	118	83	96	589
6	32	32	31	29	15	66	38	57	300
7	16	16	14	13	4	25	18	17	123
8	6	6	4	1	1	11	8	7	44
9	5	2	0	2	1	4	4	3	21
10	1	0	1	0	0	0	1	1	4
11	1	1	0	0	0	1	0	0	3
Free dye	1830	2217	1942	1724	2032	2269	2123	1944	16081

Total plasmids	7421
No labelled	1124
Labelled	6297
Efficiency	**85%**